

OPEN THIN WALLED COLUMNS

THE INFLUENCE OF SHAPE  
ON THE STRENGTH OF  
OPEN THIN WALLED COLUMNS

by

SUBBANARASU DIVAKARAN, B.E.

A Thesis

Submitted to the Faculty of Graduate Studies  
in Partial Fulfilment of the Requirements  
for the Degree  
Master of Engineering

McMaster University

September, 1964.

MASTER OF ENGINEERING  
(Civil Engineering)

McMASTER UNIVERSITY  
Hamilton, Ontario.

TITLE: The Influence of Shape on the Strength of Open Thin  
Walled Columns

AUTHOR: Subbanarasu Divakaran, B.E. (Andhra University)

SUPERVISOR: Professor H. Robinson

NUMBER OF PAGES: viii, 116

SCOPE AND CONTENTS: This Thesis deals with the analytical and experimental study of buckling strength of thin walled channel struts of different cross sections. The influence of geometry of the cross section on the strength has been studied with the aid of the electronic computer. The experimental work consisted of testing different types of channels of thin sheeting to destruction. Conclusions have been drawn from these tests, and suggestions for further research have been made. The Appendix includes sample calculations for geometrical characteristics of the sections.

## ACKNOWLEDGMENTS

I wish to express my sincere thanks to Dr. H. Robinson, my research Supervisor, for his very valuable guidance both in theoretical and experimental work.

I wish to express my sincere thanks to the Canadian Commonwealth Scholarship and Fellowship Committee, through whose award I was able to carry out this research.

## TABLE OF CONTENTS

CHAPTER		PAGE
I	INTRODUCTION	1
II	AIMS OF THE INVESTIGATION AND MATHEMATICAL ANALYSIS	15
III	EXPERIMENTAL WORK AND RELATED DISCUSSION	57
IV	COMPARISON OF EXPERIMENTAL RESULTS WITH THEORY	97
V	CONCLUSIONS	100
VI	SUGGESTIONS FOR FURTHER RESEARCH	102
	REFERENCES	105
	APPENDIX A	107
	APPENDIX B	114
	APPENDIX C	116

## LIST OF ILLUSTRATIONS

	Page
1. Fig. 1.1	5
2. Photograph 1.1	6
3. Photograph 1.2	7
4. Fig. 1.2	8
5. Photograph 1.3	12
6. Fig. 2.1	16
7. Fig. 2.2(a)	17
8. Fig. 2.2(b)	18
9. Fig. 2.3	23
10. Fig. 2.4	25
11. Fig. 2.5	31
12. Fig. 2.6(a)	43
13. Fig. 2.6(b)	44
14. Fig. 2.6(c)	46
15. Fig. 2.6(d)	47
16. Fig. 2.7(a)	49
17. Fig. 2.7(b)	50
18. Fig. 2.8(a)	53
19. Fig. 2.8(b)	54
20. Fig. 3.1	59
21. Fig. 3.2 & Fig. 3.3	60

# LIST OF ILLUSTRATIONS (CONTINUED)

	Page
22. Photograph 3.1	62
23. Photograph 3.2(a)	63
24. Photograph 3.2(b)	64
25. Photograph 3.2(c)	66
26. Fig. 3.3(a)	67
27. Fig. 3.3(b)	68
28. Fig. 3.3(c)	69
29. Fig. 3.3(d)	70
30. Fig. 3.3(e)	71
31. Fig. 3.3(f)	72
32. Fig. 3.3(g)	73
33. Fig. 3.3(h)	74
34. Fig. 3.3(k)	75
35. Fig. 3.4(a) & Fig. 3.4(b)	76
36. Fig. 3.4(c) & Fig. 3.4(d)	77
37. Fig. 3.4(e)	78
38. Fig. 3.5(a)	79
39. Fig. 3.5(b)	80
40. Fig. 3.6(a)	87
41. Fig. 3.6(b)	90
42. Fig. 3.7	91

## NOMENCLATURE

$A$	Cross sectional area
$B$	Flange width of channel
$C$	Coefficient governing the effective width
$d$	Depth of channel
$E, E_t$	Young's Modulus, Tangent Modulus
$e$	Distance of centroid from web plate
$G, G_t$	Shear Modulus, Tangent Shear Modulus
$I_{xx}, I_{yy}$	Second Moments of area about axes XX and YY
$I_p$	Polar Moment of Inertia
$K_\phi$	Coefficient of interaction in torsion and flexure
$K_\tau$	Torsional rigidity
$L$	Length of the column
$m$	Developed length of section
$M_t, M_{ts}$	Moments of external forces
$p$	Perpendicular distance from centroid to the tangent to the curve at any point $x, y$
$Q$	Ratio of web width to flange width
$R_x, R_y, R_\beta$	Geometrical constants governing buckling in torsion and flexure
$r_x, r_y, r_\beta$	Radii of gyration in flexure across XX, YY and torsional radius of gyration about Z axis
$t$	Wall thickness
$U_w$	Potential energy of external loads
$u, \bar{u}$	Displacement parallel to " $\xi$ " axis
$V$	Strain energy



$v, \bar{v}$	Displacements parallel to " $\eta$ " axis
$w, w_x, w_y$	External load and its components in the directions XX and YY
$x_0, y_0$	Co-ordinates of shear centre with respect to the principal axes.
$\alpha_1, \alpha_6$	Geometrical constants for cross sections
$\beta$	Angle of rotation of section
$\Gamma$	Warping stiffness
$\delta_c$	Compression of longitudinal fibre
$\epsilon, \epsilon_i$	Longitudinal strains
$\phi_i$	Angle made by the "i"th plate element to the " $\eta$ " axis
$\nu$	Poisson's ratio
$\sigma_g$	Axial stress
$\gamma$	Ratio of Tangent Modulus to Young's Modulus
$\eta_i$	Displacement of 'i'th plate in the direction of the " $\eta$ " axis

## CHAPTER I

### INTRODUCTION

1.1 The possibility of occurrence of torsional column failure was first recognised when open thin walled sections were used in aircraft structures, and experience revealed that columns of open cross section tend to bend and twist simultaneously under axial loading. The importance of this physical phenomenon lies in the fact that the critical load (Buckling load) for these columns may be much less than the elastic critical load as obtained by Euler for flexural buckling, on account of the onset of twisting deformation caused by low torsional stiffness of the open cross sections.

1.2. Wagner introduced the theory for such columns with his concept of unit warping<sup>1</sup>. He based his theory on the arbitrary assumption that the centre of rotation of the cross section under torsion and flexure was the centre of shear. This is, in general, not the case, and Bleich<sup>2</sup> and Ostenfeld<sup>3</sup> have given more general analysis applicable to both symmetric and unsymmetric sections. Making use of the theorem of stationary potential energy Bleich demonstrated that the usual differential equations for flexural buckling were valid for singly symmetric sections like channels, provided the displacements of the centre of shear rather than the displacement of the centroid were considered. Kappus, Lundquist, and Fligg<sup>4,5</sup> established an exact theory by which they showed that the centre of rotation will be such as to make potential energy a minimum.

1.3 All the above theories assume plane cross sections warp but that there is no distortion in their geometry in the plane of their cross sections, i.e., the various parts of the cross sections retain the same relative orientation even with warping. It is also assumed that overall failure of the section in torsional flexural buckling takes place and is not accompanied by local buckling. Attempts have been made<sup>6</sup>, by Chilver and others to clearly define regions of local and overall buckling without success. Separate analysis of local and overall buckling can only give approximate values, since it is unrealistic in so far as it separates a single phenomenon into two separate and arbitrary phenomena. An analysis to cover local and overall buckling simultaneously would be mathematically intractable. However, a large number of tests would enable clear identification of the type of buckling, as a function of the parameters denoting the geometrical configuration, the size of the flange and web, the size of lip, and the thickness of the sheeting. From such results, it would be possible to earmark ranges of these parameters in which either local or primary buckling may be anticipated. This would mean that, when a new section is to be assessed for its strength, it would be first seen if it would fail by primary buckling or local buckling. When the mode of buckling has thus been ascertained, the relevant design formulae can be chosen to determine working loads.

1.4 It has been observed from tests carried out by Kollbrunner<sup>8</sup> and Chilver<sup>6</sup> that most of the experimental points lie well above the theoretically predicted values of strength for thin walled cross sections like

angles, channels, and lipped channels. This would indicate that the present theoretical approach makes a conservative estimate of strength, and leaves a good extent of the load potential unused. To ensure development of specifications and codes of practice designed to make the fullest use of this potential in thin-walled sections, it would be necessary to conduct extensive testing, and phenomenological studies. Winter<sup>9</sup> and associates tested lipped channels, and top hat sections and have reported the results. The lack of agreement between theoretical and experimental results has shown that there is need for a large number of tests before any design specifications can be made. The importance of the effect of initial imperfections on the critical loads is another aspect which has remained unexplored. In view of the large reserve of strength beyond the initial buckling load of these sections, an elasto-plastic approach may be more appropriate.

1.5 A complete and comprehensive bibliography of work done in this field in Europe is furnished in Kollbrunner's treatise<sup>10</sup> on buckling.

1.6 The open sections commonly used so far are angles, lipped channels, channels and lipped angles. Channels with inward and outward lips have been frequently employed. The incipience of lateral buckling of individual plate elements certainly depends on the constraint or the lack of it at the free edges. The lips so far used provide constraint in a direction transverse to the plane of the flange plate element in a channel and transverse

to the legs of angles. But the stiffening lip, by itself, has a very low transverse stiffness. We can observe, while testing such channels under compression, that the lips buckle and distort very early in the loading process. The very early setting in of the waving in these lips reduces their contribution to the lateral stiffness of the outstanding flange. It may be that, because of this, increase in strength is not in direct proportion to the increase in cross sectional area caused by the provision of straight lips. The present investigation has been undertaken to determine other shapes of flange stiffening or web stiffening which would improve efficiency of the section as a whole. Fig.1.1 shows the various shapes proposed for this purpose.

The circular lips in these sections have multidirectional stiffness, and therefore stiffen the outstanding flanges, and the web plate against local buckling. Preliminary tests have shown that increase in strength can be achieved by the provision of such lips in the cross sections (Photographs 1.1 and 1.2).

1.7 Provision of lips in the cross sections also help to stiffen it torsionally. In many instances these lips prevent overall buckling and restrict failure to local buckling. This fact can be appreciated better from the theoretical analysis presented subsequently. A channel section 8 inches by 4 inches and 36 inches long has been selected for the purpose of studying the influence of geometry of the cross section on the critical load, and on the possibility of torsional collapse. Referring to Fig.1.2, a,b,c, the distance from the centroid to the shear centre along the X axis of symmetry

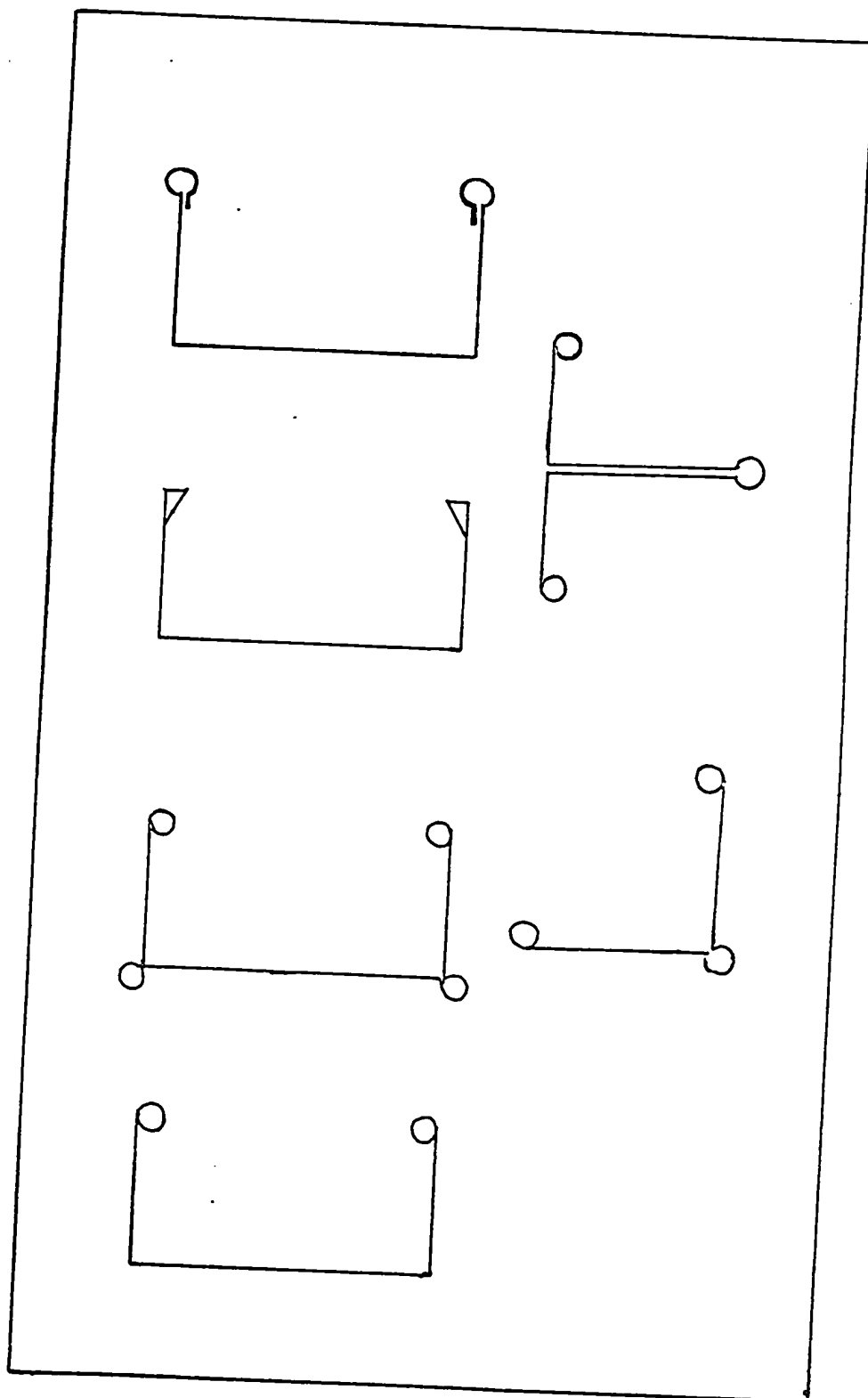
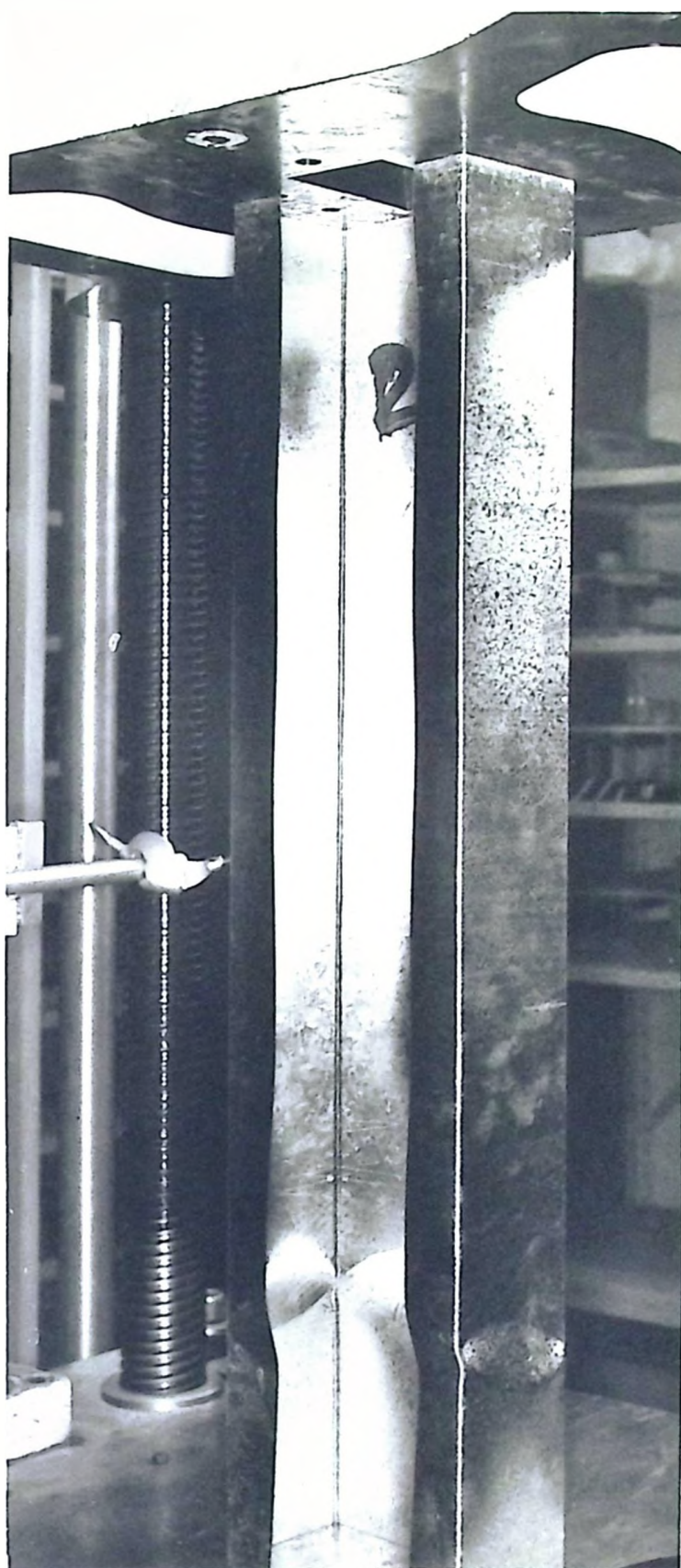


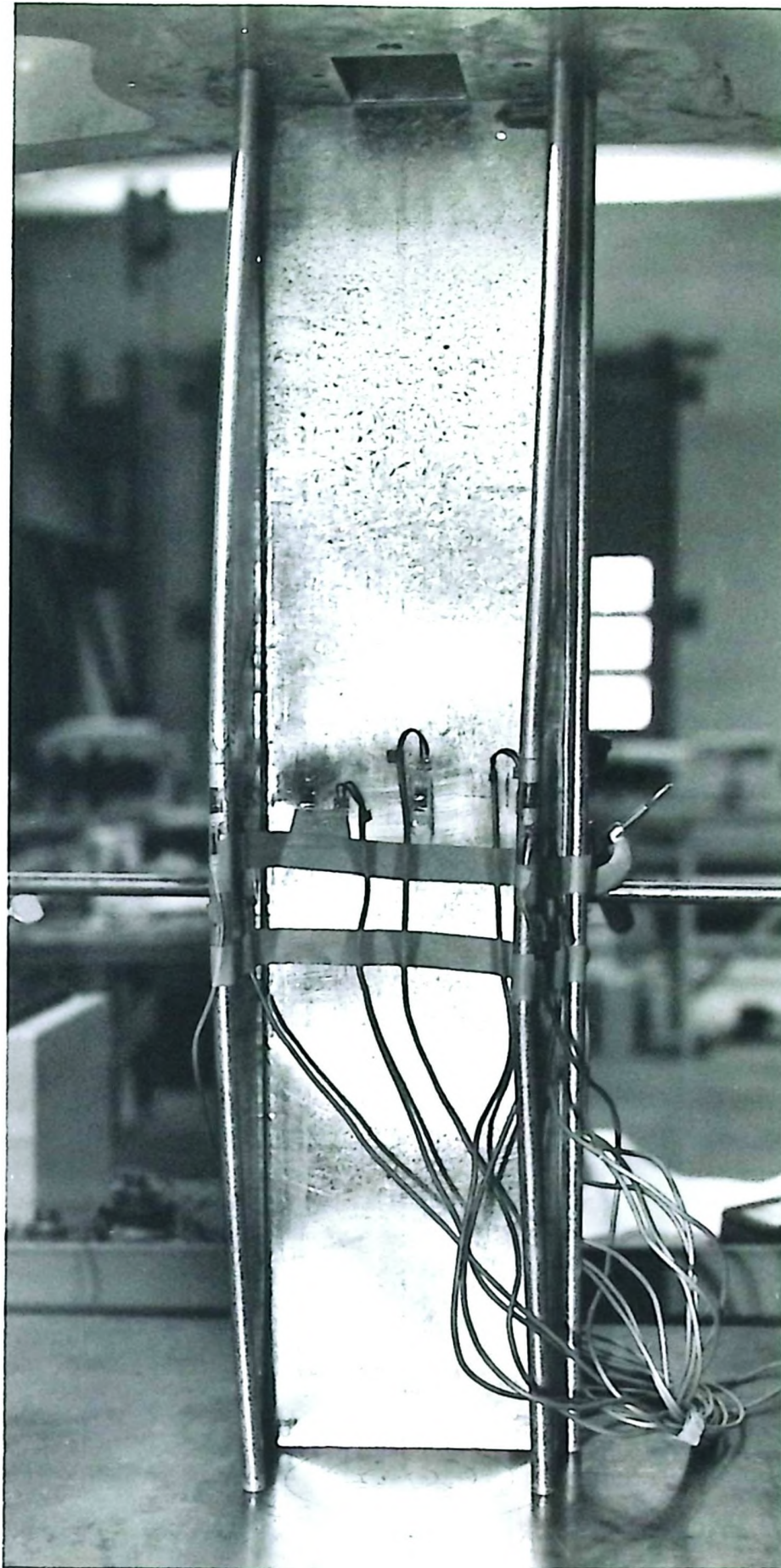
FIG. 1.I



PHOTOGRAPH 1.1

STRAIGHT LIPPED CHANNEL AT FAILURE





PHOTOGRAPH 1.2

CHANNEL WITH FOUR BULBS AT FAILURE



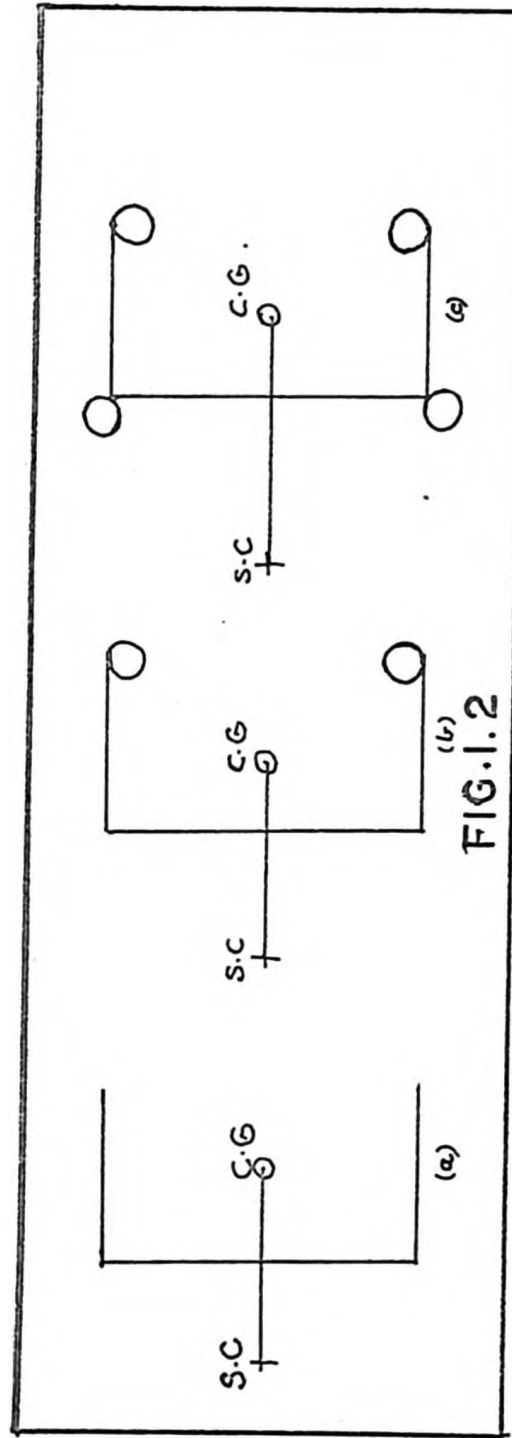


FIG.1.2

is obtained from the relation:

$$x_o = \frac{1}{I_{xx}} \int_0^m y t \alpha_c ds \quad y_o = -\frac{1}{I_{yy}} \int_0^m x t \alpha_c ds \quad (1.1)$$

$$\alpha_c = \int_0^s p ds \quad (1.2)$$

where "x,y", are the co-ordinates of any point on the centre line of the cross section

"m" the full developed length of the section from one tip to the other

" $I_{xx}$ " Moment of inertia about axis XX

"p" the perpendicular distance from centroid to the tangent at the point (x,y) on the centre line of the cross section.

The shear centre is the point through which the resultant shear stress on the section due to the shear field passes. If an external load passes through the centre of shear, the section bends without twisting. If a torque T acts on the section and it rotates through an angle  $\theta$ , then

$$T = K_1 \theta$$

where  $K_1$  is the uniform torsional stiffness. For a wall of uniform thickness "t", K equals  $G m t^3/3$ , where G is the elastic modulus in shearing. The warping stiffness for a cross section ( $T$ ) is obtained from the relation obtained by Bleich<sup>2</sup>:

$$\text{Warping stiffness } \Gamma = \frac{d^2}{4} \left[ I_{yy} + A e^2 \left( 1 - \frac{d^2 A}{4 I_{xx}} \right) \right]$$

where "d"      depth of channel in inches  
           "A"      area of channel in square inches  
           "e"      distance of Centroid from the web centre line  
 $I_{xx}, I_{yy}$       Moments of inertia about xx and yy resply  
           " $\Gamma$ "      Warping stiffness

The above equation is approximate and is within one percent of the values for bulbed channels, channels with circular lips as determined by Goodiers solution. Table 1.1 provides the geometrical properties of four different sections of channels.

1.8      It may be observed that provision of circular lips increases the warping stiffness considerably. When warping is restrained by flat end supports as in ordinary construction it is reasonable to expect a greater torsional stiffness for sections with greater warping rigidity. This aspect of the problem has not received its due attention, and in exploratory tests it was obvious that the warping rigidity had much to do with the prevention of torsional displacements of the section. The theoretical analysis and evaluation of geometrical constants bring out the mathematical relationship between warping stiffness and torsional radius of gyration.

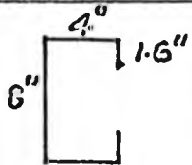

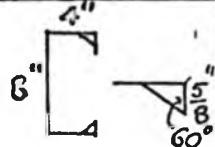
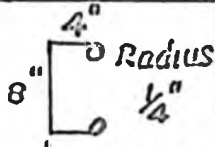
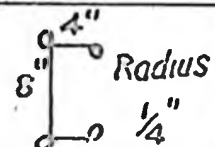
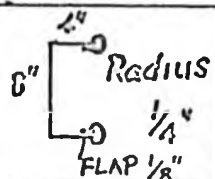
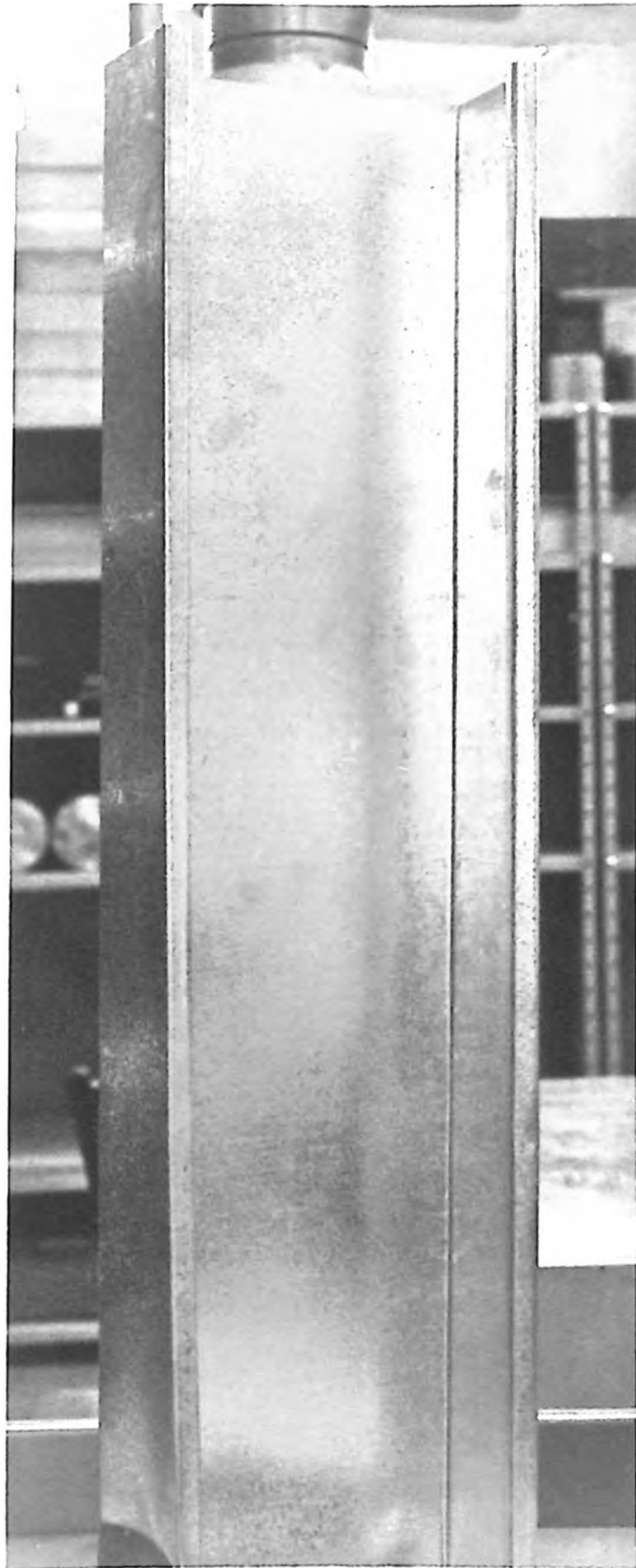
Section.	$R_x$	$R_y$	$R_p$	$R_E$	Warping stiffness per unit "t"	$I_{xx}$ per unit "t"	$I_{yy}$ per unit "t"	$I_P$ about shear centre/"t"	Remarks.
	3.26	1.59	1.068	0.973	 449.2	204.09	48.67	393.76	
	3.382	1.56	1.145	1.017	484.5	221.66	48.32	375.47	
	3.448	1.664	1.159	1.05	555.2	214.86	52.87	413.33	
	3.284	1.61	1.31	1.16	782.7	270.0	57.92	455.95	
	3.41	1.674	1.33	1.155	766.	224.93	54.182	433.13.	

Table 1.1



PHOTOGRAPH 1.3

1.9 Post buckling strength of thin walled members is an important aspect which should be considered in this context. Just because a thin walled structural element has buckled, it cannot be presumed to have been destroyed. In fact, it can take several times the initial buckling load before finally collapsing. Even at ultimate failure the collapse leaves a large portion of the elements completely undamaged (See photographs 1.2 and 1.3). This emphasizes the fact that just because the structural element shows up ripples on its surface it should not be considered to have collapsed. \*

---

\* It would be of interest to refer to a residential block built in West Germany, and reported in Der Stahlbau, July, 1962. In this German structural frame, channels of 7 cm x 4 cm, and wall thickness varying from 2 mm to 3 mm (0.0775 - 0.118") have been used as columns. The thicknesses correspond to U.S. gauges 14 to 6. The spacing of the columns is very close, viz. 3 to 4 feet. In air frame design it is taken for granted that buckling of the skin panels will be normally encountered, and should be ignored so long as the strength is unimpaired. In the same manner, a small amount of buckling in a thin walled structural member, is not significant so long as it does not impair the strength of the element concerned. Therefore, it should be possible to define strength of these elements in relation to their out of plane buckling, for the purpose of formulating a design code. In most cases, however, the structural frame will be encased with a fireproof material and the ripples would not be seen on the surface.

1.10 Failure of a thin walled element has to be defined arbitrarily - because very heavy distortions will certainly be ruled out. To start with, we may say failure can be said to occur when lateral displacement exceeds 5 times the thickness of element. In a similar manner any widening of the open section under loading can also be specified - for instance, for a channel with 8" web and 4" flanges, it should be acceptable if the outstanding edges of the channel flanges, approach towards or recede from each other by 0.25", i.e.  $1/32$  of the width. These limitations would satisfy aesthetics. Besides, the working load of the structure is still only a fraction of the ultimate load.

1.11 For a state of loading under which the stresses in the section nowhere exceed the limit of proportionality, Timoshenko<sup>11</sup> among others, developed the concept of effective width. However, beyond the limit of proportionality it may not be correct to use these relations. An empirical approach can be made use of as in Bleich's work<sup>2</sup>. Also, with the now generally accepted tangent modulus concept it is possible to develop formulae which are simpler to use.

## CHAPTER II

### AIMS OF THE INVESTIGATION AND MATHEMATICAL ANALYSIS

2.1 The analysis detailed in the following pages closely follows the method derived by Bleich<sup>2</sup>, as it is the most suitable approach for sections made up of rectilinear plate elements. The relevant part of this development is outlined in the following. Figure 2.1 shows the cross section of a column of uniform section composed of a number of flat plates - which are very thin when compared to their lengths  $X, Y, Z$ , represents the system of axes corresponding to the undeformed configuration. We also consider axes " $\xi, \eta$ " originally merging with  $X$  and  $Y$ , but under-going displacements and rotation along with the cross section. The components of displacement parallel to " $\xi, \eta$ " axes are  $\bar{u}$  &  $\bar{v}$  (Fig. 2.1).

Under external loading the displacements of any point in the plane will be a function of the displacements  $\bar{x}, \bar{y}$ , of the centroid and the rotation " $\beta$ ". Also these displacements can be treated as a function of  $\bar{u}, \bar{v}, \beta$ ". It is also tacitly assumed that the geometry of the cross section does not alter, and displacements are considered to be rigid body movements and rotations. Even though each plate element can bend in its own plane, and its cross section remains plane, the compression member as a whole may warp. The planes of adjacent plates may be different altogether after deformation. This assumption is reasonable since, away from the supports, use can be made of St. Venant's principle and also any variation in warping



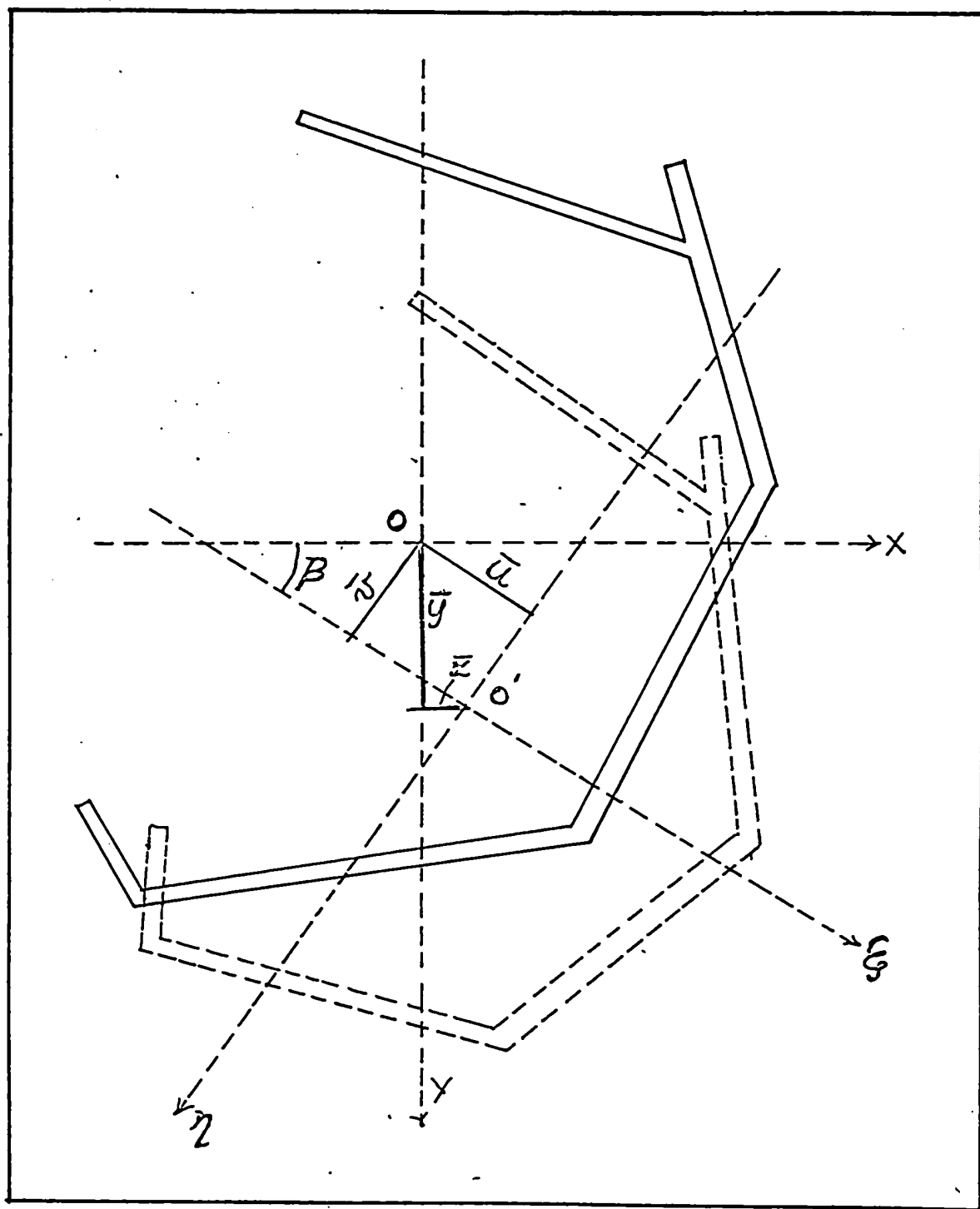


FIG. 2.1

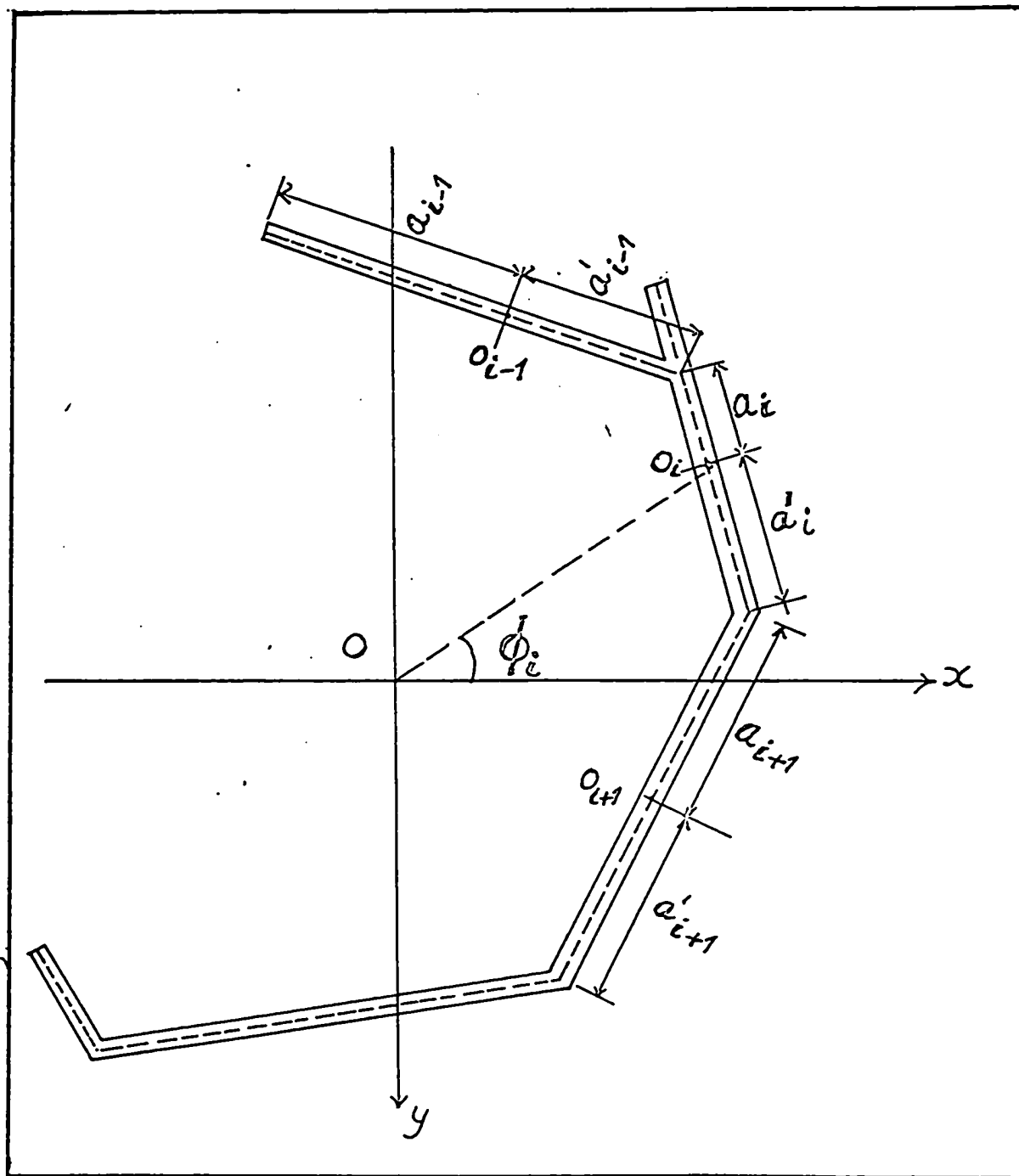


FIG. 2.2(a)

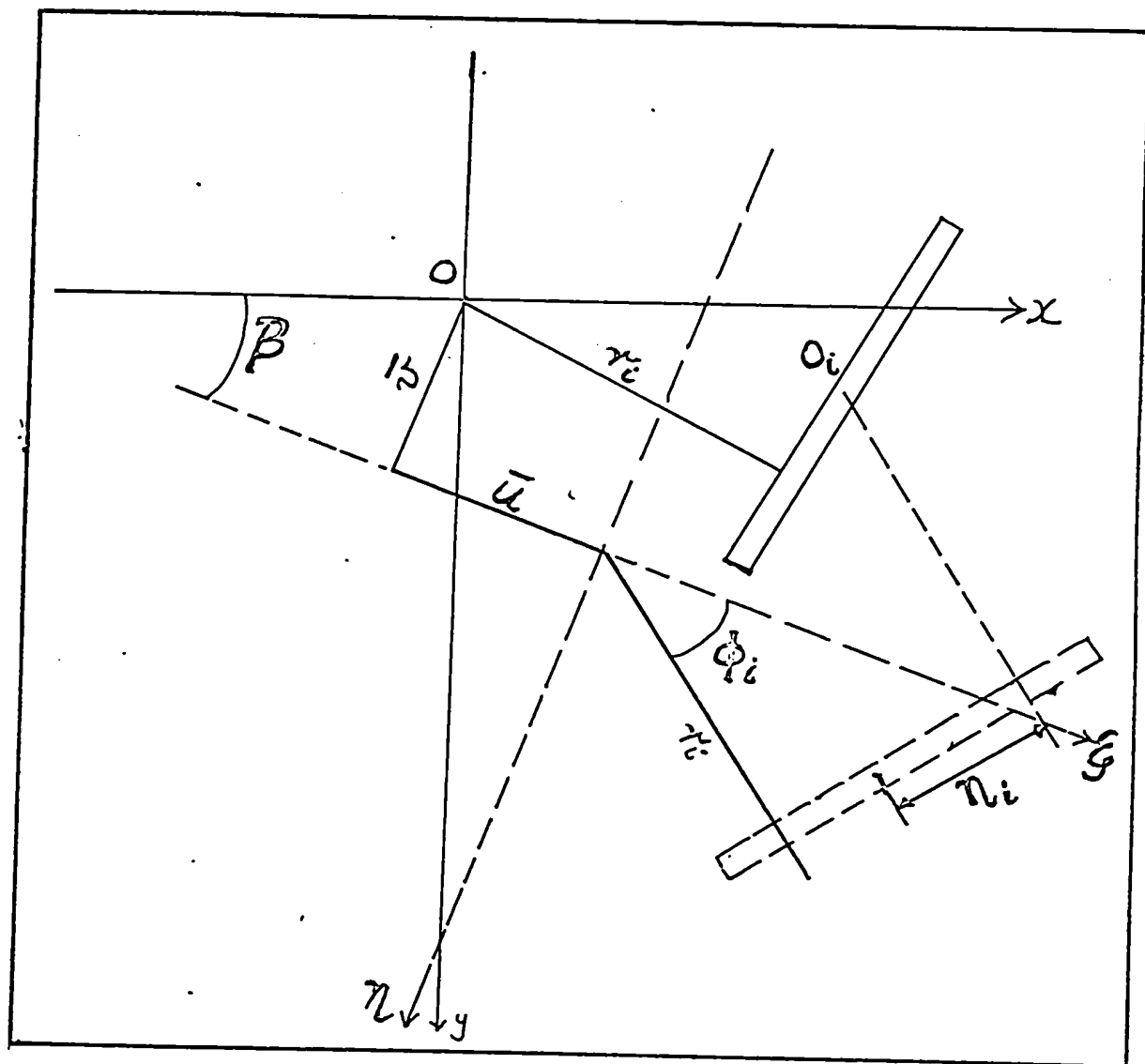


FIG.2.2 (b)

within the small thickness of the plate element itself ignored. Considering the "i"th plate element along with the "i-1"th and the "i+1"th plate (see Fig. 2.2b), since " $\beta$ " is small it may be assumed  $\cos \beta$  equals 1 and  $\sin \beta$  equals " $\beta$ ".

Then, " $\eta_i$ " the displacement parallel to the  $\eta$  axis is

$$\eta_i = -\bar{u} \sin \phi_i + \bar{v} \cos \phi_i + \beta r_i$$

The curvature of the "i"th plate in its own plane is  $\frac{d^2 \eta_i}{d\eta^2} = \eta_i''$

and the longitudinal strain at the centroid is  $\bar{\epsilon}_i$ . The strain energy of one plate element, due to direct and flexural deformation, is

$$\frac{1}{2} \int (EI \eta_i''^2 + EA_i \bar{\epsilon}_i^2) d\eta \quad (2.1)$$

For all "n" plates in the cross section the strain energy is

$$V_1 = \frac{1}{2} \int \sum_{i=1}^n (EI \eta_i''^2 + EA_i \bar{\epsilon}_i^2) d\eta \quad (2.2)$$

the integral being carried over the whole range " $L$ ".

At each corner where two plates join the longitudinal strain should be the same so that the conditions of continuity are satisfied. Considering the "i-1"th plate and the "i"th plate then

$$\bar{\epsilon}_{i-1} + a'_{i-1} \eta_{i-1}'' = \bar{\epsilon}_i - a_i \eta_i'' \quad (2.3)$$

For "n" such plate elements there are "n-1" junctions and hence "n-1" compatibility equations:

If the average longitudinal strain " $\epsilon$ " is defined by the equation

$$A\epsilon = \sum_{i=1}^n A_i \epsilon_i \quad (2.3b)$$

where A equals  $\sum_{i=1}^n A_i$

If " $\epsilon_1$ " is the difference between the strain " $\bar{\epsilon}_1$ " and the average strain " $\epsilon$ ", it can be written

$$\epsilon_i = \bar{\epsilon}_i - \epsilon \quad (2.4)$$

Equation 2.3 can be rewritten as follows:

$$\epsilon_{i-1} + a'_{i-1} \eta''_{i-1} = \epsilon_i - a_i \eta''_i \quad (2.5)$$

Also from equation 2.3b

$$\sum_{i=1}^n A_i \epsilon_i = 0 \quad (2.6)$$

There are "n-1" relations 2.5 and the "n"th equation is given by 2.6. It is possible, therefore, to express strain differences " $\epsilon_1$ " in terms of curvatures " $\eta''_i$ ". By substituting values of " $\bar{\epsilon}_1$ " in terms of " $\epsilon_1$ " in equation 2.2 the resulting equation is:

$$V_1 = \frac{E}{2} \int \left[ \sum_{i=1}^n (I_i \eta''_i{}^2 + A_i \epsilon_i^2) + A \epsilon^2 \right] d\eta \quad (2.7)$$

the mixed terms of " $\epsilon_1$ " and " $\epsilon$ " vanishing because of relation 2.6. Differentiating the equation giving values of " $\eta_i$ " in terms of  $\bar{u}, \bar{v}, \phi$  it can be written

$$\eta_i'' = -\bar{u}'' \sin \phi_i + \bar{v}'' \cos \phi_i + \gamma_i \beta'' \quad (2.8)$$

The above relation shows that the curvatures are linear functions of  $\bar{u}''$ ,  $\bar{v}''$ , and  $\beta''$ , since  $\phi$  is an invariant for any particular plate and depends solely on the geometry of the section.

Using this function " $\eta_i$ " a general expression for strain energy " $V$ " is obtained as,

$$V = \frac{E}{2} \int (\alpha_1 \bar{u}''^2 + \alpha_2 \bar{v}''^2 + \alpha_3 \beta''^2 + \alpha_4 \bar{u}'' \bar{v}'' + \alpha_5 \bar{u}'' \beta'' + \alpha_6 \bar{v}'' \beta'' + A \epsilon^2) d\eta \quad (2.9)$$

where " $\alpha_1$ ", " $\alpha_2$ ", --- " $\alpha_6$ " depend upon the geometry of the section. It can be shown that

$$\alpha_1 = I_y, \alpha_2 = I_x, \alpha_4 = I_{xy} = 0 \quad \text{since } XX, YY \text{ are principal axes.}$$

Putting now " $\alpha_5$ " =  $2 R_y$ , " $\alpha_6$ " =  $2 R_x$ ,  $\alpha_3 = R_\beta$

the expression for strain energy becomes

$$V_1 = \frac{1}{2} \int (EI_y \bar{u}''^2 + EI_x \bar{v}''^2 + 2ER_y \bar{u}'' \beta'' + 2ER_x \bar{v}'' \beta'' + ER_\beta \beta''^2 + EA \epsilon^2) d\eta \quad (2.10)$$

The constants  $R_x$ ,  $R_y$ ,  $R_\beta$ , occur in this problem and not in ordinary flexure. These can be evaluated for any section by using the relations 2.4, 2.5, 2.6. If the section is symmetrical about the "x" axis  $R_y = 0$ ; if about the "y" axis  $R_x = 0$ . When there is symmetry about both "x" and "y" axis only  $R_\beta$  has a value the others vanishing simultaneously.

2.2 While considering strain energy due to shear it is permissible to ignore the bending shear as its contribution is much smaller than the torsional shear. If  $T$  is the torque at any section, the strain energy for the whole column can be written as

$$V_s = \frac{1}{2} \int T \frac{d\beta}{dz} dz = \frac{1}{2} \int GK \beta'^2 dz \quad (2.11)$$

where  $G$  is the shear modulus of the material.

$K$  for narrow rectangular section is  $dt^3/3$ , and for a section composed of such sections only we can, with reasonable accuracy, add the values for individual plates.

Thus  $K$  equals  $\sum_{i=1}^n \frac{1}{3} d_i t_i^3$

The strain energy due to bending and torsion may now be written thus:

$$V = V_b + V_s = \frac{1}{2} \int (EI_y \bar{u}''^2 + EI_x \bar{v}''^2 + 2ER_y \bar{u}'' \beta'' + 2ER_x \bar{v}'' \beta'' + ER_\beta \beta''^2 + GK \beta'^2 + AE \epsilon^2) dz \quad (2.12)$$

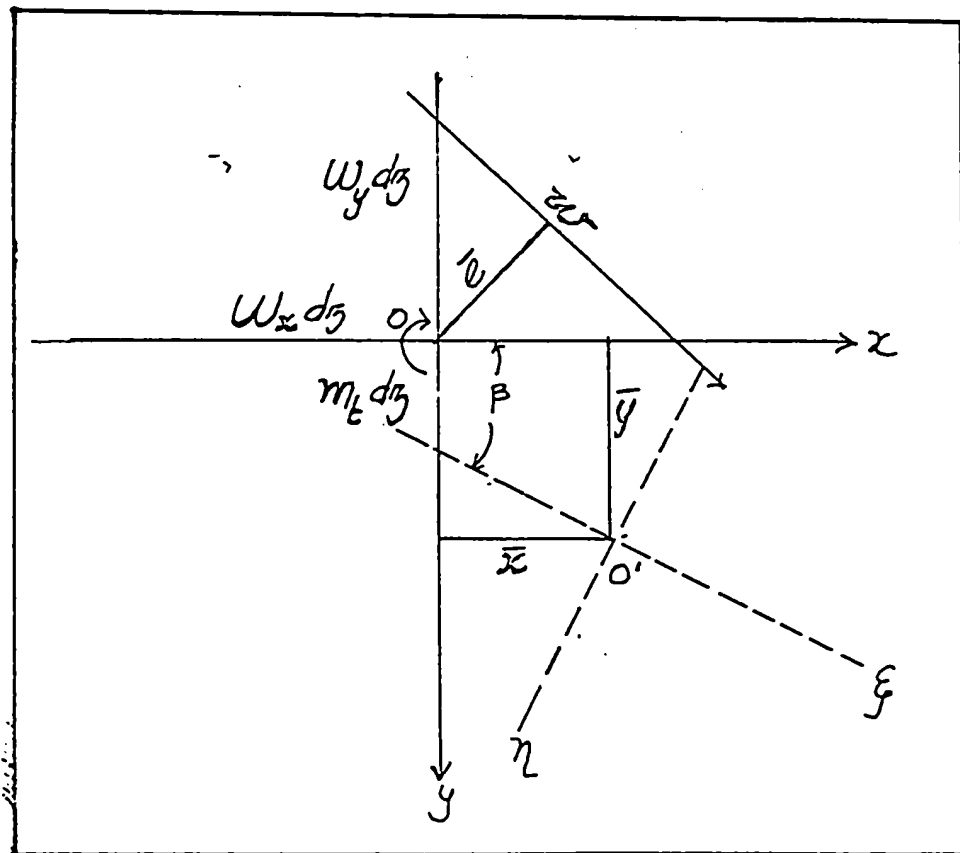


FIG 2.3



2.3 It is now possible to evaluate the potential energy of the external loads (Fig. 2.3)

$$U_W = - \int (\bar{x} \omega_x + \bar{y} \omega_y + \beta \bar{m}_t) d\eta \quad (2.13)$$

Transforming this into a function of  $\bar{u}$ , and  $\bar{v}$  by using

$$\bar{x} = \bar{u} \cos \beta - \bar{v} \sin \beta$$

$$\bar{y} = \bar{u} \sin \beta + \bar{v} \cos \beta$$

where it has been tacitly assumed " $\beta$ " to be small so that  $\sin \beta$  equals " $\beta$ " and  $\cos \beta$  equals 1 nearly. It may now be assumed that  $\bar{x} = \bar{u}$ , and  $\bar{y} = \bar{v}$  without appreciable error. The potential energy of external loads may be expressed thus:

$$U_W = - \int (\bar{u} \omega_x + \bar{v} \omega_y + \beta \bar{m}_t) d\eta \quad (2.14)$$

The final expression for potential energy is

$$\begin{aligned} \Pi^S = U_W + V_S + V_L = \\ \frac{1}{2} \int (EI_y \bar{u}''^2 + EI_x \bar{v}''^2 + 2ER_y \bar{u}'' \beta'' + 2ER_x \bar{v}'' \beta'' + ER_\phi \beta''^2 \\ + GK\beta'^2 + AE\epsilon^2 - 2\bar{u} \omega_x - 2\bar{v} \omega_y - 2\beta \bar{m}_t) d\eta \end{aligned} \quad (2.15)$$

If this integral should have an extremum value the variation " $\delta \Pi^S$ " should tend to zero which yields the following Eulerian equations.

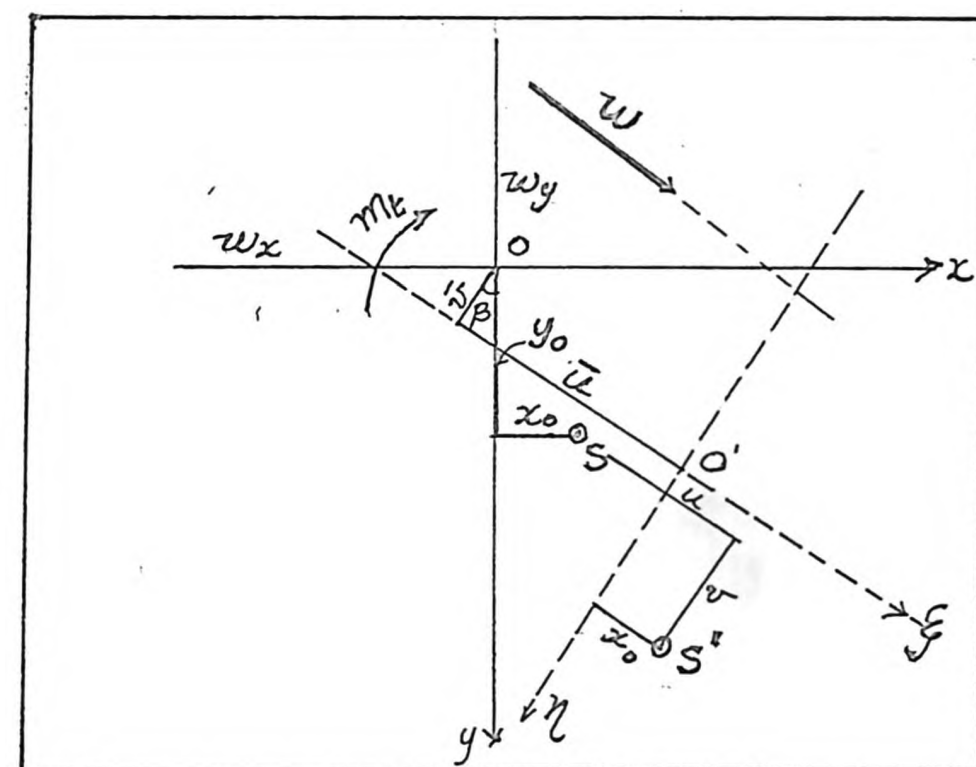


FIG.2.4

$$EI_y \bar{u}^{iv} + ER_y \beta^{iv} = w_x \quad (2.16a)$$

$$EI_x \bar{v}^{iv} + ER_x \beta^{iv} = w_y \quad (2.16b)$$

$$ER_y \bar{u}^{iv} + ER_x \bar{v}^{iv} + ER_\beta \beta^{iv} - GK \beta'' = \bar{m}_t \quad (2.16c)$$

$$EA \epsilon = 0 \quad (2.16d)$$

It is interesting to compare these equations with those obtained by conventional theory of bending

$$EI_y \bar{u}^{ii} = -M_y \quad EI_x \bar{v}^{ii} = -M_{xx} \quad \text{which on differentiating twice}$$

yield

$$EI_y \bar{u}^{iv} = w_x \quad EI_x \bar{v}^{iv} = w_y$$

The additional terms containing  $R_x$  and  $R_y$  &  $R_\beta$  show the influence of torsion and flexure.

2.4 An arbitrary origin  $S, (x_0, y_0)$  is chosen of which the displacements will be designated "u" and "v" and " $\beta$ ". Now from Fig. 2.4 it may be written  $\bar{u} = u + y_0 \beta$  and  $\bar{v} = v - x_0 \beta$  (2.17)

Since  $x_0$  and  $y_0$  remain the same before and after deformation, and are arbitrary it is possible to assume  $x_0 = R_y / I_x$  and  $y_0 = -R_x / I_y$

Now the relations (2.17) become

$$\bar{u} = u - \frac{R_y}{I_y} \beta \quad \bar{v} = v - \frac{R_x}{I_x} \beta \quad (2.18)$$

If these values are introduced into 2.16 the following relations are obtained

$$EI_y u^{iv} = \omega_x \quad (2.19a)$$

$$EI_x v^{iv} = \omega_y \quad (2.19b)$$

$$ER_y u^{iv} + ER_x v^{iv} + E\left(R_\beta - \frac{R_y^2}{I_y} - \frac{R_x^2}{I_x}\right) \beta^{iv} - GK\beta'' = \bar{m}_t \quad (2.19c)$$

We can refer  $\bar{m}_t$  with respect to the new origins, (shear centre) in which case

$$m_{ts} = \bar{m}_t + y_o \omega_x - x_o \omega_y \quad (2.20)$$

Using 2.19a and (b) as substitutions in (c) the relation becomes

$$E\left(R_\beta - \frac{R_y^2}{I_y} - \frac{R_x^2}{I_x}\right) \beta^{iv} - GK\beta'' = \bar{m}_t + y_o \omega_x - x_o \omega_y \quad (2.21)$$

Comparing 2.20 and 2.21 the right hand expressions of the equalities are identical. If a new constant " $\Gamma$ " is defined as follows

$$\Gamma = R_\beta - \frac{R_y^2}{I_y} - \frac{R_x^2}{I_x} \quad (2.22)$$

the equations 19 reduce to

$$EI_y u^{iv} = w_x \quad (2.23a)$$

$$EI_x v^{iv} = w_y \quad (2.23b)$$

$$ET\beta^{iv} - GK\beta'' = m_{ts} \quad (2.23c)$$

Equations 2.23 are similar to the conventional equations in bending except that all displacements "u" and "v" are referred to the centre of shear rather than the centroid. From 2.23, if  $\beta$  equals zero, " $m_{ts}$ " equals zero which means that the resultant of the external loads should pass through S-(definition of the centre of shear). Also if there is no bending displacement  $w_x$  and  $w_y$  are both zero, then the centre of shear becomes the centre of rotation in pure torsion. The above state of affairs may not be true in the neighbourhood of the extremities of the bar.

The value of the warping constant " $T$ " is calculated by Timoshenko and Goodier in a different manner, and is more accurate than the form used here in the case of angles and tees, where the distance of the section from the shear centre is also small. In the case of channels, however, Bleich's values are within 0.5 percent of the Goodier values, and yet can be obtained in a much simpler manner.

**2.4 COLUMNS WITH AXIAL LOADING.** An axially loaded column remains straight until the buckling load is reached, and if the expression (Equation 2.12) for strain energy is employed, "u", "v" remain zero prior to buckling.

When buckling does take place it is convenient to use values of tangent moduli  $E_t$  and  $G_t$ . But the term  $E\epsilon^2$  in the integral cannot be avoided except by considering datum for energy to be the initially straight but compressed state. Also it is necessary to reckon the potential energy of external loads from the same datum. Hence, it can be written that

$$V = \frac{1}{2} \int (E_t I_y u''^2 + E_t I_x v''^2 + E_t T \beta''^2 + G_t K \beta'^2) d\eta \quad (2.24)$$

If  $E_t/E = \tau$ , then  $E_t = E\tau$  where " $\tau$ " is a function of the stress. It may also be assumed  $G_t = G\tau$ , though it would be more precise to assume  $G_t = G\sqrt{\tau}$  as in the theory of plates. But " $\tau$ " is actually smaller in value than " $\sqrt{\tau}$ ", as " $\tau$ " is less than 1. The analysis, would therefore be conservative and acceptable.

If the above simplification is used the expression for potential energy becomes

$$V = \frac{1}{2} \int (E\tau I_y u''^2 + E\tau I_x v''^2 + E\tau T \beta''^2 + G\tau K \beta'^2) d\eta \quad (2.25)$$

The tangent modulus theory is assumed to be realistic as has been established by Shanley and use is made of  $E_t$  rather than Von Karman's reduced or effective modulus. It may be noted that  $E_t = d\sigma/d\epsilon$ .

If the datum for potential energy of external loads is assumed as the initially straight but compressed configuration, there are two effects to be considered; the change of longitudinal stress in fibres

causing a change in strain, and a displacement entirely due to curvature.

If the new stress in a fibre is  $\sigma_y + \delta \sigma_y$  the change in strain is

$\frac{\delta \sigma_y}{E_t}$ . Work done will be

$$U_W = -(\sigma_y + \delta \sigma_y) \frac{dA}{E_t} \int_0^L \delta \sigma_y d\eta$$

Ignoring higher order terms of small quantities and setting constant shortening of fibre over length "L" as  $\delta_c$  the relation becomes

$$U_W = -\sigma_y dA \left( \delta_c + \frac{1}{E_t} \int_0^L \delta \sigma_y d\eta \right) \quad (2.26)$$

If the whole cross section is considered, " $U_W$ " becomes

$$U_W = -\sigma_y \int_A \delta_c dA - \frac{\sigma_y}{E_t} \int_A \int_0^L \delta \sigma_y d\eta dA. \quad (2.27a)$$

Since there is no change in axial loading during the buckling process

$$\int_A \delta \sigma_y dA = 0$$

Hence,

$$U_W = -\sigma_y \int_A \delta_c dA \quad (2.27b)$$

" $\delta_c$ " can be determined in a manner similar to a line in one plane:

$$\begin{aligned} \delta_c &= \int_0^L \left[ \sqrt{1 + \left( \frac{d\Delta x}{d\eta} \right)^2 + \left( \frac{d\Delta y}{d\eta} \right)^2} - 1 \right] d\eta = \underline{\underline{\quad}} \\ &= \int_0^L \left\{ \left[ \left( 1 + \frac{1}{2} \left\{ \left( \frac{d\Delta x}{d\eta} \right)^2 + \left( \frac{d\Delta y}{d\eta} \right)^2 \right\} \right) \right] - 1 \right\} d\eta = \underline{\underline{\quad}} \end{aligned}$$

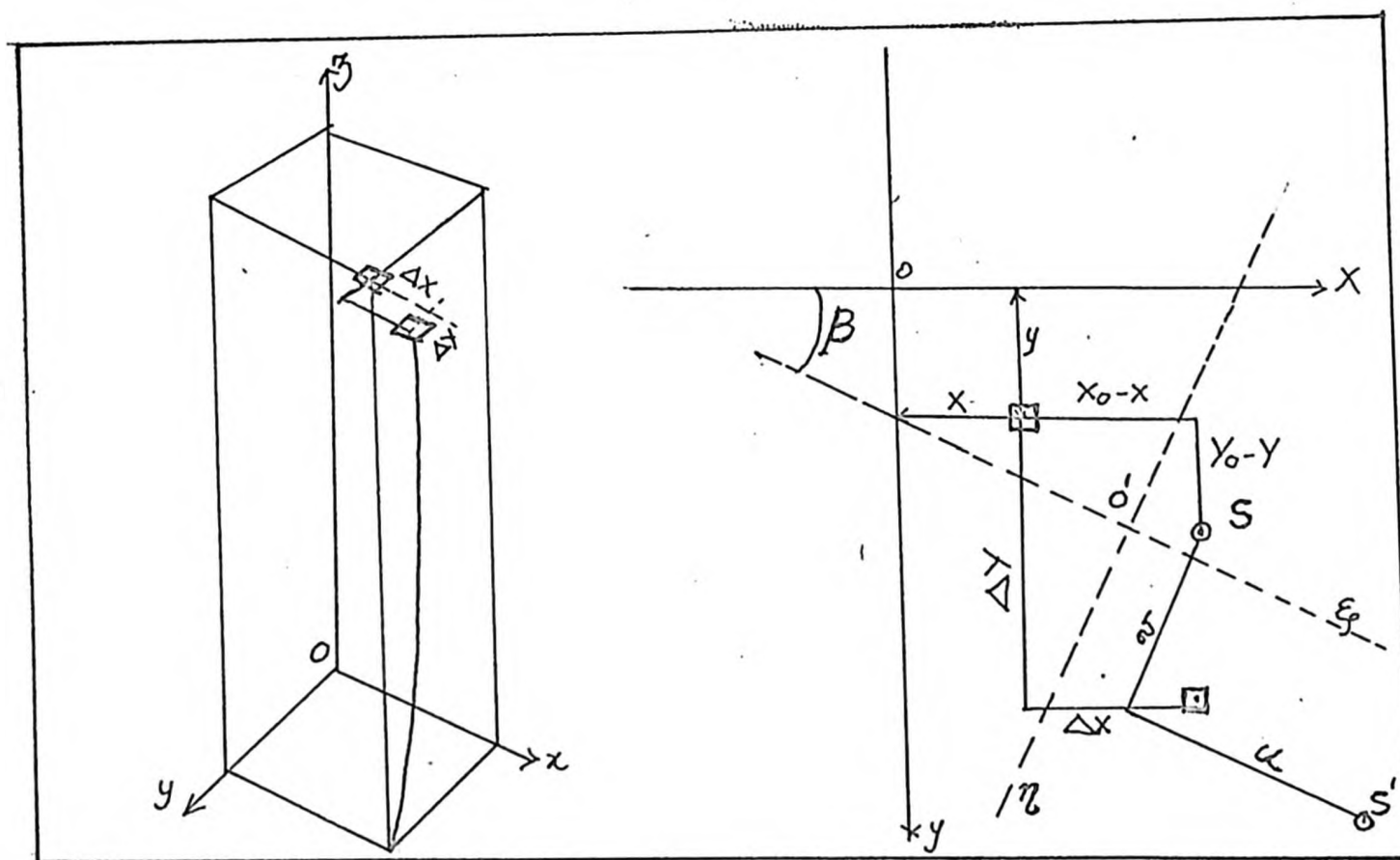


FIG.2.5



$$\frac{1}{2} \int_0^L \left[ \left( \frac{d\Delta_x}{d\eta} \right)^2 + \left( \frac{d\Delta_y}{d\eta} \right)^2 \right] d\eta \quad (2.28)$$

It is possible to express " $\Delta_x$ " and " $\Delta_y$ " in terms of  $u$ ,  $v$ , and " $\beta$ ".

$$\Delta_x = x_0 - x + (u - x_0 + x) \cos \beta - (v - y_0 + y) \sin \beta = u + (y_0 - y) \beta \quad (2.29a)$$

$$\Delta_y = y_0 - y + (u - x_0 + x) \sin \beta + (v - y_0 + y) \cos \beta = v - (x_0 - x) \beta \quad (2.29b)$$

The equations 2.29 with simplification are admissible as only small values of " $u$ ", " $v$ " and " $\beta$ " are considered. If these values are introduced into 2.28, it leads to double integrals with respect to  $dz$  and  $dA$ , and if the following geometrical relations are observed

$$\int_A dA = A \quad \int_A x dA = 0 \quad \int_A y dA = 0$$

$$\int_A \left[ (x - x_0)^2 + (y - y_0)^2 \right] dA = I_p = \text{Polar moment of inertia about shear centre.}$$

the potential energy  $U_w$  reduces to

$$U_w = \frac{1}{2} \int_0^L \left[ -\sigma_3 A (u'^2 + v'^2) - 2\sigma_3 A y_0 u' \beta' + 2\sigma_3 A x_0 v' \beta' - \sigma_3 I_p \beta'^2 \right] d\eta \quad (2.30)$$

The potential energy then becomes

$$\begin{aligned} \Pi^S = \frac{1}{2} \int_0^L [ & E\gamma I_y u''^2 + E\gamma I_x v''^2 + E\gamma T \beta''^2 + G\gamma K \beta'^2 - \sigma_3 A (u'^2 + v'^2) \\ & - 2\sigma_3 A y_0 u' \beta' + 2\sigma_3 A x_0 v' \beta' - \sigma_3 I_p \beta'^2 ] d\eta \end{aligned} \quad (2.31)$$

From the theorem of stationary potential energy the Eulerian equations (2.32) are obtained,

$$E\gamma I_y u^{IV} + \sigma_3 A u'' + \sigma_3 A y_0 \beta'' = 0 \quad (2.32a)$$

$$E\gamma I_x v^{IV} + \sigma_3 A v'' - \sigma_3 A x_0 \beta'' = 0 \quad (2.32b)$$

$$\sigma_3 A y_0 u'' - \sigma_3 A x_0 v'' + E\gamma T \beta^{IV} + (\sigma_3 I_p - G\gamma K) \beta'' = 0 \quad (2.32c)$$

## 2.5 COLUMNS WITH ONE AXIS OF SYMMETRY.

For sections like channels, if there is symmetry about the  $x$  axis  $y_0$  is zero. Then,

$$E\gamma I_y u^{IV} + \sigma_3 A u'' = 0 \quad (2.33a)$$

$$E\gamma I_x v'''' + \sigma_y A v'' - \sigma_y A x_0 \beta'' = 0 \quad (2.33b)$$

$$- \sigma_y A x_0 v'' + E\gamma T \beta'''' + (\sigma_y I_p - G\gamma K) \beta'' = 0 \quad (2.33c)$$

Equation 2.33a yields

$$\sigma_{y(x)} = \frac{\pi^2 E \gamma}{\left(\frac{l}{r_y}\right)^2} \quad (2.34)$$

Equations 2.33b and 2.33c do not contain "u" but only v and "β". This means in the direction "y" buckling and twisting are intertwined, and the stress "σ<sub>y</sub>" obtained from the conventional theory, viz

$$\sigma_{y(y)} = \frac{\pi^2 E \gamma}{\left(\frac{l}{r_x}\right)^2}$$

is not correct.

If simply supported ends are only considered for  $x = 0$  and  $x = l$ ,  $u = 0$ ,  $\beta = 0$ ,  $u'' = 0$ ,  $\beta'' = 0$ , are the boundary conditions which help reduce the constants of integration from 8 to 2.

"v" and "β" may be expressed as

$$v = C_1 \sin \frac{n\pi y}{L}, \quad \beta = C_2 \sin \frac{n\pi y}{L}$$

If this value is used in the original differential equations nonvanishing values of "v" and "β" are possible only when the determinant of their coefficients vanishes. The critical stress can be expressed as

$$\sigma_{y(y)} = \frac{\pi^2 E \gamma}{\left(\frac{l}{R_E}\right)^2}$$

where  $R_E$  is the equivalent radius of gyration obtained from the quadratic relation.

$$\begin{vmatrix} 1 - \frac{\tau_y^2}{\tau_E^2} & x_o \\ x_o & \frac{I_p}{A} \left( 1 - \frac{\tau_\beta^2}{\tau_E^2} \right) \end{vmatrix} = \left( 1 - \frac{\tau_y^2}{\tau_E^2} \right) \left( 1 - \frac{\tau_\beta^2}{\tau_E^2} \right) - \frac{A x_o^2}{I_p} \quad (2.35)$$

where  $\tau_\beta$  is

$$\sqrt{\frac{T}{I_p} + \frac{\ell^2}{\pi^2} \frac{GK}{EI_p}} \quad (2.36)$$

and  $\tau_y$  is the radius of gyration about y axis.

If the Poisson's ratio for steel is assumed 0.30 and the ratio

$$\frac{G}{E} = \frac{1}{2(1+\nu)} = \frac{1}{2.6} \quad \text{the expression for } \tau_\beta \text{ becomes}$$

$$\tau_\beta = \sqrt{\frac{T}{I_p} + 0.0390 \frac{\ell^2 K}{I_p}} \quad (2.37)$$

The equivalent radius of gyration assumes the form,

$$\tau_E = \pm \sqrt{\frac{(\tau_y^2 + \tau_\beta^2) \pm \sqrt{(\tau_y^2 + \tau_\beta^2)^2 - 4\tau_y^2 \tau_\beta^2 \left( 1 - \frac{A x_o^2}{I_p} \right)}}{2 \left( 1 - \frac{A x_o^2}{I_p} \right)}} \quad (2.38)$$

$(1 - \frac{Ax_o^2}{I_p})$  may be written  $(1 - \frac{x_o^2}{r_o^2})$  where  $r_o^2 = \frac{I_p}{A}$  and

$r_o$  is the polar radius of gyration about the centre of shear. Winter, Chajes and associates call  $(1 - \frac{x_o^2}{r_o^2})$  the interaction coefficient  $K_\phi$ .

It can be appreciated that to keep  $r_o$  large the value of this coefficient of interaction should be large although this is not a direct relationship or proportionality. It is possible to calculate deformation corresponding to the roots of the quadratic equation in  $r_E$  (2.38) and the centre of rotation for the section is found to be

$$x_c = 0, \quad y_c = \frac{y_o}{1 - \frac{r_E^2}{r_y^2}}$$

If torsional stiffness of a section is small  $r_E$  is close to  $r_p$  and the centre of rotation can be assumed to merge with the centre of shear.

The formula

$$\sigma_{xc} = \frac{\pi^2 E \gamma}{(\frac{l}{r_E})^2}$$

can be used for end conditions other than pinned by substituting the effective lengths as in Euler formulae for simple buckling in flexure.

2.6 Recently, Winter<sup>9</sup> and his team have enlarged on the Timoshenko Goodier<sup>11</sup> approach. For singly symmetrical sections the critical load in torsional flexure is given by the two roots of the quadratic

$$\tau_o^2 (P - P_x)(P - P_\phi) - P^2 x_o^2 = 0$$

which can also be written as

$$\frac{P}{P_\phi} + \frac{P}{P_x} - K_\phi \left( \frac{P^2}{P_\phi P_x} \right) = 0$$

where  $P_x = \frac{\pi^2 EI_x}{L^2}$

Pure flexural buckling load

$$P_\phi = \frac{1}{\gamma_o^2} \left( GK + \frac{\pi^2 E \Gamma}{L^2} \right)$$

Pure torsional buckling load

$$E \Gamma =$$

Warping stiffness

$$K_\phi = \left\{ 1 - \left( \frac{x_o}{\gamma_o} \right)^2 \right\}$$

Shape factor where  $x_o$  is the distance between the centroid and shear centre and  $\gamma_o$  is the polar radius of gyration about the shear centre.

$P =$  critical load

For  $P$  to have a large value the factor  $K_\phi$ , the coefficient of interaction has to be large. The largest value of  $K_\phi$  will be unity when " $x_o$ " equals zero, i.e. when the shear centre coincides with the centroid as in doubly symmetrical sections. However, critical load  $P$  depends also upon the critical load in pure torsional buckling ( $P_\phi$ ) and the critical load in pure flexure about axis YY ( $P_x$ ). The values of  $P_\phi$  and  $P_x$  are also governed by the cross sectional geometry. Thus an increase in the coeff-

icient of interaction " $K_\phi$ " alone will not mean a higher critical stress in torsional flexural buckling. The coefficient of interaction furnishes only an idea of closeness or otherwise of the values of the critical load to the torsional critical load  $P_\phi$ . Coefficient of interaction unity implies that the crippling load in torsional flexural buckling is the same as the crippling load needed to cause buckling in torsion ( $P_\phi$ ). In this case  $P$  equals  $P_\phi$ . Smaller values of " $K_\phi$ " imply that buckling will be due to combined bending and twisting.

## 2.7 SCOPE OF THE PRESENT INVESTIGATION.

The material used in the present investigation was G.I. sheeting of U.S. gauge 24, of thickness 0.0239". The length available for column testing on the testing machine was only 36 inches between the platens. A channel section 8" x 4" was chosen so that failure by flexure and torsion may result. It has been established elsewhere<sup>2</sup> that combined bending and twisting is likely to occur in short lengths of columns of channel cross sections. (Besides this, a section of these cross sectional dimensions, when fully analysed for buckling as a column and as a beam, could be used as a structural element for single storey ridged portal frames). The present phase of the investigation covers buckling under axial compression only. Another noteworthy feature of the sections studied in this series is the very high thinness ratio, i.e., the ratio of the widest plate in the cross section to its thickness. The actual value here is 335, calculated on the web width of 8 inches.

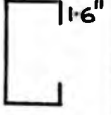
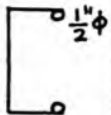

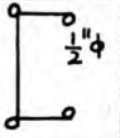
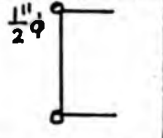
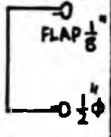
2.8 The significant geometrical constants for these channels with circular lips at the ends of the flanges, and channels with 4 circular lips in their cross section, have been computed by using nondimensional parameters. The parameter  $Q$  is the ratio of the web width to the flange width, and the parameter  $R$  is the ratio of the radius of the bulb to the flange width. Thus  $Q$  and  $R$  inter-relate the flange, the circular lips and the web in respect of their dimensions. Except for the radius of gyration for pure torsional buckling ( $R_\beta$ ) and that for torsional flexural buckling ( $R_E$ ), all other quantities are linear functions of the thickness of the sheeting.  $R_\beta$ ,  $R_E$  vary as " $t^{1.5}$ ", as obtained in equation 2.36. The very small thickness of sheeting, viz. 0.0239", does not influence the values of  $R_\beta$  and  $R_E$  significantly and this influence has been ignored without much loss of accuracy. In attempting to rationalize a design procedure, the equivalent radius of gyration concept used by Chwalla and other European investigators is employed. This would lead to an expression for critical stress in torsional flexural buckling " $\sigma_c$ "

$$\sigma_c = \frac{\pi^2 E_t}{(l/R_E)^2}$$

where " $l/R_E$ " is the equivalent slenderness ratio and  $E_t$  is the Tangent Modulus of the material. In general, the value of  $R_E$  is smaller than  $R_y$ , and  $R_\beta$ , in magnitude for short lengths of open cross sections. When thickness is small as in the present case,  $R_E$  remains less than  $R_\beta$  even for longer lengths. This is where thin walled sections differ from hot rolled sections on account of their thinness. Table 2.8 shows the values of  $R_x$ ,  $R_y$ ,  $R_\beta$ ,  $R_E$  for different cross sections and also the ratio  $R_E^2/A_w$ ,



TABLE 2.8

Section 8"x4"	$R_x$	$R_y$	$R_\beta$	$R_E$	$R_E^2 / A_w$	Remarks & Serial No.
	3.26	1.59	1.068	0.973	0.0485	1
	3.448	1.664	1.159	1.05	0.0575	2
	3.382	1.560	1.145	1.017	0.0540	3
	3.284	1.610	1.310	1.160	0.0605	4
	3.430	1.538	1.119	0.914	0.0437	5
	3.41	1.674	1.330	1.155	0.0690	6

A being the area expressed in terms of the developed width of sections concerned. The ratio  $R_E^2/A_w$  takes into account the different cross sectional areas of the sections and reduces it to a single parameter for comparison. The length being constant, critical stress is directly proportional to  $R_E^2$ . The following is the order in which the sections can be placed starting from the section having the largest value of this parameter, and proceeding in the descending order.

1. Channel No. 6 (Table 2.8)
2. Channel No. 4 ( do )
3. Channel No. 2 ( do )
4. Channel No. 3 ( do )
5. Channel No. 1 ( do )
6. Channel No. 5 ( do )

## 2.9 OPTIMUM SHAPE

Using the I.B.M. 7040 computer the following geometrical properties were calculated for varying values of non-dimensional parameters Q and R:

1. Equivalent radius of gyration  $R_E$
2. Radius of gyration for pure torsional buckling  $R_\beta$
3. Warping Stiffness "  $\Gamma$  "

Of the above quantities,  $R_E$  and  $R_\beta$  were computed as ratios, which, when multiplied by the flange width in any system of units, would yield the corresponding radius of gyration. Warping stiffness "  $\Gamma$  " is of the sixth power of linear dimensions, and the non-dimensional coefficient will

have to be multiplied by the sixth power of the flange width. All values refer to unit thickness of sheeting. For any given sheeting the value of the warping stiffness obtained from the curves will have to be further multiplied by the magnitude of the actual sheet thickness. It should be borne in mind that  $Q$  and  $R$ , relate the flange width, web width and the radius of the bulb.

Figs. 2.6(A) and 2.6(B) show the variation of the non-dimensional parameter governing equivalent radius of gyration with varying values of  $Q$  and  $R$ . Fig. 2.6(A) refers to a channel with flange bulbs only, and this fact is marked on the figure for easy identification. Fig. 2.6(B) refers to a channel with 4 bulbs and contains a sketch of the section for identification. Referring to Fig. 2.6(A), for any value of  $Q$  less than 0.625, increasing values of parameter  $R$  (increase in bulb radius) reduces  $R_E$  except that when  $R$  changes from 0.09 to 0.12,  $R_E$  tends to increase in this range. In the range of  $Q$  from 0.625 to 1.50, for all values of  $R$ , the parameter governing  $R_E$  increases with  $Q$ . For any given  $Q$  in this range increase in bulb radius results in decrease in  $R_E$ . For a value of  $Q$  greater than 1.5 and less than 2, the curve corresponding to  $R = 0.03$  has smaller ordinates than the curve for  $R = 0.06$ . On the whole, in the range of  $Q$  from 0.625 to 1.50 change in radius results in a larger change in  $R_E$ , than in the range of  $Q$  from 1.50 to 2.0. In the range of  $Q$  from 1.50 to 2.0 the curves for  $R = 0.03, 0.06, 0.09$  are very close to one another. Even the curve for  $R = 0.12$  does not show a much smaller ordinate for  $R_E$  than the rest at  $Q = 2.0$ .

Referring to Fig. 2.6(B) for the channel with 4 bulbs, the curves for  $R_E$  for various radii  $R = 0.03, 0.06, 0.09, 0.12$  are very close to one

Equivalent  $R_e$  per unit flange width

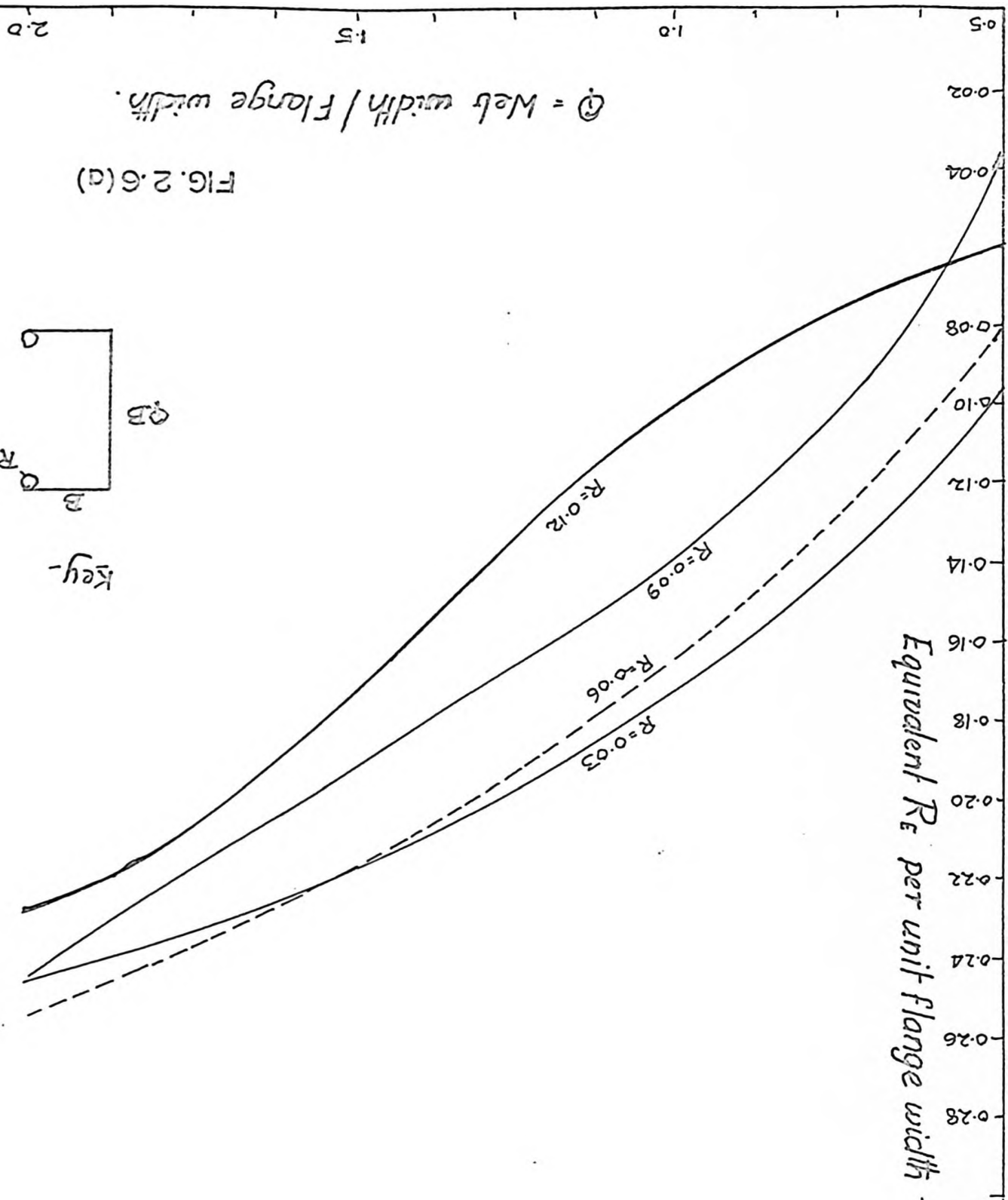
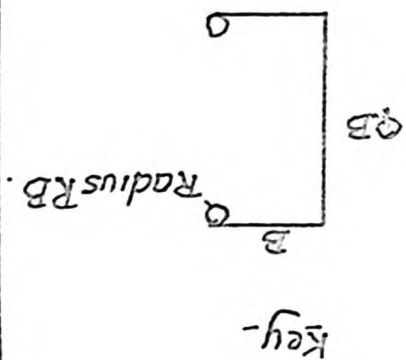
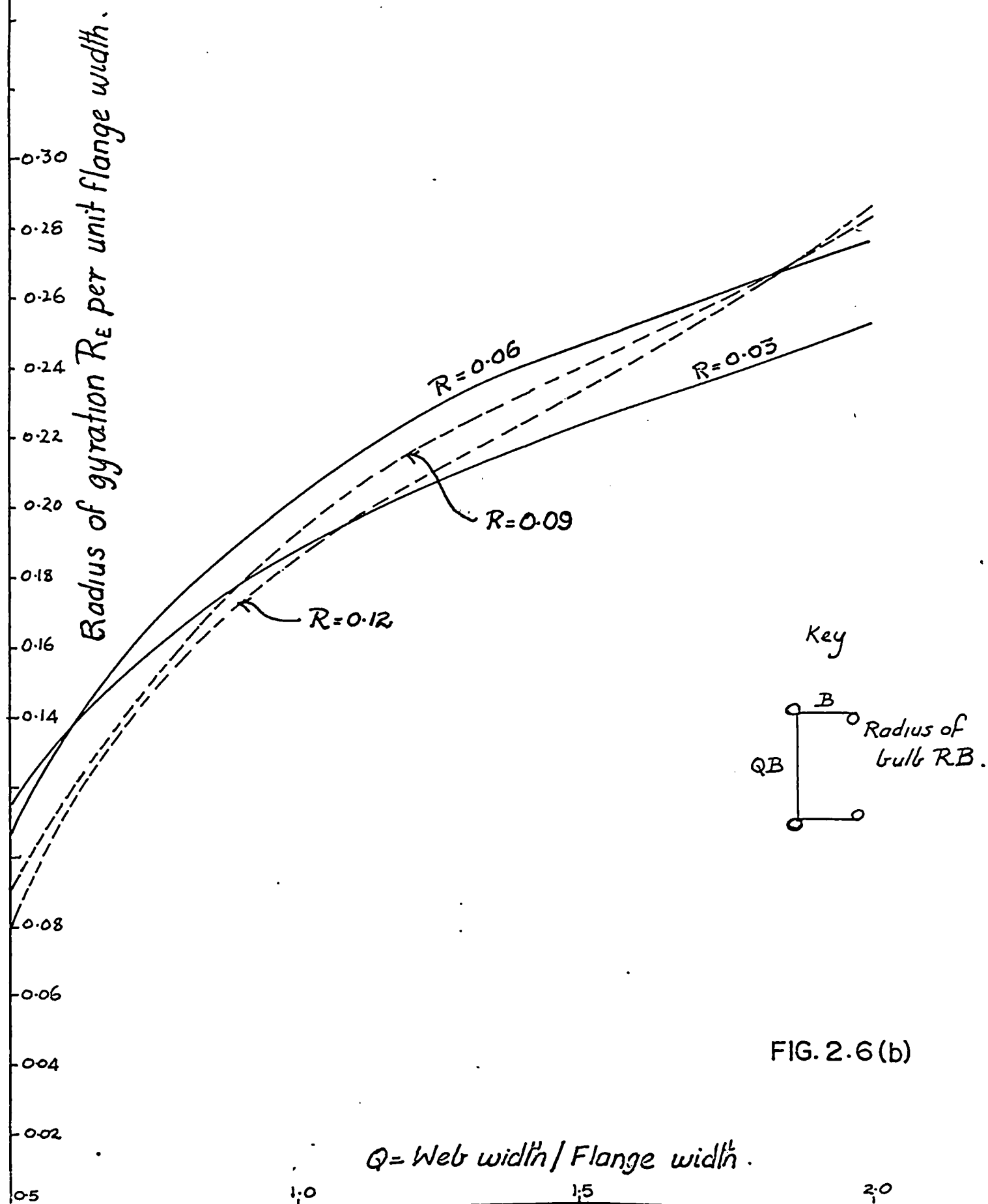


FIG. 2.6 (a)

$Q = \text{Web width} / \text{Flange width}$





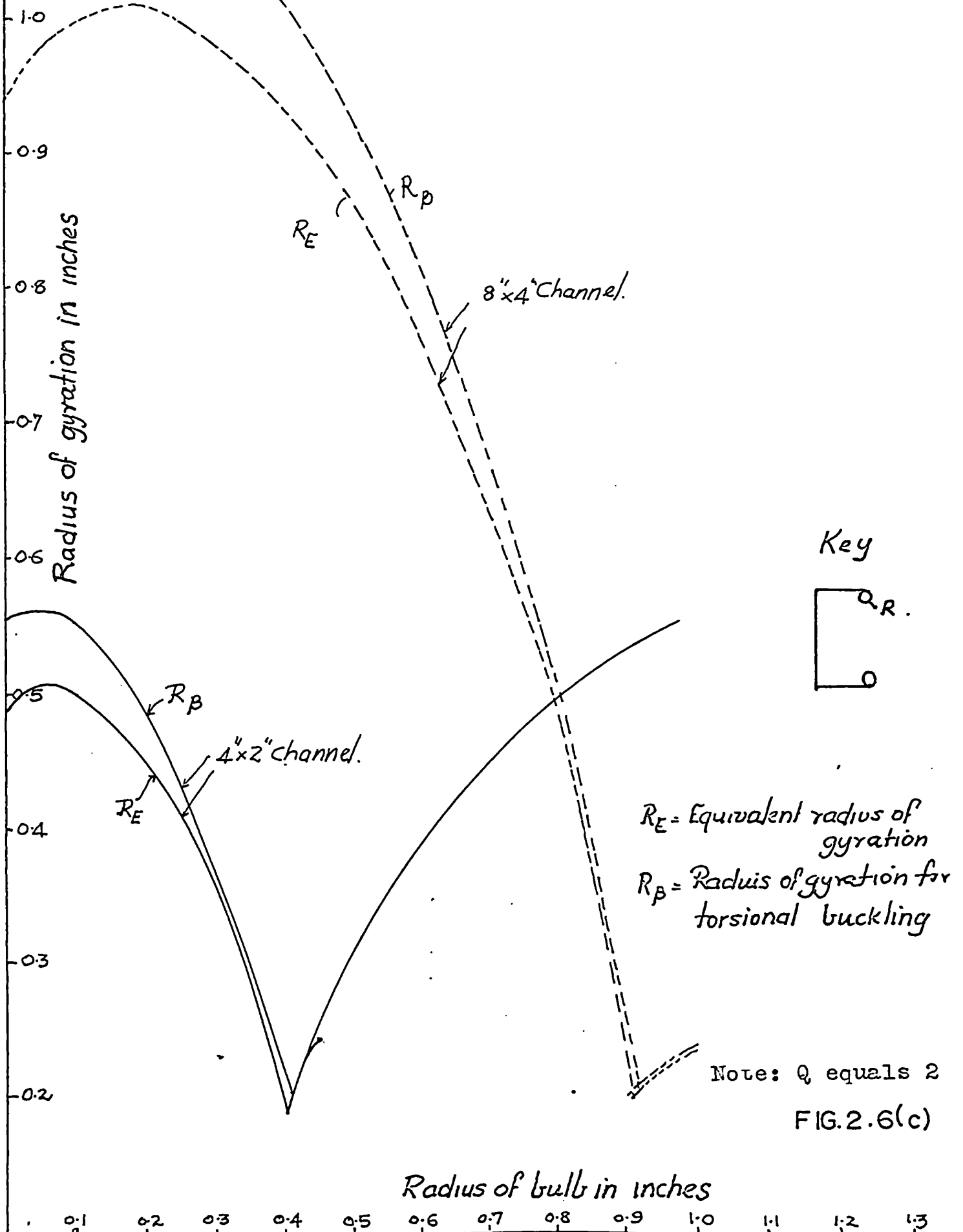
another. This means that the influence of change in bulb radius is much less evident in this case than in the channel considered in Fig. 2.6(A). In Fig. 2.6(B), in the range of  $Q = 0.5$  to  $0.75$ , the largest parameter for equivalent radius of gyration is given by the smallest radius of bulb  $R = 0.03$ . From  $Q = 0.75$  to  $Q = 1.44$  the largest value of  $R_E$  occurs with a radius of bulb  $0.06$  times the flange width. From  $Q = 1.44$  to  $Q = 1.875$ , a radius corresponding to  $R = 0.09$  provides the greatest  $R_E$ . From  $Q = 1.875$  to  $Q = 2.0$ , radius corresponding to  $R = 0.12$  furnishes the greatest value of  $R_E$ .

Comparing the graphs in Fig. 2.6(A) and 2.6(B), the curves in (B) show greater ordinates than in (A) for the values of  $Q$  between  $0.625$  and  $2$ . Comparison is made in the following of some specific points to emphasize this trend.

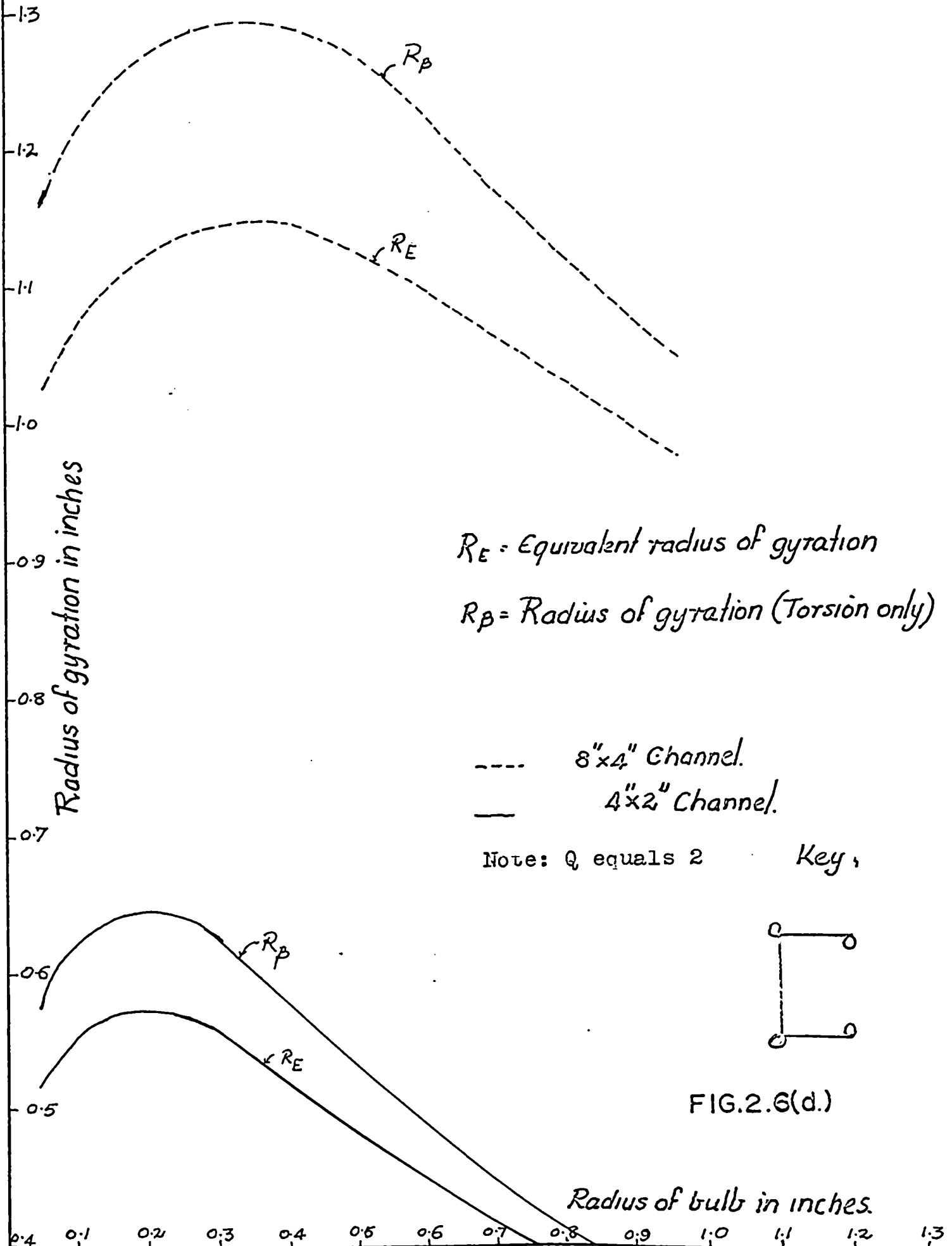
At a radius of  $R = 0.03$ , for parameter  $Q = 1.0$ , the channel with 2 bulbs (Fig. 2.6(A)) has an equivalent  $R_E = 0.1735$ . The channel with 4 bulbs (Fig. 2.6(B)) has a value  $0.1895$ . At  $R = 0.06$  and  $Q = 1.0$  the values for the channels with 2 bulbs and the channel with 4 bulbs are  $0.164$  and  $0.196$  respectively. At the same ratio  $Q = 1.0$ , at  $R = 0.09$ , the two values are  $0.118$  and  $0.1375$  respectively for the channels in Figs 2.6(A) and (B). At  $R = 0.12$ , with  $Q$  at a value 1 again, the values for  $R_E$  are  $0.10$  and  $0.1745$  for the two channels.

The change in this parameter defining the equivalent radius of gyration at a constant value of  $Q = 1.5$  can now be studied. The values referred to here are again in the same order, viz. value for 2 bulbed channel (Fig. 2.6(A)) followed by the value for 4 bulbed channel (Fig. 2.6(B)). At  $R = 0.03$ , the values are  $0.218$  and  $0.2315$ . At  $R = 0.06$ , the values are

# Variation of radii of gyration with shape.



Variation of radii of gyration with shape.





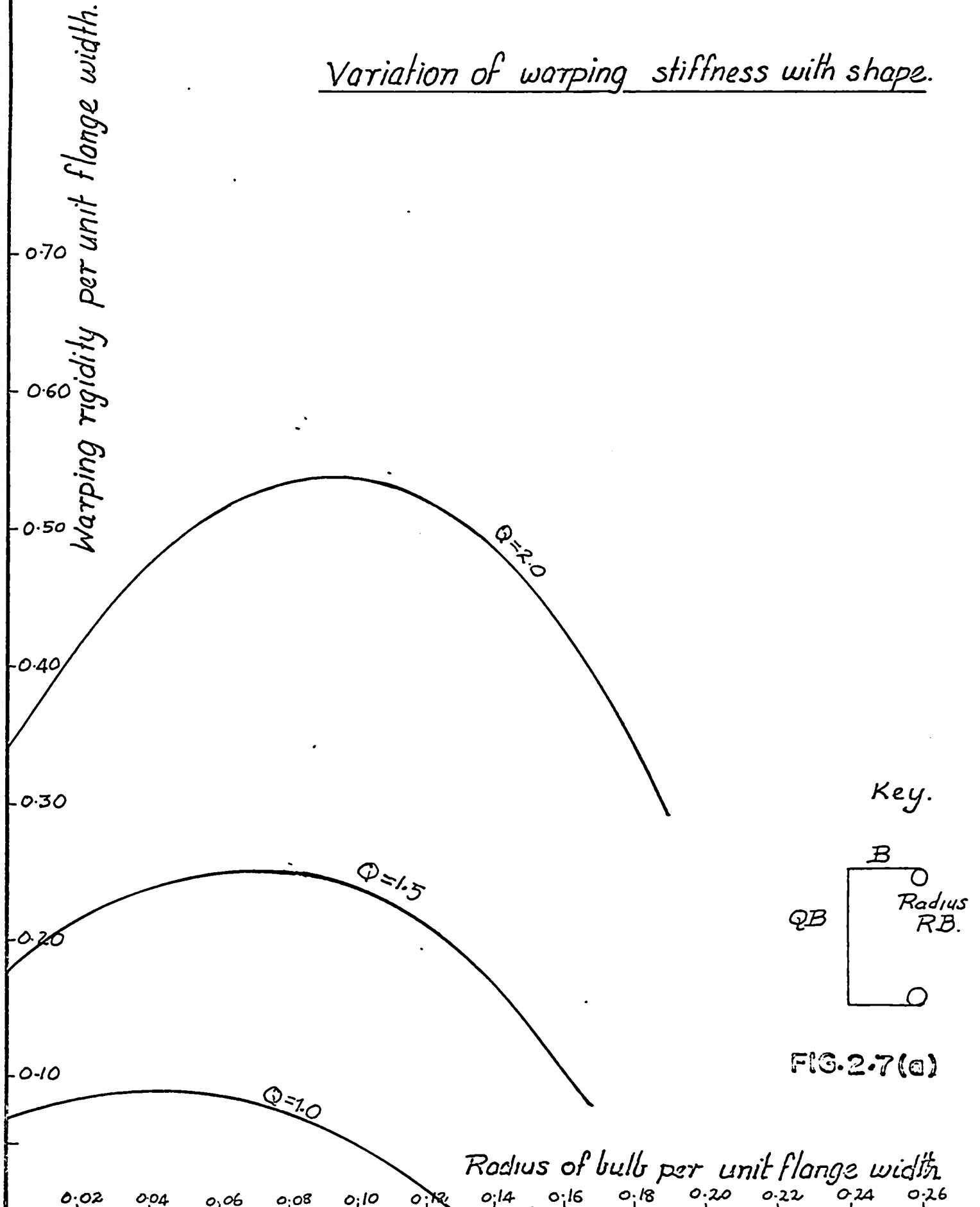
0.2315 and 0.2455. At  $R = 0.09$  the values are 0.202 and 0.253. At  $R = 0.12$ , the values are 0.1775 and 0.2415.

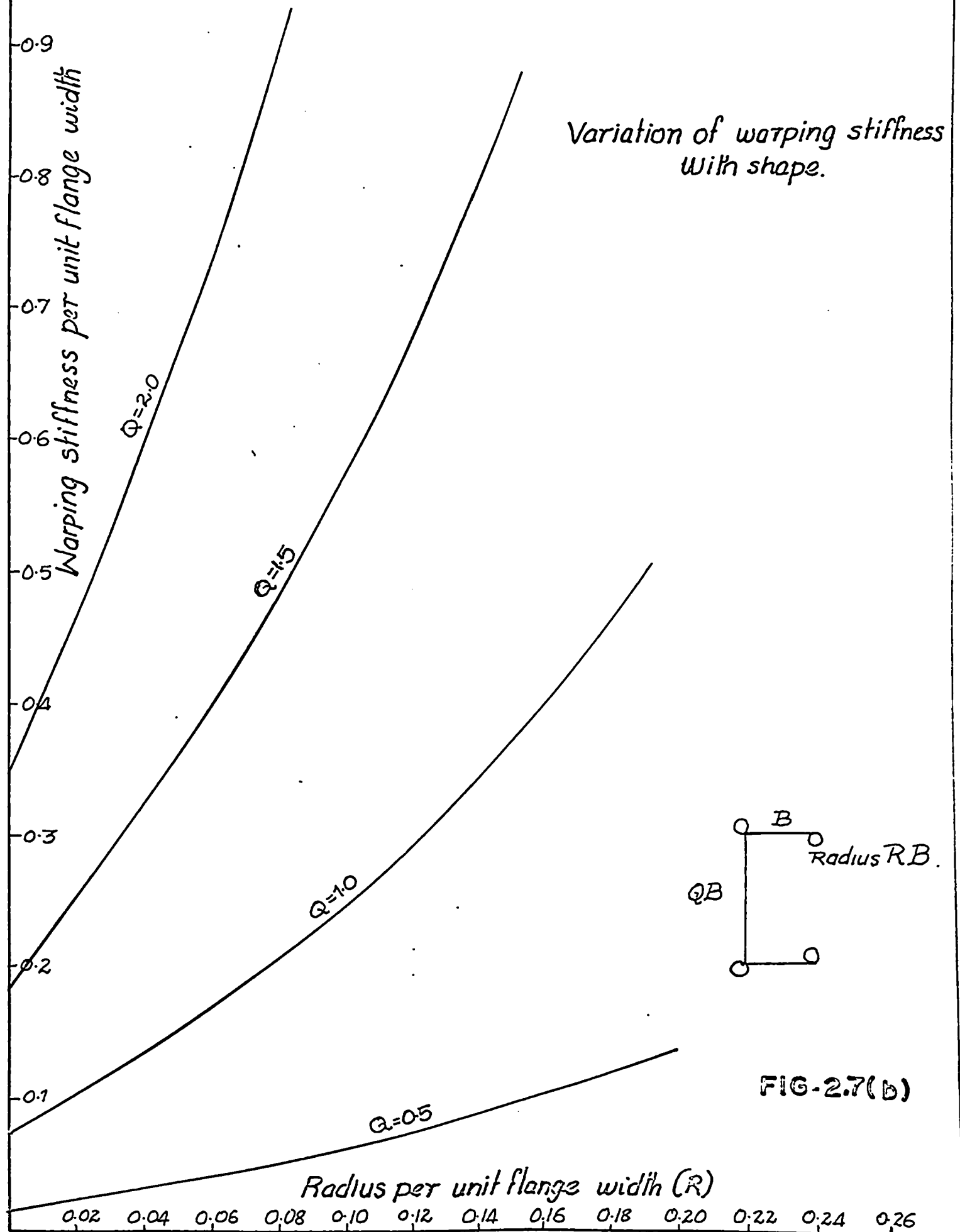
At a constant value of  $Q = 2.0$ , at  $R = 0.03$ , the values for  $R_E$  are 0.247 and 0.257. At  $R = 0.06$ , the values are 0.253 and 0.276. (Fig. 2.6(A) and (B) ). At  $R = 0.09$ , the values are 0.244 and 0.283, and at  $R = 0.12$  they are 0.228 and 0.215 respectively. (See also Table 2.8).

To emphasize the influence of shape on  $R_E$  and  $R_p$ , in any particular section, computations were made for 8" x 4" and 4" x 2" channels with 2 bulbs and with 4 bulbs. The curves showing the actual values of the two radii of gyration  $R_E$  and  $R_p$  in inches can be seen in Figs. 2.6(C) and 2.6(D). Referring to Fig. 2.6(C), the 8" x 4" channel has maximum  $R_E$  when the radius of the bulb is 0.2", and the 4" x 2" channel has maximum at bulb radius of 0.07". It is also to be noted that the curves for  $R_E$  and  $R_p$  fall off steeply from the maximum and for radius of bulb 0.8" to 0.9" both the radii of gyration are sensibly the same for an 8" x 4" channel. For a 4" x 2" channel the two curves are very close to each other in the region  $R = 0.3"$  to  $0.4"$ .

Referring to Fig. 2.6(D) pertaining to a channel with 4 bulbs,  $R_E$  is a maximum at a radius of bulb equal to 0.35 inch for 8" x 4" channel and at a radius equal to 0.2" for 4" x 2" channel. Compared to Fig. 2.6(C), the curves in Fig. 2.6(D) fall away at a flat slope from the maximum. This means that the reduction in equivalent radius of gyration with increasing radii of bulb is more gradual in this case. The curves for equivalent radius of gyration  $R_E$ , in this case, are well below those for  $R_p$  indicating that a pronounced torsional flexural buckling is more likely in such

Variation of warping stiffness with shape.





sections than in those with 2 bulbs.

Fig. 2.7(A) and (B) shows that the variation in the non-dimensional parameter governing warping rigidity " $\Gamma$ " increases initially, reaches a maximum and decreases with further increase in radius. To obtain warping rigidity of a section the parameter " $\Gamma$ " shown on Fig. 2.7(A) and (B), will have to be multiplied by the sixth power of the flange width first, and then further multiplied by the thickness of sheeting. Comparing maximum ordinates at  $Q = 1.0$  and  $Q = 2.0$ , the values of " $\Gamma$ " are 0.09 and 0.54 respectively. Hence, increase in  $Q$  has a significant effect on " $\Gamma$ ". The maximum warping rigidity for  $Q = 2.0$  occurs at a radius of 0.09 times the flange width.

Referring to Fig. 2.7(B), for a 4 bulbed channel, the constant " $\Gamma$ " continuously increases with  $R$ . This increase is steep for higher values of  $Q$  of 1.5 and 2, and is flatter for values of  $Q$  of 1 and 0.5. For instance, at a radius per unit flange width of 0.04, " $\Gamma$ " for  $Q = 2.0$  is 0.61 and for  $Q = 1.0$ , it is 0.135. Here also the influence of increase in  $Q$  is significant. Comparing Figs. 2.7(A) and 2.7(B) it can be seen that the values of the warping rigidity for the 4 bulbed channel are always larger than those for the 2 bulbed channels. At  $Q = 1$ , the maximum value for coefficient " $\Gamma$ " is 0.09, corresponding to a bulb radius of 0.04 times flange width (Fig. 2.7(A)). The 4 bulbed channel, however, has a value of 0.105 for the values  $Q = 1.0$  and  $R = 0.04$ .

At  $Q = 1.5$ , the maximum value for the coefficient " $\Gamma$ " is 0.255 (Fig. 2.7(A)) at a radius equal to 0.065 of the flange width. At corresponding value of  $Q$  and  $R$ , the 4 bulbed channel (Fig. 2.7(B)) has a " $\Gamma$ " value of 0.45.

At a value of  $Q = 2.0$ , the maximum value for " $\Gamma$ " in a 2 bulbed channel (Fig. 2.7(A)) is 0.54 at a radius of 0.09 times the flange width. For the 4 bulbed channel for the corresponding value of  $Q$  and  $R$ , the value of " $\Gamma$ " is nearly 1.0. From the above it may be observed that increase in " $\Gamma$ " is much larger in 4 bulbed channels, notwithstanding its cross sectional area being larger, than the 2 bulbed channel. One reason for this is that in the case of 2 bulbed channels the centroid tends to shift away from the web plate for increasing bulb radii, whereas in a 4 bulbed channel, the web bulbs balance the flange bulbs and help maintain a small distance between the web and the centroid, even with increasing radius. Study of the influence of geometrical shapes on the warping stiffness can best be made only by preparing graphs as in 2.7(A) and (B), for varying proportions. The variation in the warping rigidity does not bear a simple relation to the cross sectional dimensions of the channel, and computations must be made for each different combination of web, flange, and lip dimensions. Because of this, no generalisation can be made of the influence of geometry on the warping stiffness.

Considering the influence of shape on the "coefficient of interaction",  $(1 - \frac{x_o^2}{r_o^2})$ , Fig. 2.8(A) provides a comparison between two different sizes of the two bulbed and 4 bulbed sections. Both for 8" x 4" channel and 4" x 2" channel the value of the coefficient of interaction is greater when 4 bulbs are provided. Further, increase in radius causes a decrease in the coefficient of interaction in both cases. The rate of decrease is larger for smaller sections than for larger one, as can be seen from the slopes of the descending segments of the curves. Another

Variation of coefficient of interaction with radius of bulb.

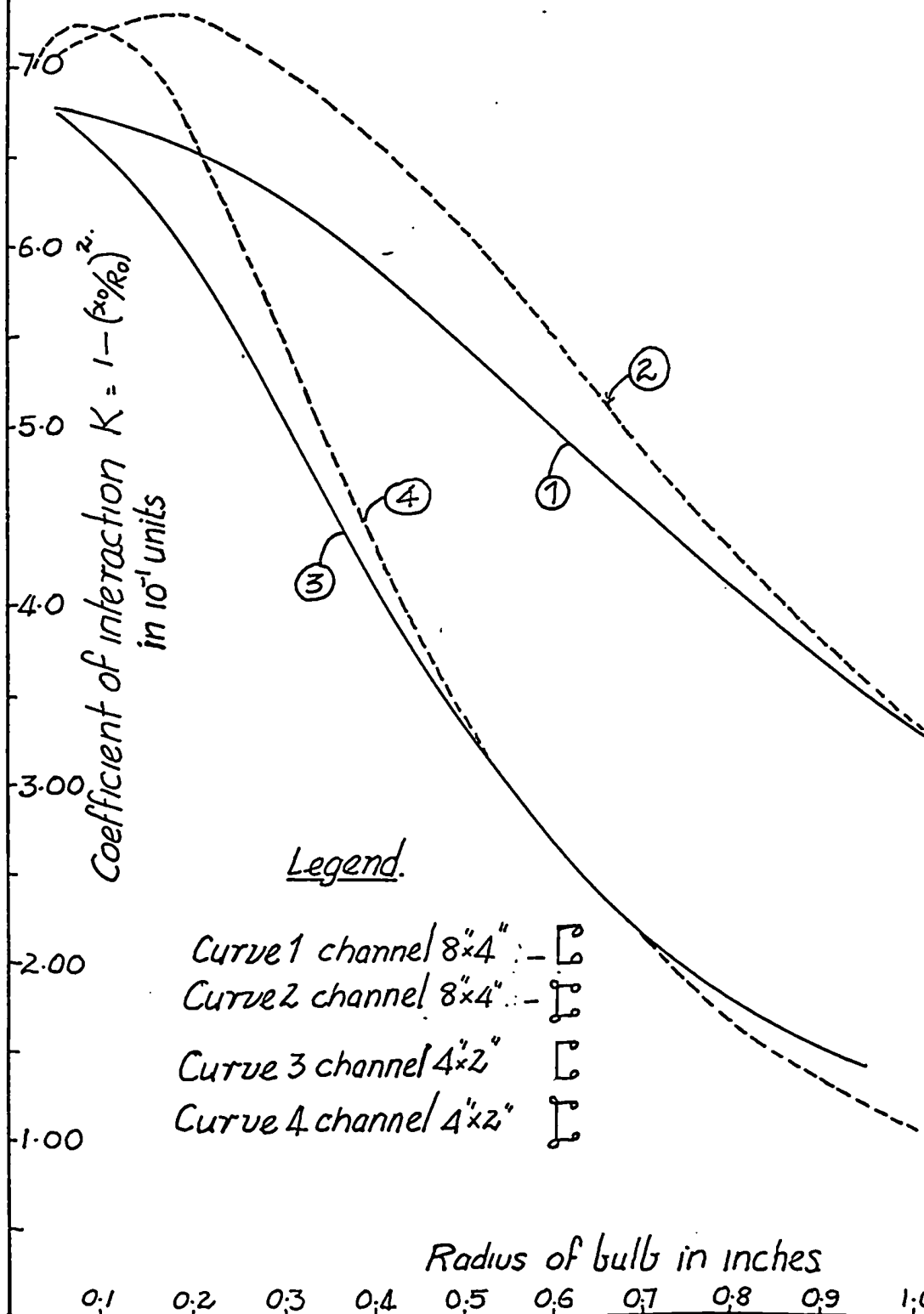
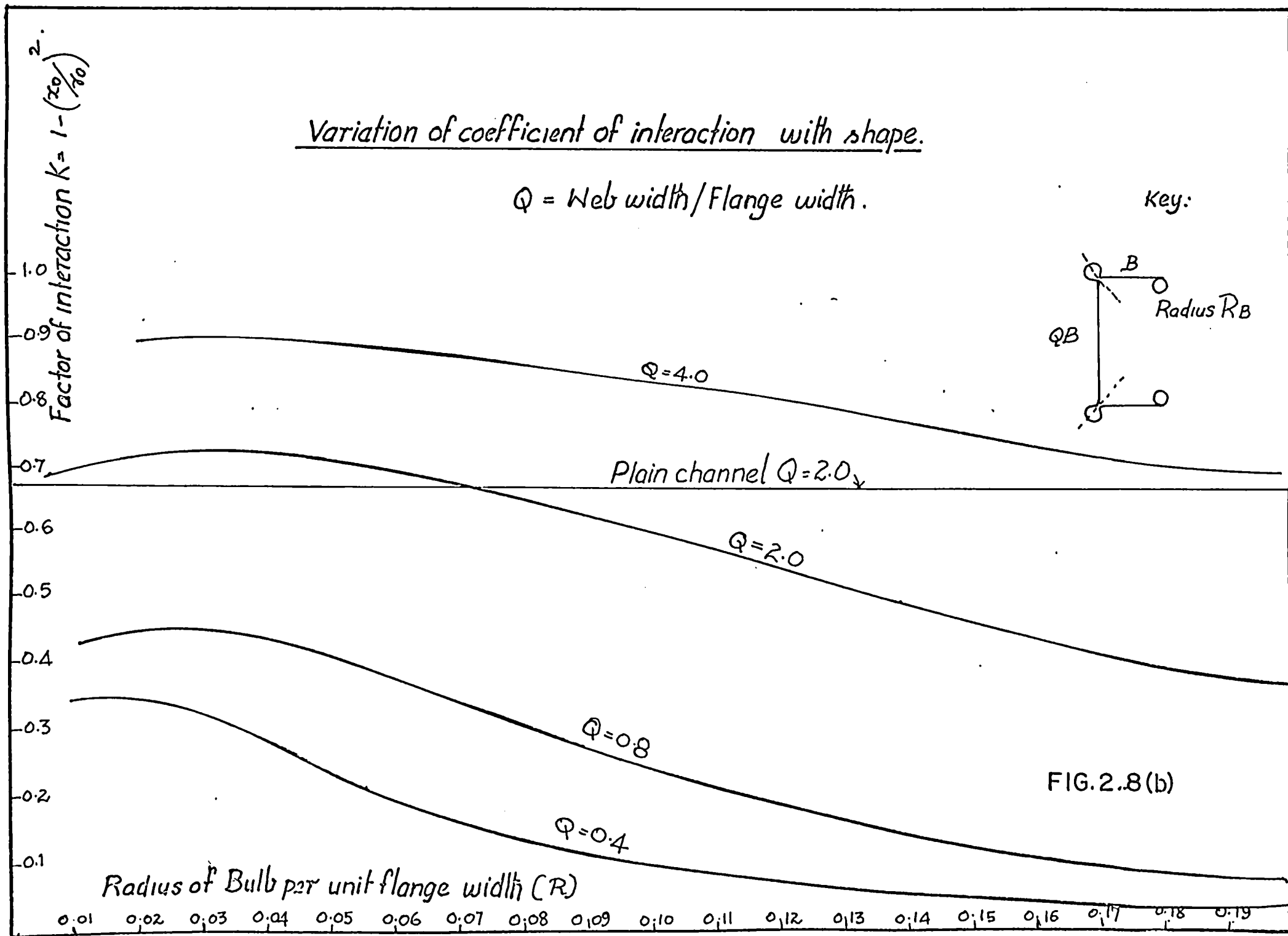


FIG. 2.8(a)



significant point is that with increasing radius of bulbs, the coefficients of interaction for both 2 bulbed and 4 bulbed channels approach each other closely. From the point of view of the constant of interaction " $K_{\phi}$ " which should be high for a greater critical load, there is no significant difference between the two types of channels at larger radii of bulbs. (See the range  $R = 0.5$  to  $0.9$  for  $4" \times 2"$  channel and  $R = 0.8$  to  $1.0$  for the  $8" \times 4"$  channel, in Fig. 2.8(A). Figure 2.8(A) and (B) indicate that the channel sections  $8" \times 4"$  and  $4" \times 2"$  sections show a coefficient of interaction less than unity. This would mean that these sections are likely to fail by torsional flexural buckling. This was an important criterion in the final choice of sections for experimental work.

2.10 Buckling collapse of a column is, in general, a combination of local and overall buckling. The problem of demarcating the regions of possible local buckling and possible overall buckling is mathematically very complex and remains to be solved. Only in the case of equal angle sections do the criteria for local and overall buckling yield the same critical stress. If local buckling occurs first, resulting in failure, it should be possible to employ an empirical approach for such sets of columns. Final collapse is a combination of local and overall buckling, in all but very short columns. Whether local buckling or overall buckling is the first to occur in the process of loading is an important consideration for assessment of column strength.



2.11 As a sequel to the foregoing theoretical study of the behaviour of bulbed channels, experimental work was planned and carried out as outlined in the following chapter. It can be seen from Table 2.8 that the equivalent radius of gyration  $R_E$  is less than the minimum radius of gyration in flexure " $R_y$ ", in all the sections considered. Hence, it may be expected that the sections chosen for tests would buckle in the torsional flexural mode, rather than in pure flexure. The purpose of the experimental work was to determine if failure did take place in the mode anticipated or not. Further tests would demonstrate the actual behaviour of such columns.

## CHAPTER III

### EXPERIMENTAL WORK AND RELATED DISCUSSION

3.1 As a prelude to detailed testing with complete instrumentation, a number of different channel shapes were tested in an Olsen screw type testing machine. The maximum length of column that could be accommodated on the machine was 36 inches. Fig. 3.1 shows the different 8" x 4" channel shapes chosen for the tests. These shapes are as follows:

- (a) Plain channel 8" x 4".
- (b) Channel 8" x 4" with half inch diameter bulbs at the ends of flanges.
- (c) 8" x 4" channel with bulbs at the ends of flanges, and also at the junction of webs and flanges. Diameter of bulbs is 1/2 inch.
- (d) 8" x 4" channel with triangular lips of the same developed length as a half inch bulb.
- (e) 8" x 4" channel with half inch diameter bulbs at the junctions of webs and flanges only.
- (f) 8" x 4" channel with inward lips each equal to the developed length of half inch bulb.

3.2 The results of preliminary tests are shown in Table 3.1. Actual record of test results is given in the Appendix. The values shown in Table 3.1 are average values of the loads. Section (c) carried loads in the range of 8,500 to 9,400 lbs in fully instrumented tests carried out later. In this case the values in the preliminary tests were lower because of initial imperfections. These being the first such sections attempted in forming, some denting and tool marking was unavoidable, especially in forming the web bulbs.

From the preliminary results it was decided to conduct fully instrumented tests only on sections (b), (c), (e), and (f), shown in Fig. 3.1, so as to study circular bulbs and straight lips, and compare their relative influence.

3.3 The purpose of the experimental investigation was to:

- i) observe the influence of cross sectional shape on ultimate strength as a strutt.
- ii) observe the mode of collapse and classify it as local buckling or overall buckling.
- iii) study the out-of-plane deformation of the web and the flanges at various stages of the loading to see the extent to which they could be allowed without being aesthetically unacceptable.
- iv) study the distribution of stresses in the cross section, and to determine the influence, if any, of the bulbs provided in the cross sections.

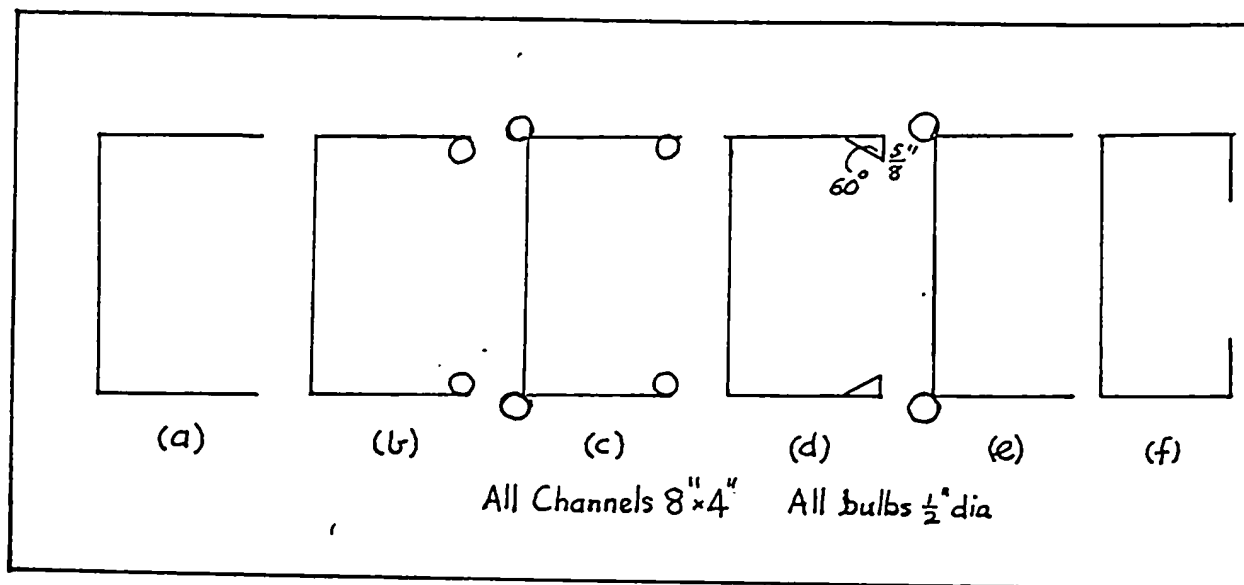


FIG 3.1







Section.						
Pult in Lbs	2738	6500	5360	6480	6500	6730
Remarks	2 tests	4 tests	2 tests	2 tests	4 tests	2 tests

TABLE 3.1

10.16 11.62 12.12 14.15

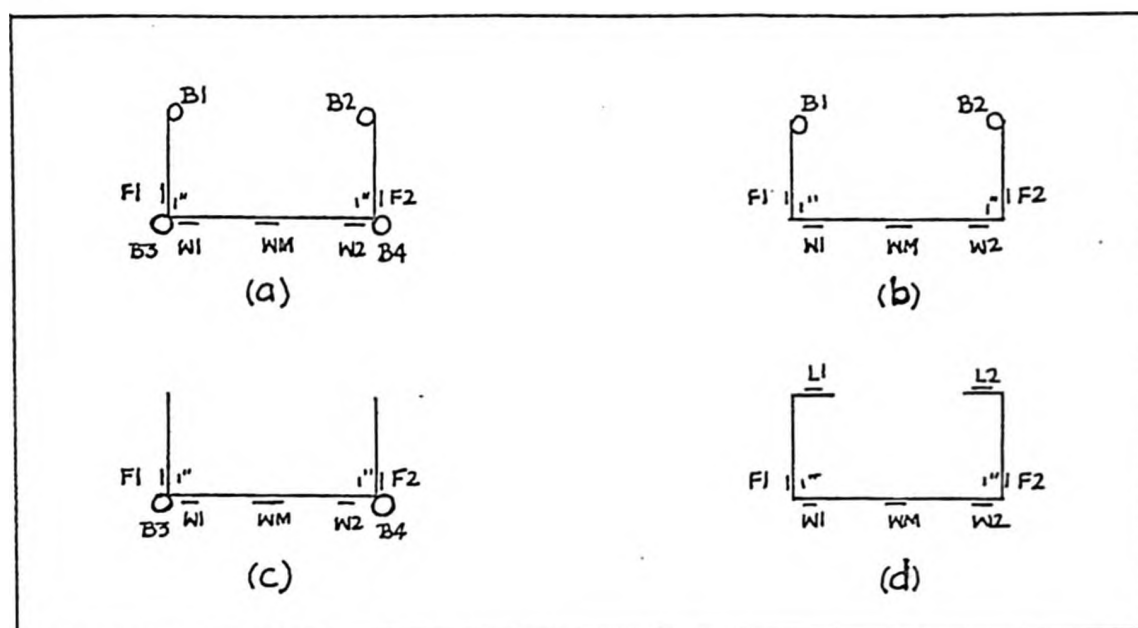


FIG. 3.2.

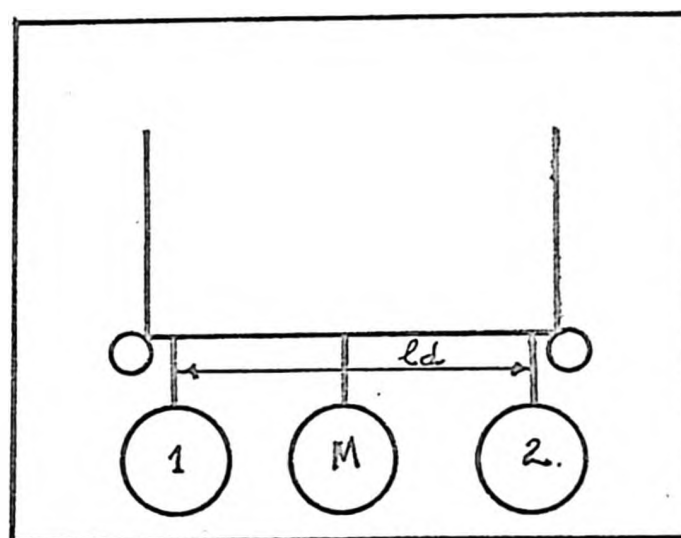
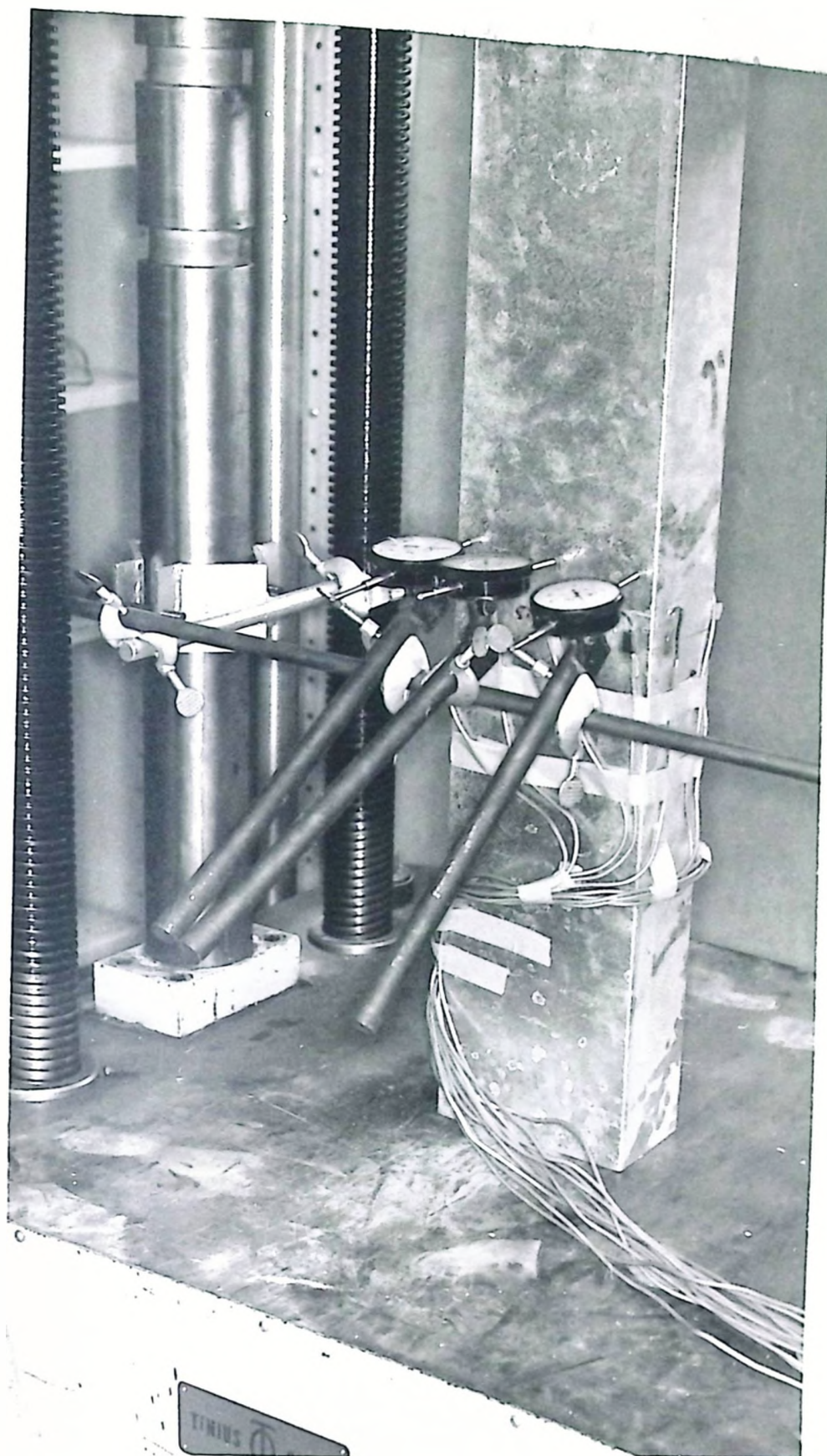


FIG.3.3.

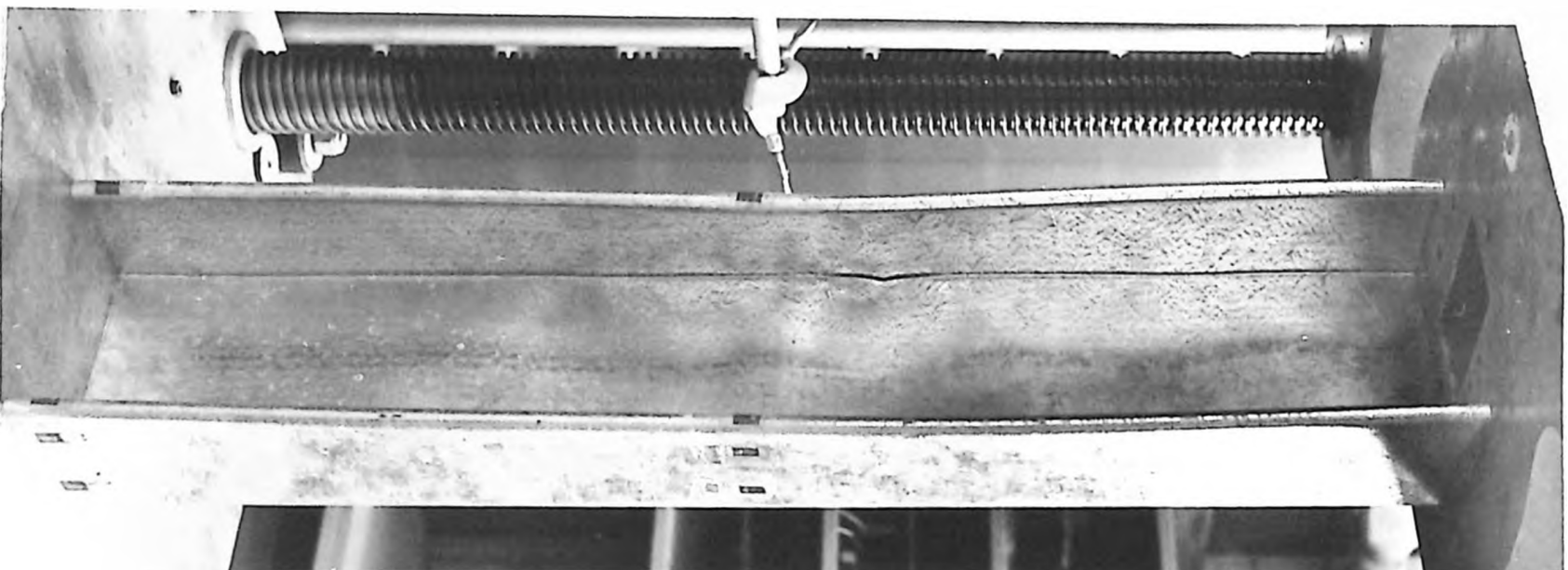
- v) arrive at a semi-empirical approach to evaluate the strength of such columns.
- vi) investigate the possibility of using these sections as structural skeletons for lightly loaded structures.

### 3.4 CONDITIONS OF TESTS

At mid height of the column, 3/8 inch Budd foil type resistance strain gauges were mounted at locations shown in Fig. 3.2(a,b,c,d). Except on the bulbs, one gauge was mounted on each face of the web or flange plate, with the idea of separating the direct and flexural strains for the analysis. The gauges were all Type C-6 with gauge factor ranging from 2 to 2.1. The gauges were all mounted parallel to the longitudinal axis of the column. A multiple switching and bridge unit with a galvanometer indicator was used for balancing the gauges at each load stage. Two dial gauges were mounted at right angles to the web plate to measure the relative rotation of the section at mid height, and one more dial gauge was provided at the middle of the web for measuring the out-of-plane displacements of the web. Photograph 3.1 and Fig. 3.3 show the arrangements. By measuring the difference in displacement at gauges (1) and (2), and dividing it by " $l_d$ ", their distance apart, the rotation " $\beta$ " is directly obtained in radians. It is to be noted that by this means overall lateral displacement normal to the web is cancelled out of the measurements. An attempt was made to obtain even bearing at the ends against the machine platens, by sand papering and smoothfiling. All the tests were conducted with a constant cross head speed of 0.0025 inches per minute. At each



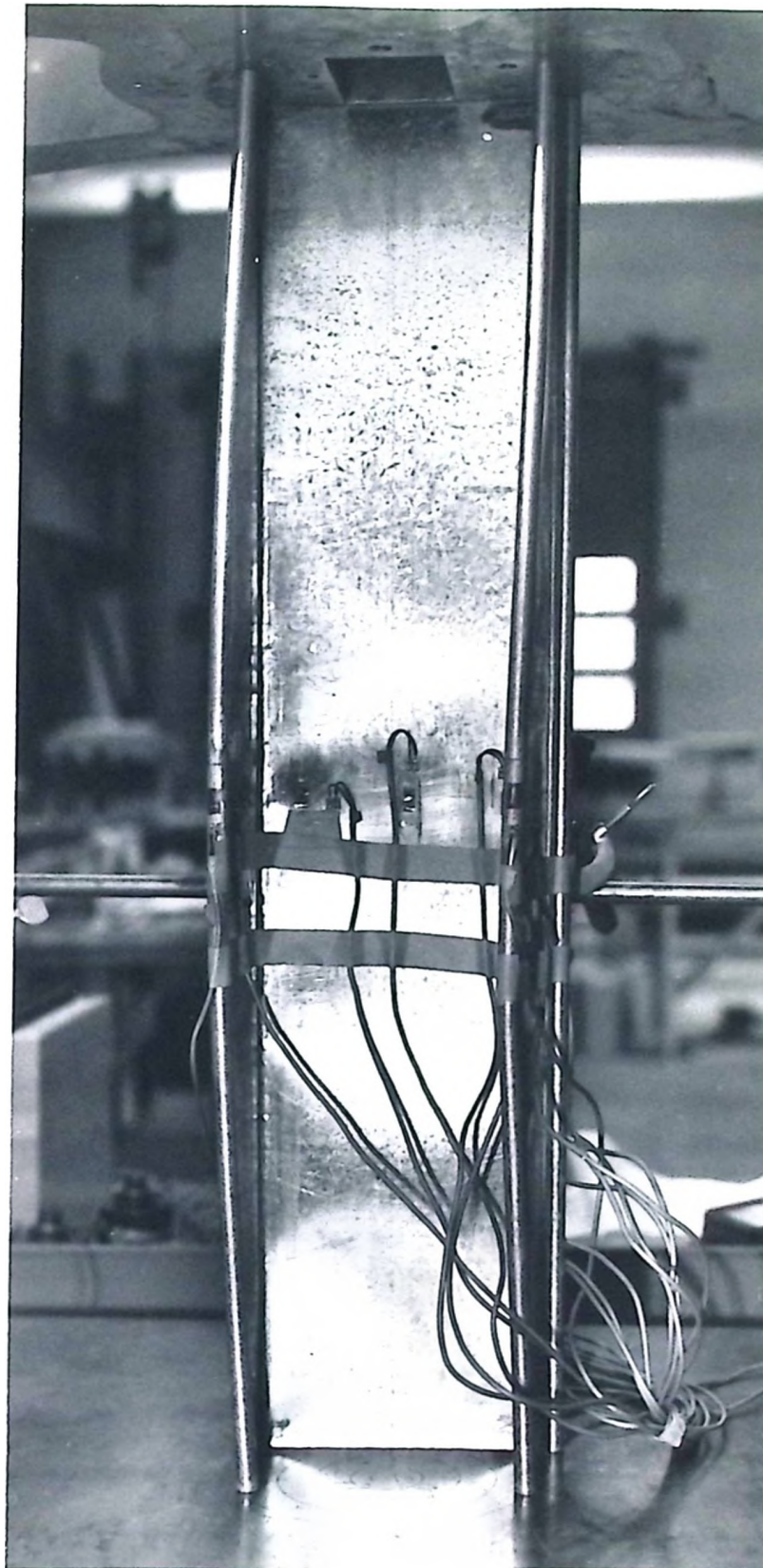
PHOTOGRAPH 3.1  
ARRANGEMENT FOR MEASUREMENT OF ROTATION OF CROSS  
SECTION



PHOTOGRAPH 3.2(a)

CHANNEL WITH FLANGE BULBS AT FAILURE





PHOTOGRAPH 3.2(b)

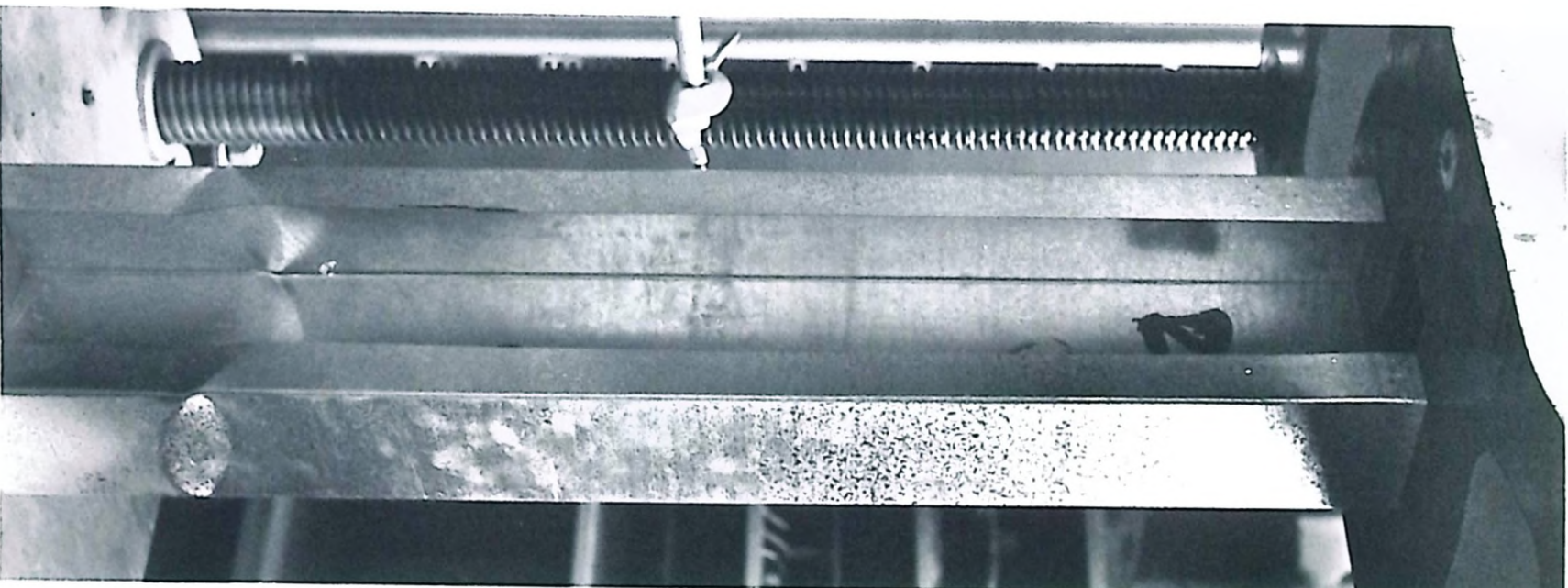
CHANNEL WITH FOUR BULBS AT FAILURE

chosen load level the screw drive was declutched and gauge readings recorded.

3.5 Since the preliminary tests had shown that all sections collapsed by local buckling, it was decided to have flat ends for the main tests also. Photographs 3.2(a) refer to failure of section (b) with two bulbs at ends of flanges, 3.2(b) refers to failure of section (c) with four bulbs. Photograph 3.2(c) shows the mode of failure of plain lipped channel. It may be noted in the photograph that the web bulbs are all still straight when the flange bulbs have gone into one half wave, and the flanges have buckled considerably.

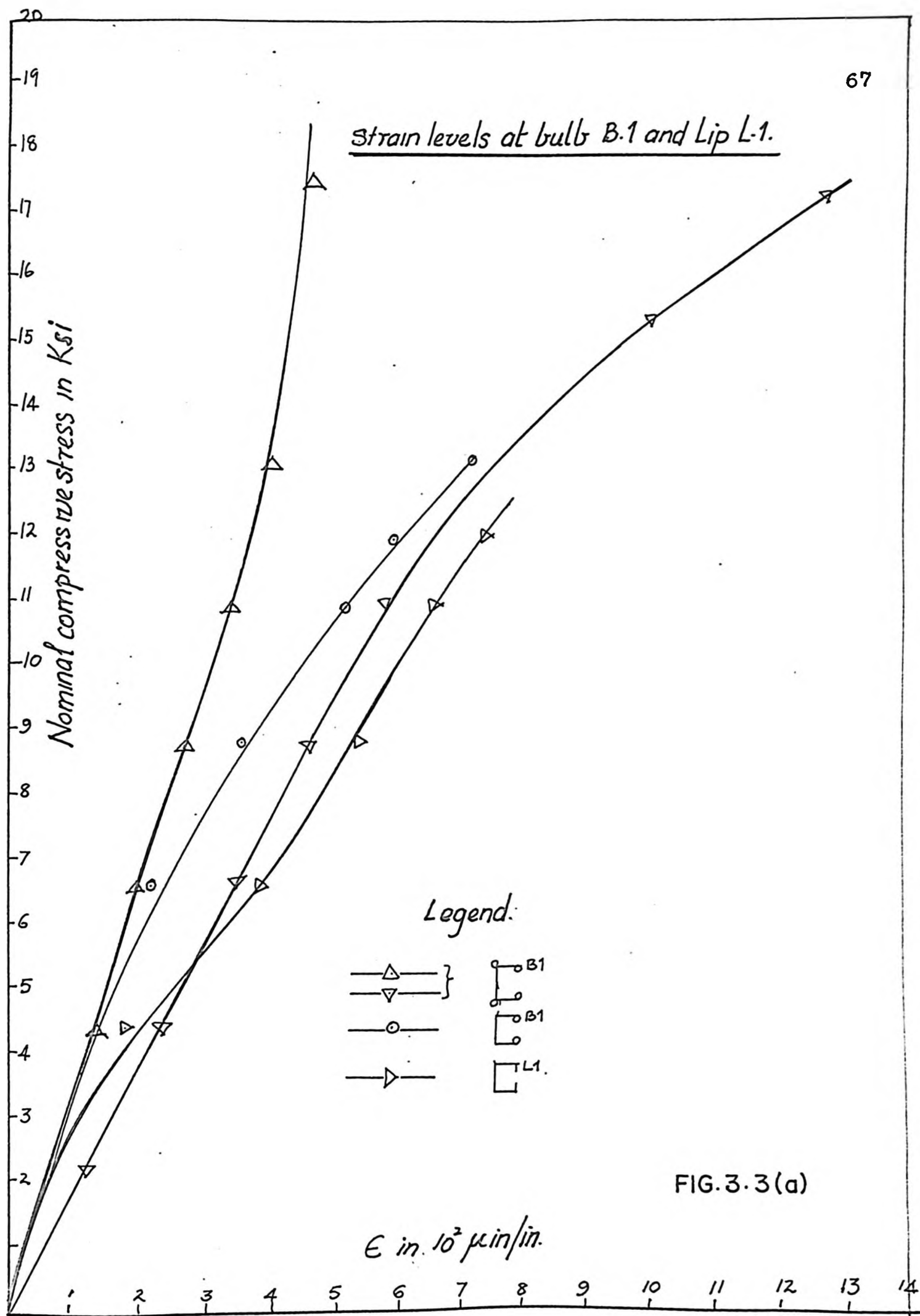
The direct longitudinal unit strains in the various sections are represented in Figs. 3.3(a,b,c,d,e,f,g,h,k). Figs. 3.4 (a,b,c,d,e) show the flexural strains at the same locations. Fig. 3.5(a) and (b) show the distribution of stress at nominal stress levels, shown on them and provide an idea of the distribution of stress over the cross section.

3.6 The movements of the middle cross section measured by the three dial gauges mounted as already mentioned, are recorded in Table 3.2. The figures mentioned here refer to the maximum values observed. It may be clearly seen that the rotation is very small. Most of the rotation occurred during end stages of loading. The maximum out-of-plane displacement does not exceed 5 times the thickness of the sheeting, i.e. 0.1195 inches. But due to the square buckling patterns on the column even this

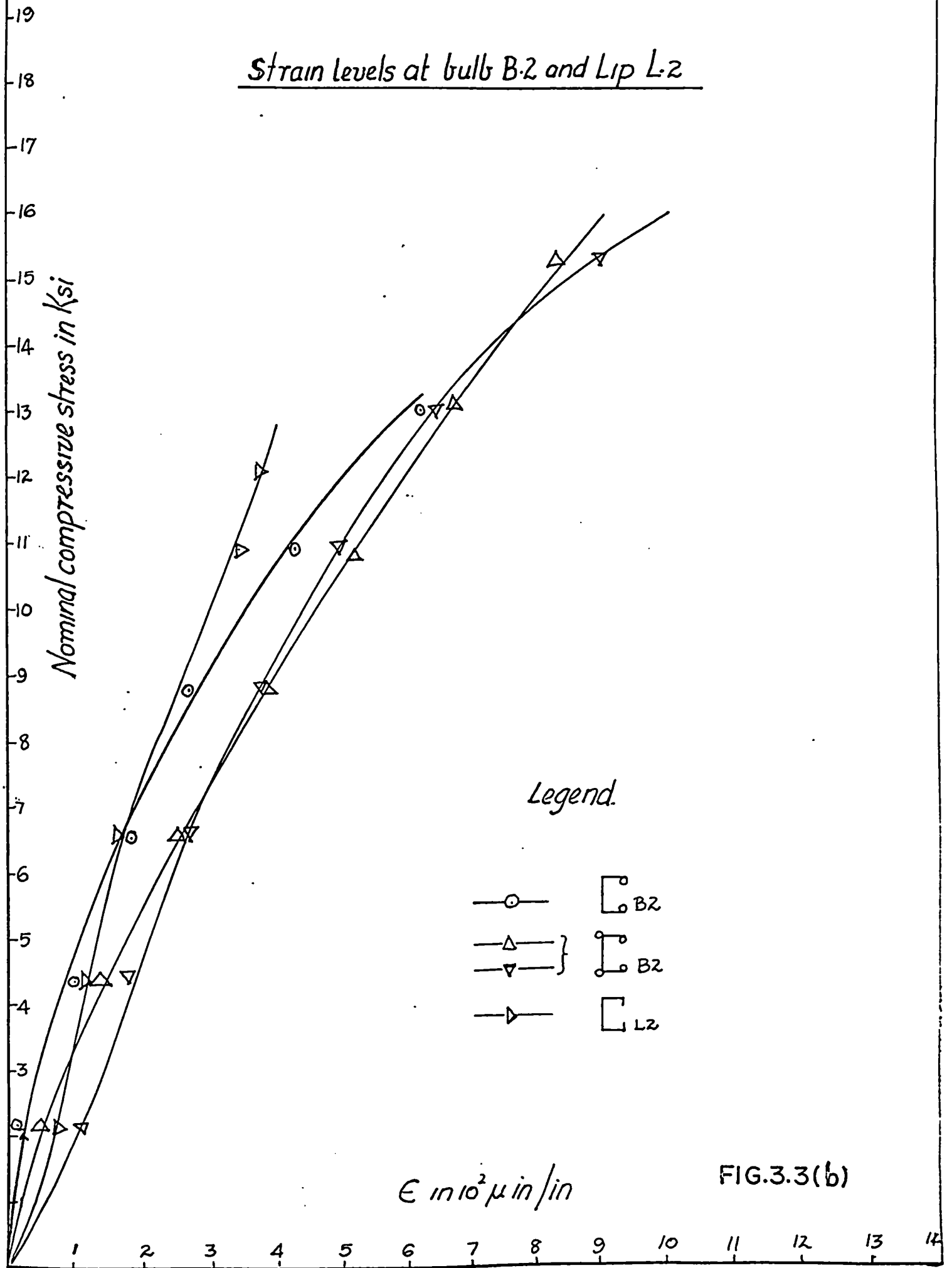


PHOTOGRAPH 3.2(c)

STRAIGHT LIPPED CHANNEL AFTER LOAD RELEASE

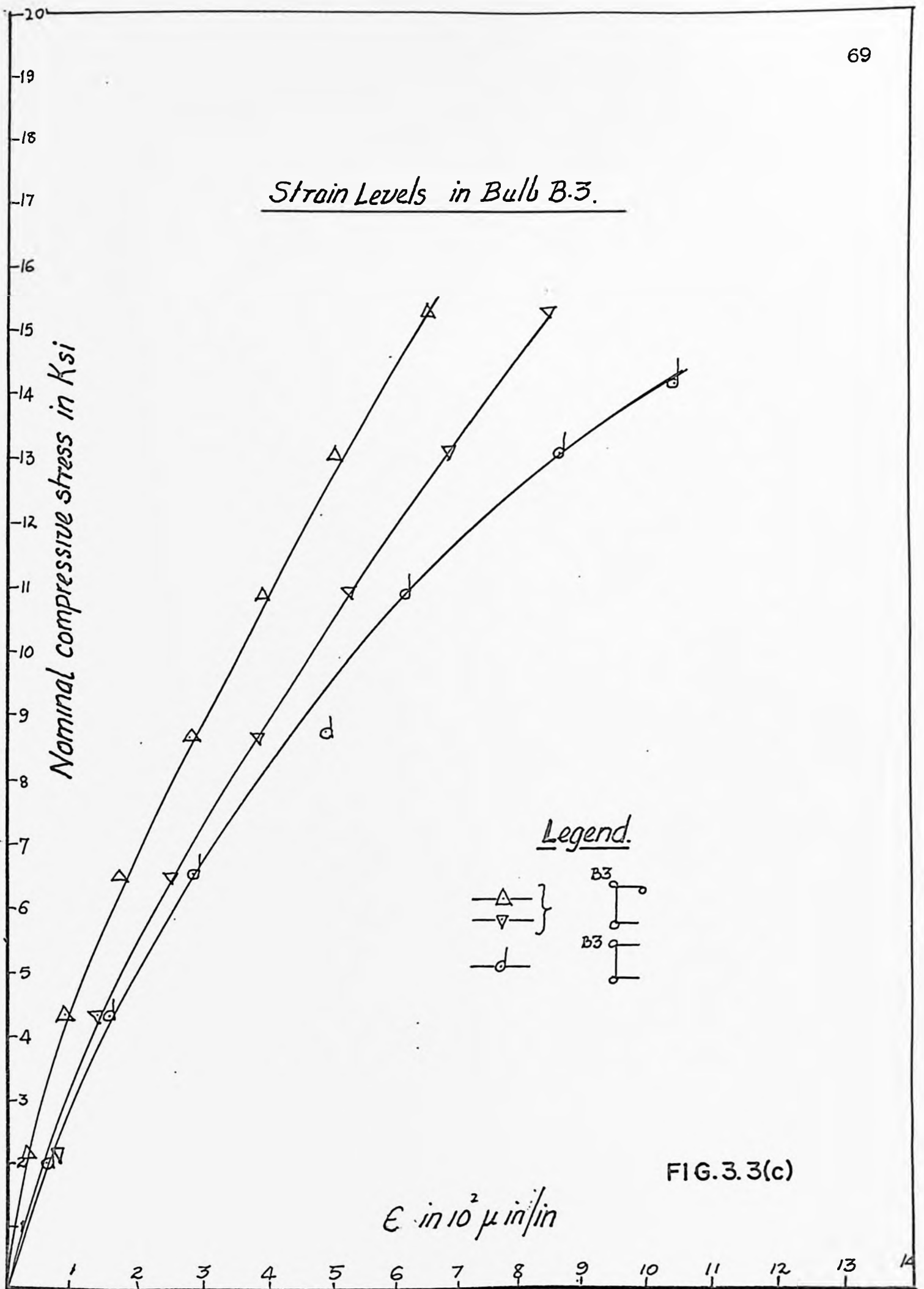


Strain levels at bulb B.2 and Lip L.2

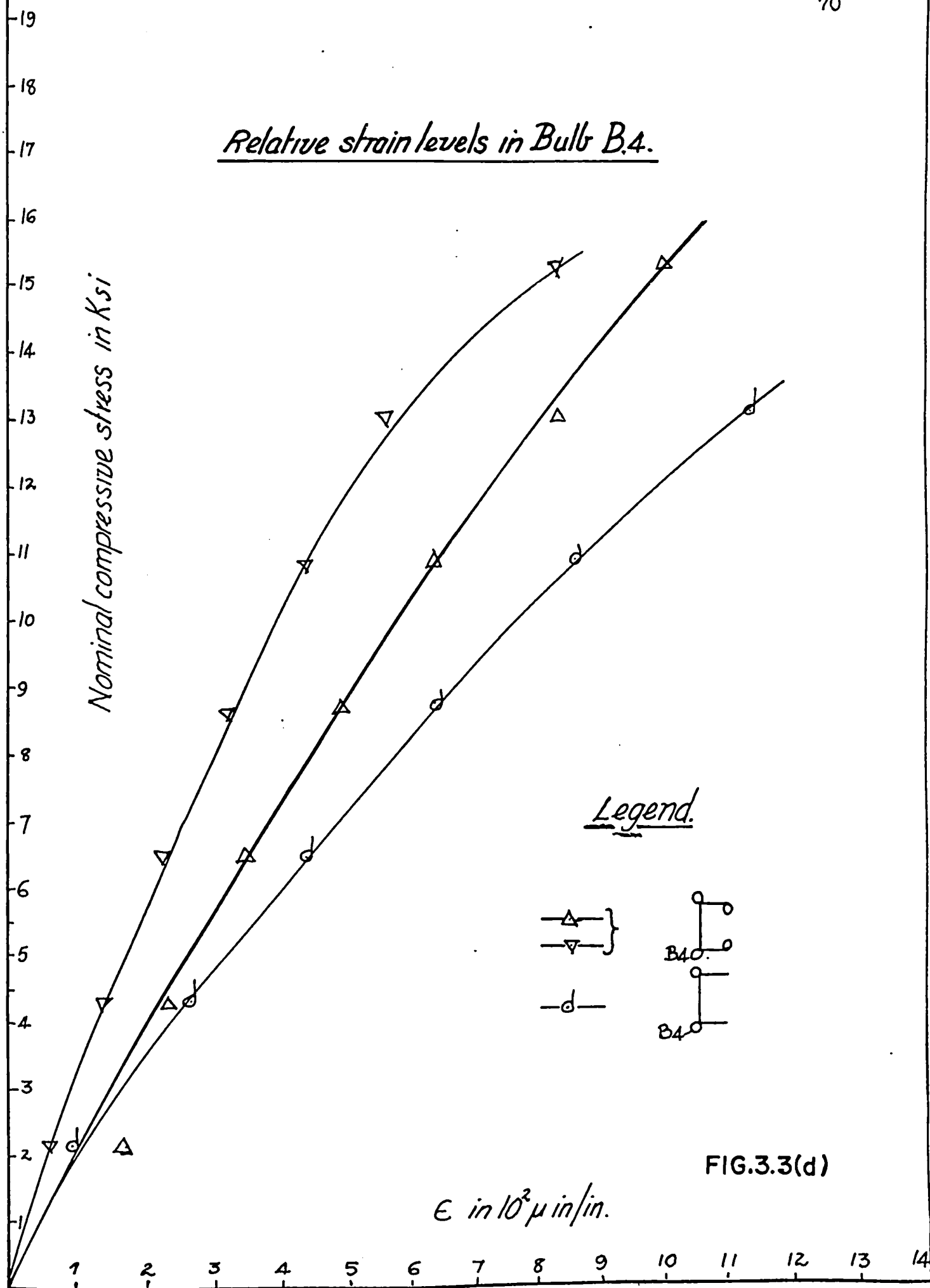




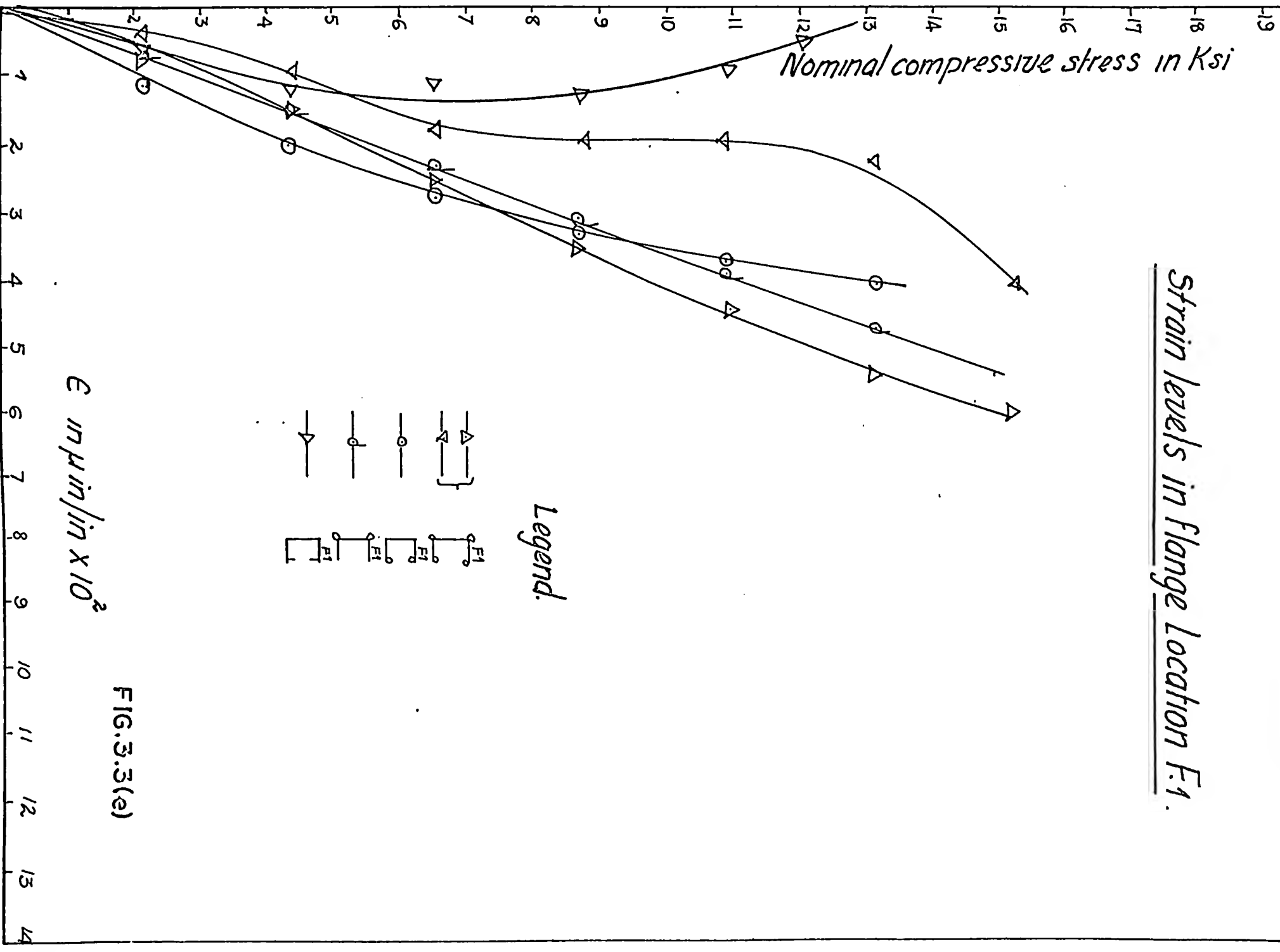
Strain Levels in Bulb B.3.



Relative strain levels in Bulb B.4.

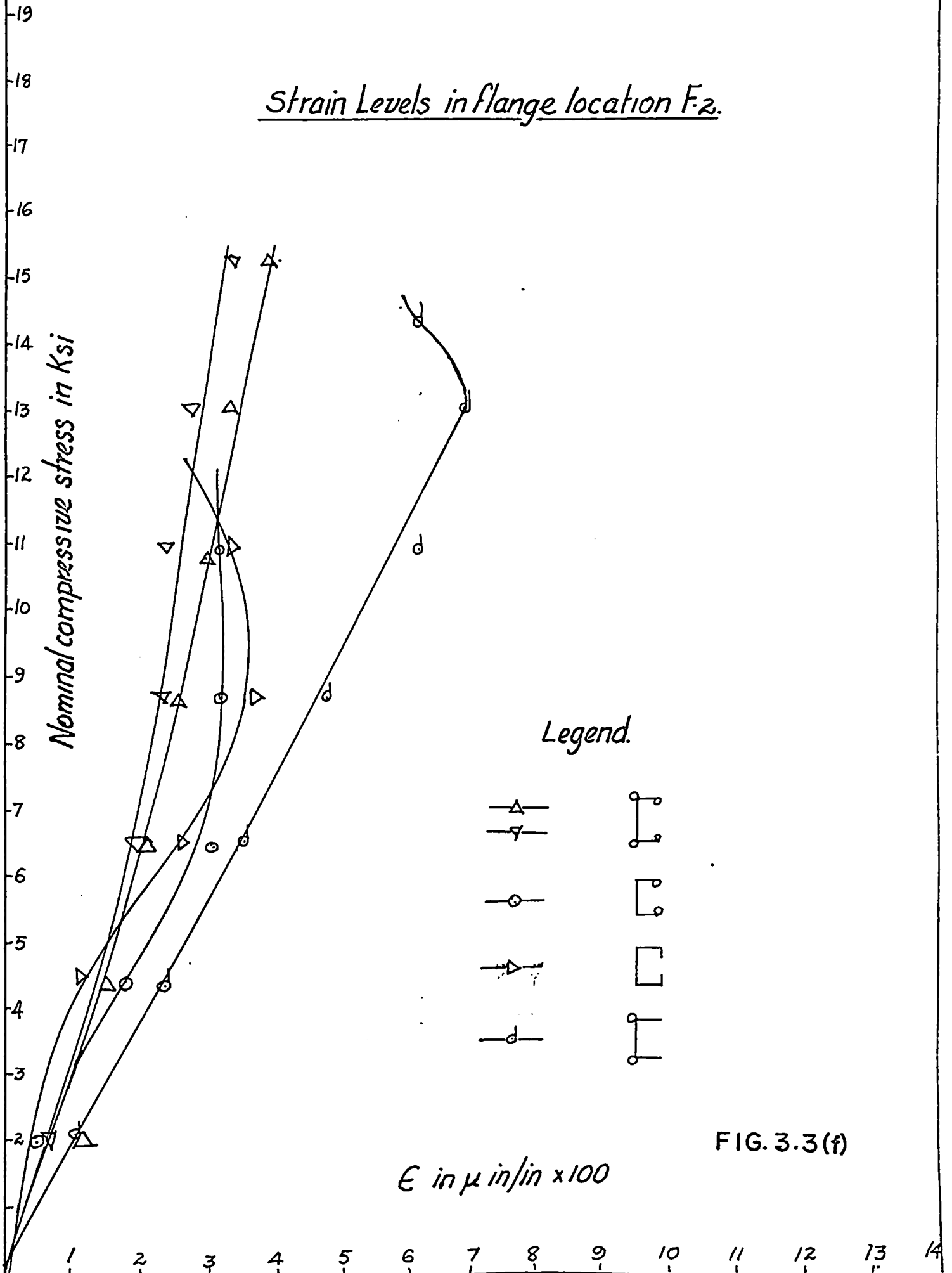


Strain levels in flange location F.1.

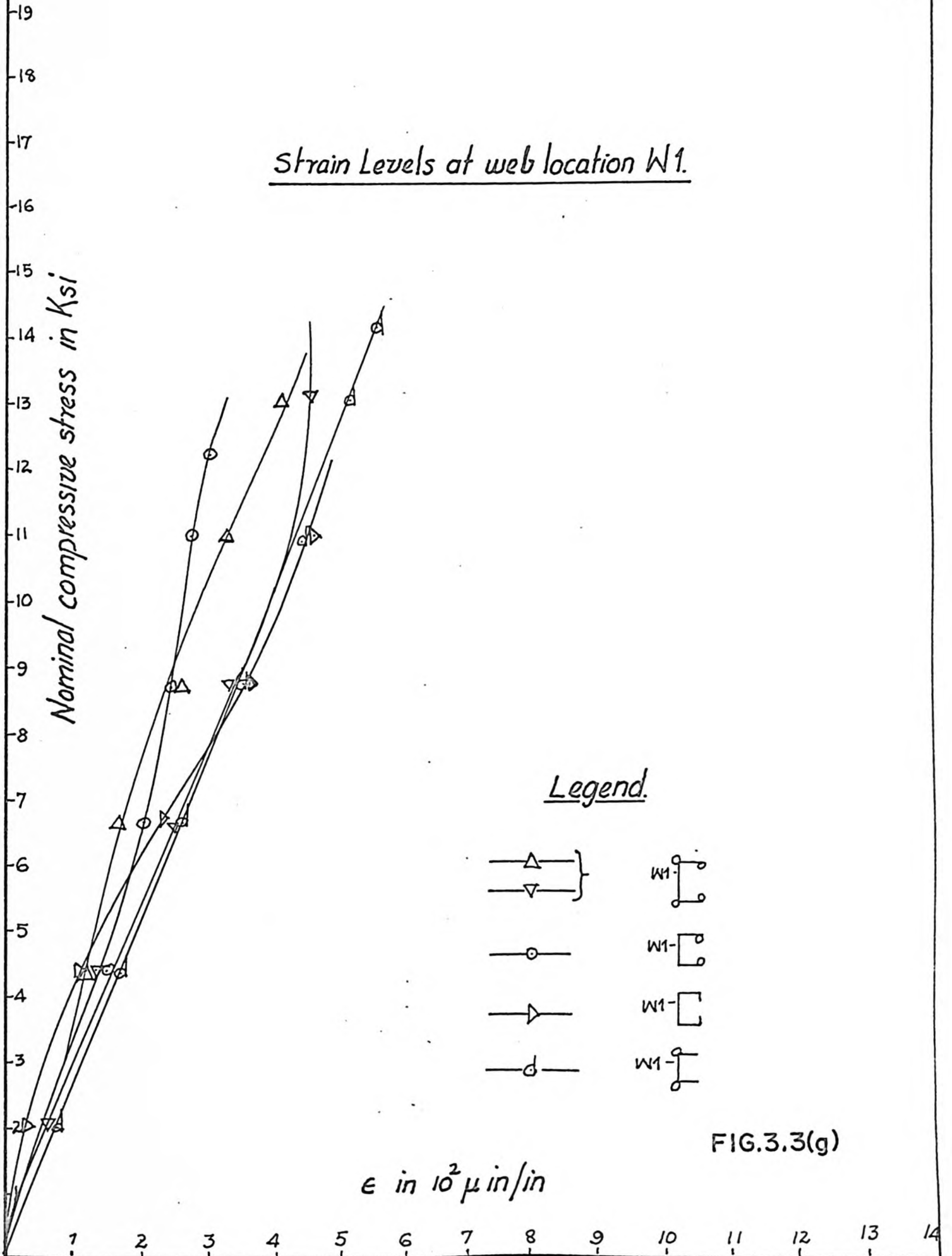


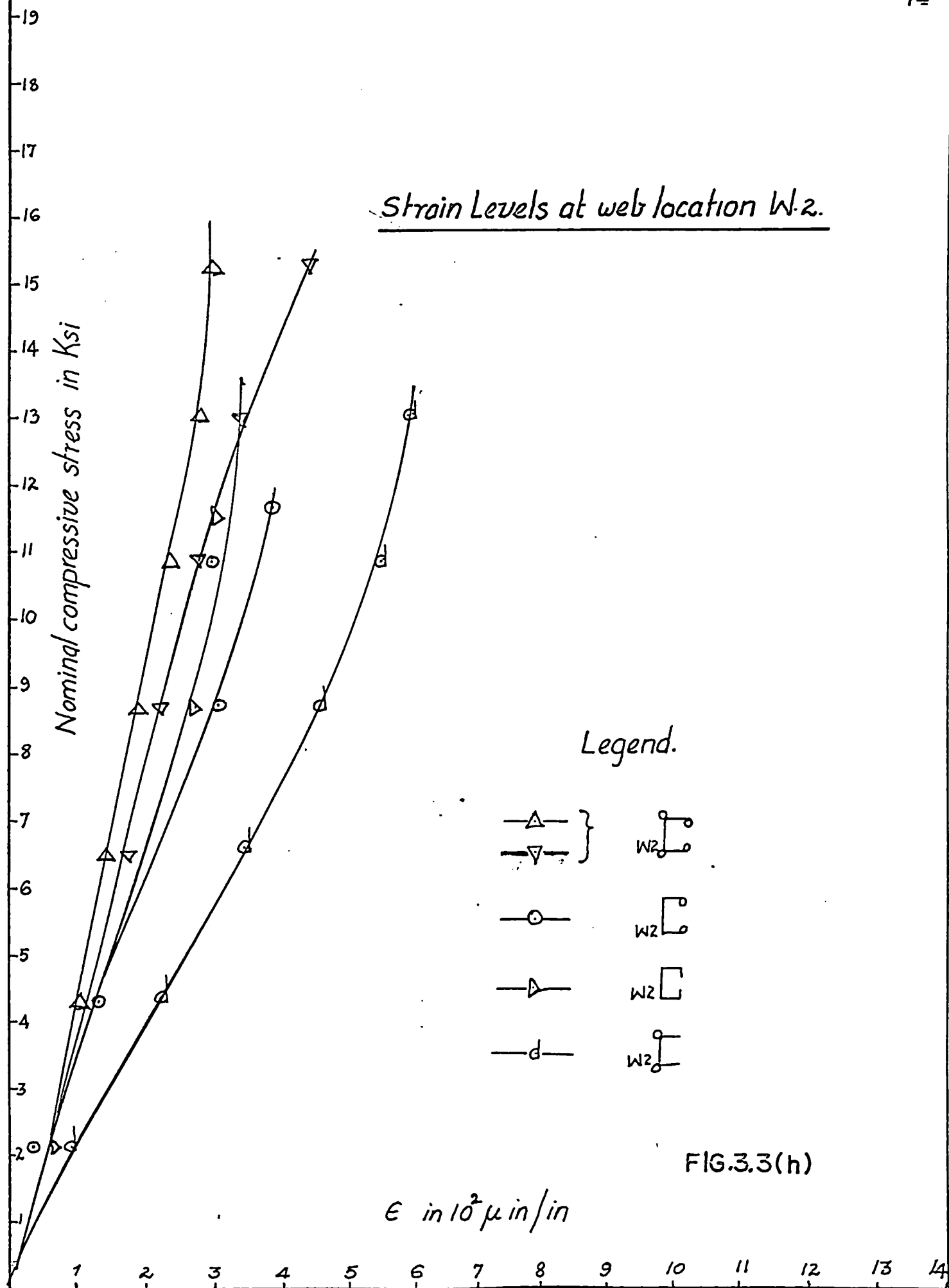


Strain Levels in flange location F.2.

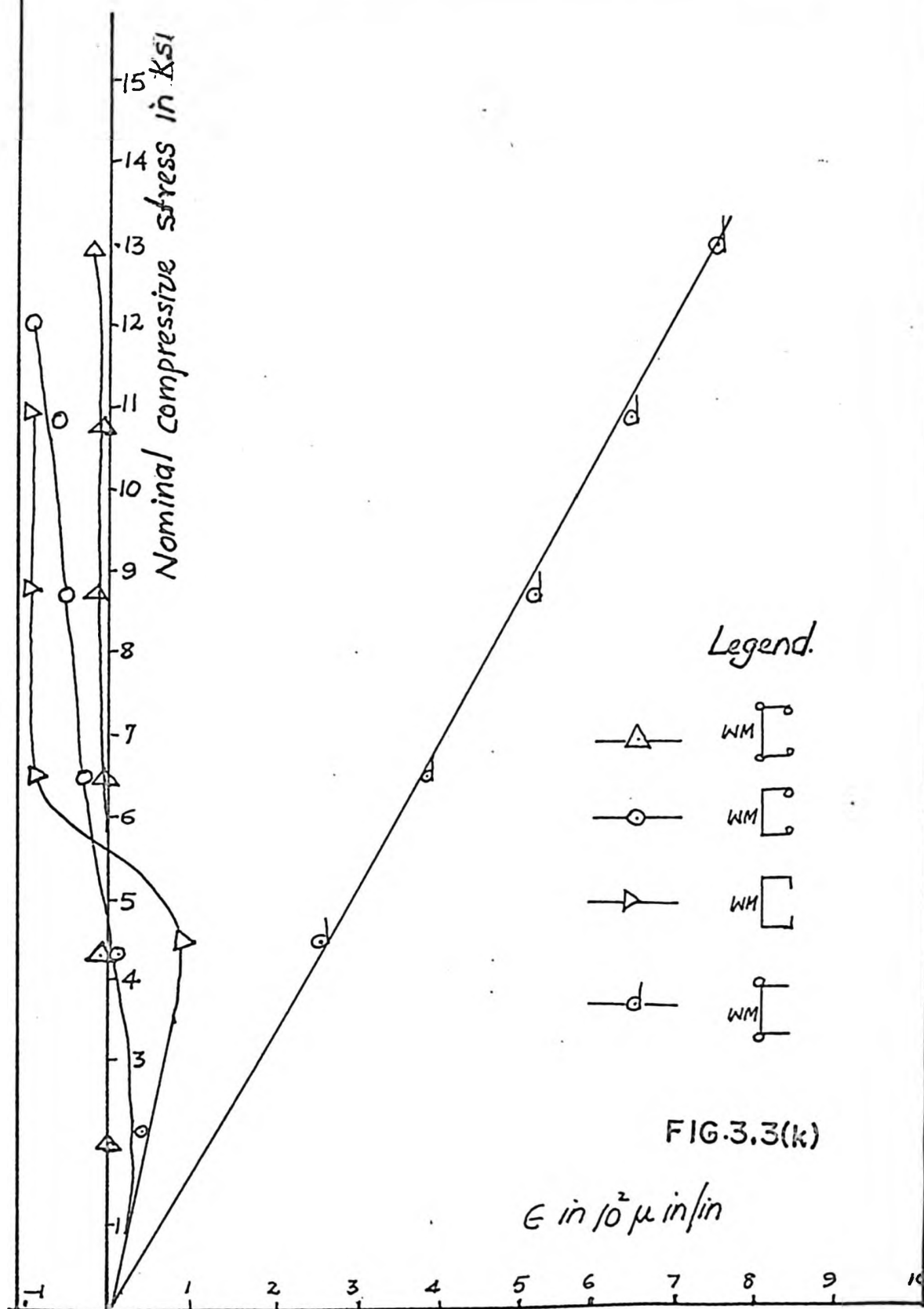


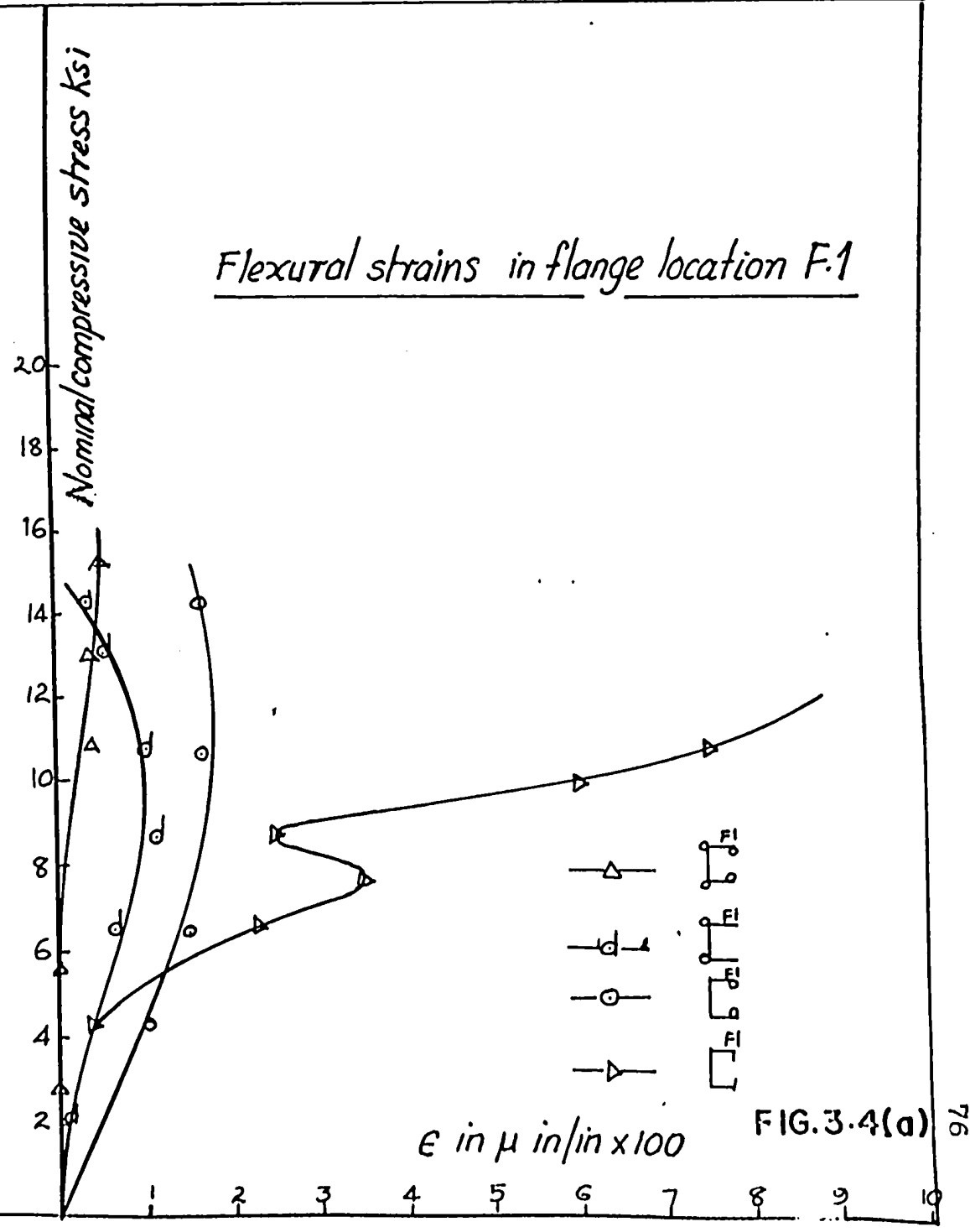
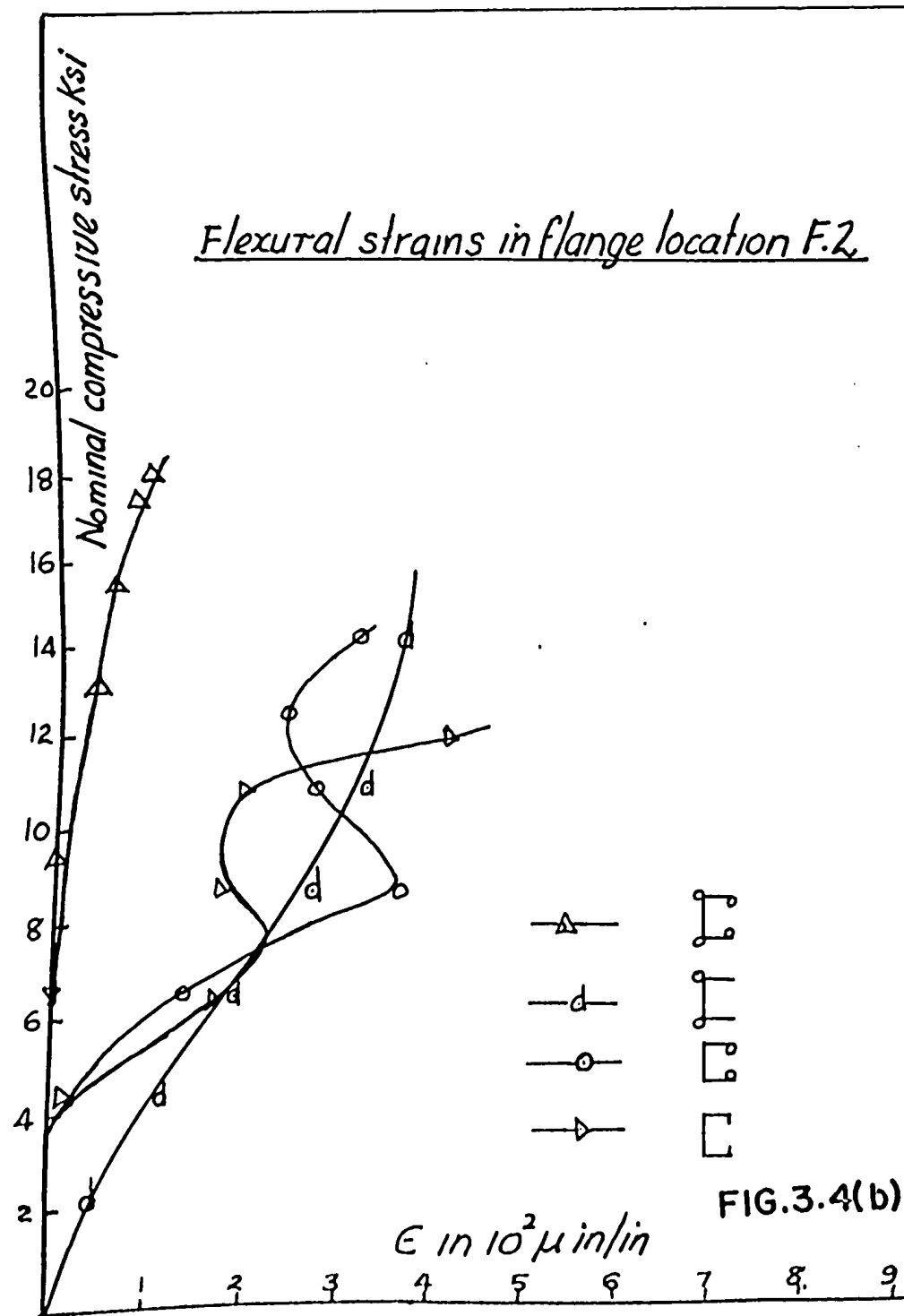
Strain Levels at web location W1.

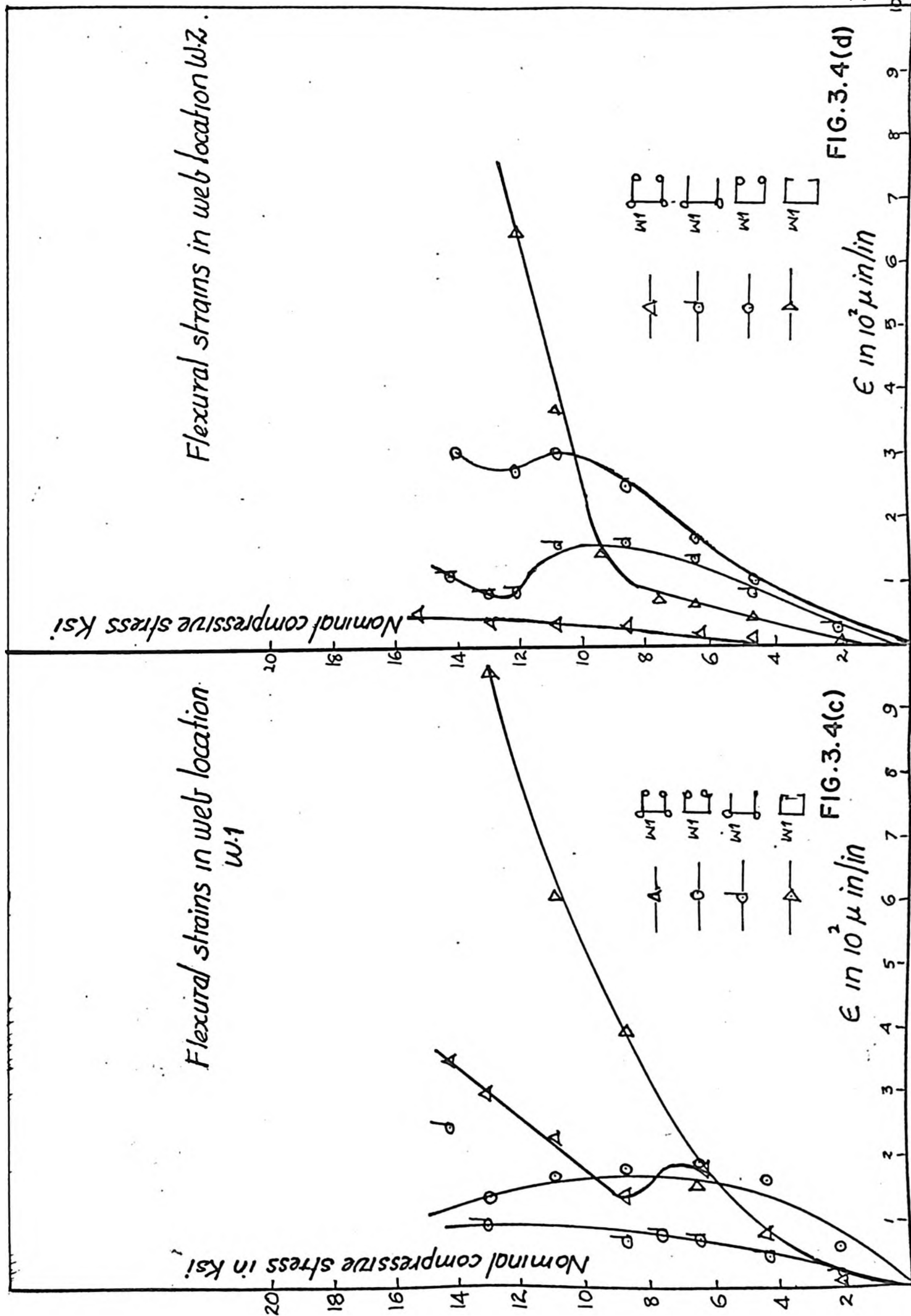


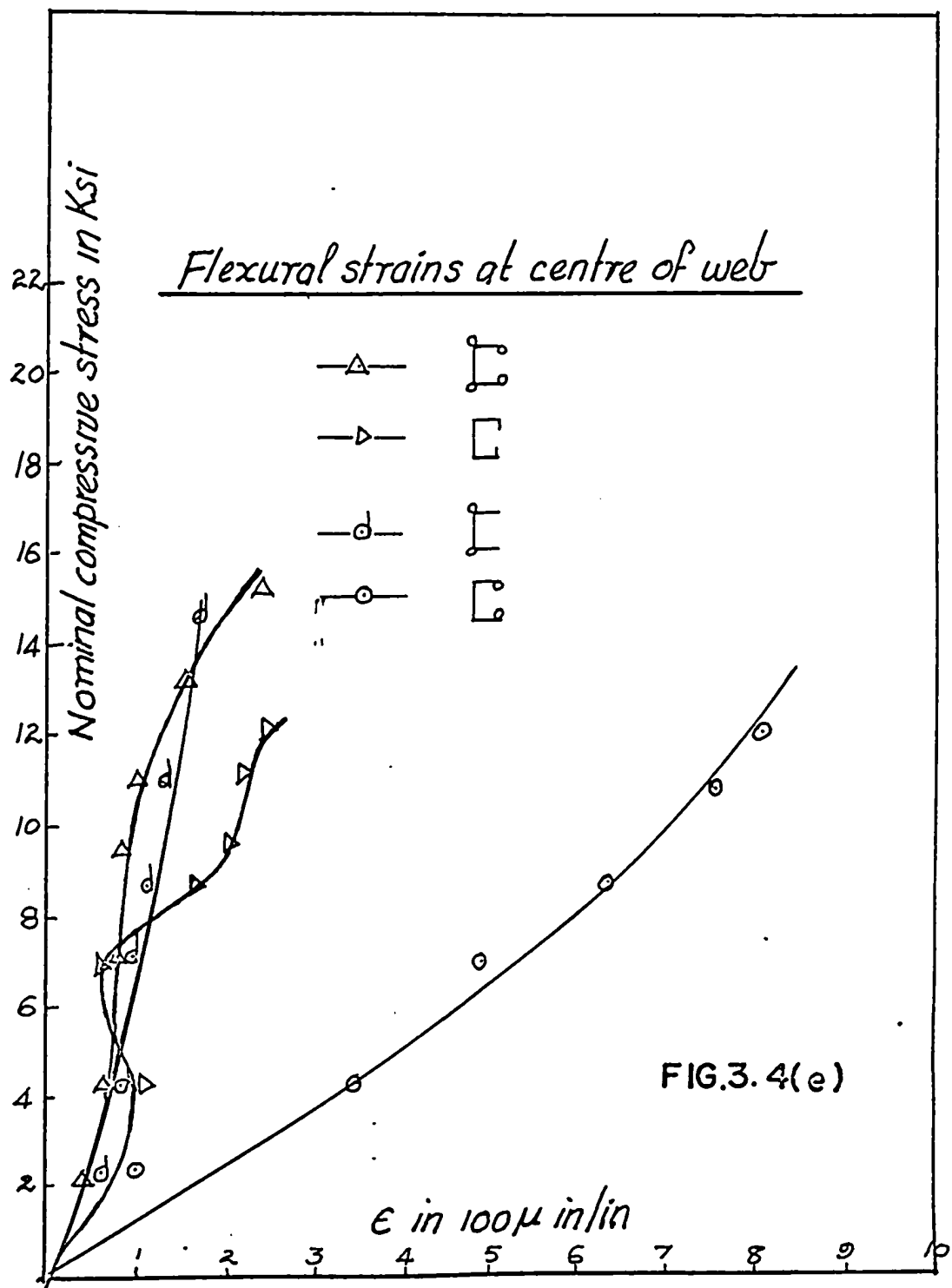


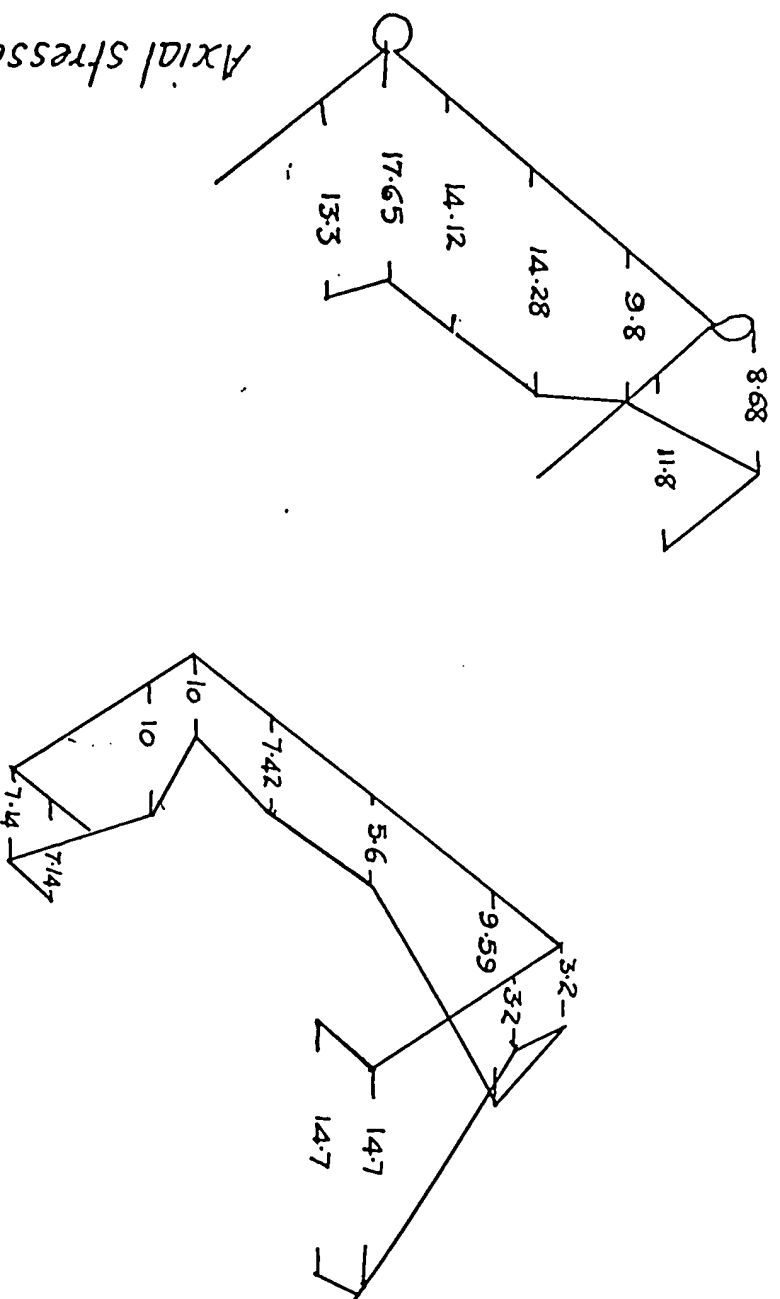
Strain levels at the centre of web











Axial stresses in cross sections  
at  
Nominal compressive stress 8.72 Ksi

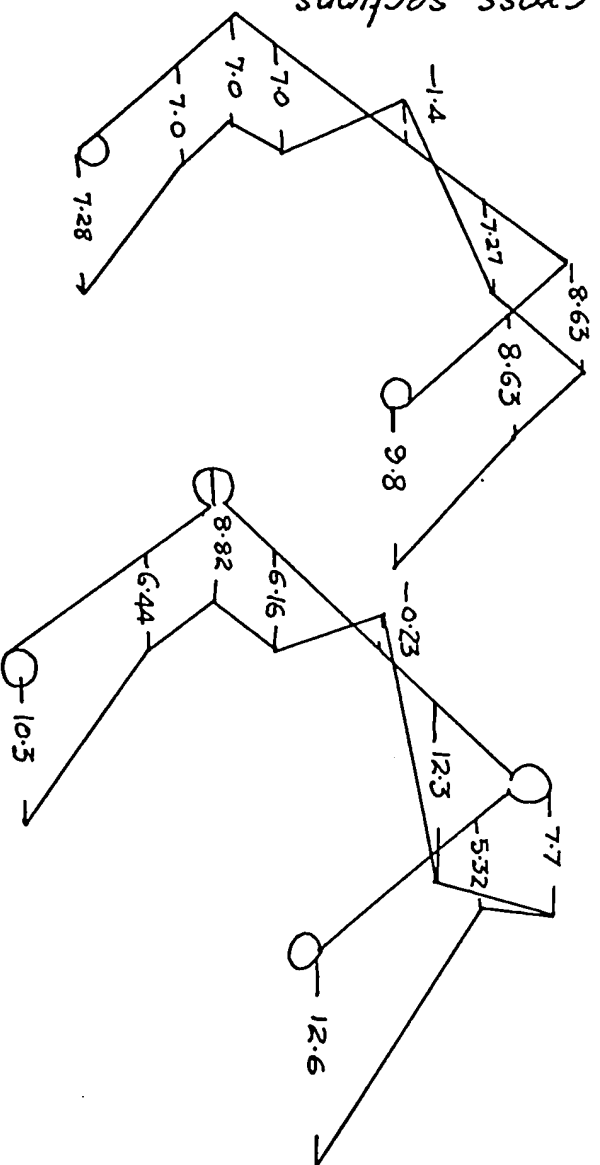


FIG. 3.5(a)



FIG.3.5(b)

Axial stresses in cross sections  
at  
Nominal compressive stress 10.9 Ksi

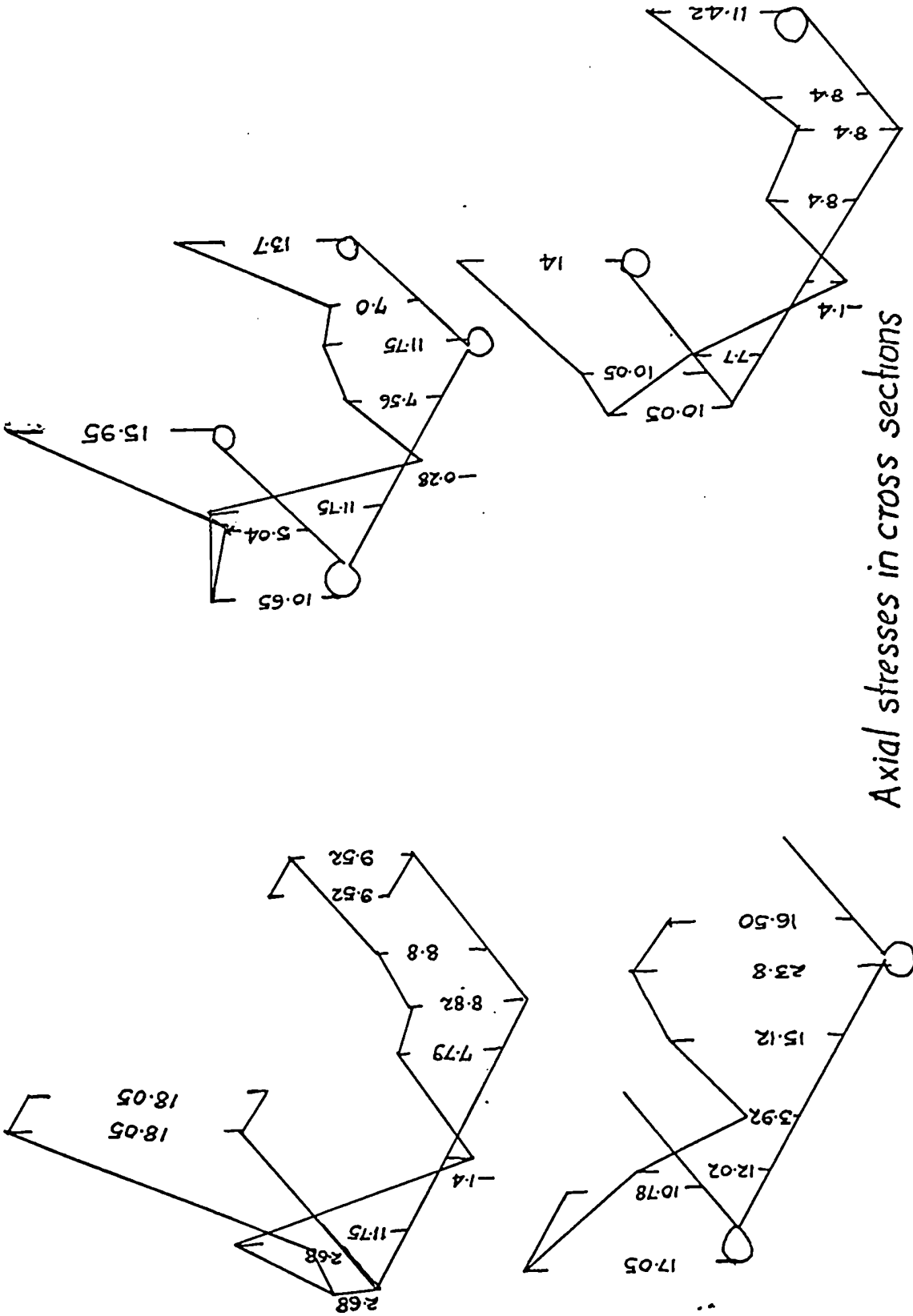






Table 3.2

Section	"p" Degrees	"δ <sub>M</sub> " Inches
	0.06	0.117
	0.23	0.028
	0.29	0.067
	0.12	0.072

movement has a disconcerting appearance. A movement of up to 3 times the plate thickness may go unnoticed, and this was not exceeded until about 80% of the load capacity was reached. Final buckling of plates at failure, occurred generally at locations other than midheight of the section, where strain gauges have been mounted.

3.7 Figs. 3.4(a to e) show flexural strains in various flange and web locations. The meandering shape of the curves indicates the changes from one mode of buckling to the other. These changes are not occurring at the same nominal compressive stress in all cases, but occur at various stress levels differing from each other. The least flexural strains at flange positions F1 and F2 occur in a 4 bulbed channel. Because of the waviness of the curves we cannot conclude whether any flange location always displays greater strains than the rest in flexure. The same conditions also exist in the flanks of the web W1 and W2. The centre of the web W1 has a low level of flexural strain in all cases except in the channel with stiffening bulbs in the flanges, in which case the strains are 4 times as large as in the rest of the sections at this location. (Fig. 3.4e).

Stiffening of the flanges with bulbs appears to be preferable to using straight lips, because the straight lips themselves get into a number of half waves whereas the bulbs remain straight until they buckle into a half wave just prior to the ultimate load.

It has been suggested<sup>13,14</sup> that the strength of a stiffened sheet may be approximately computed as the sum of the strength of the stiffeners

and of the individual sheet panels. The bulbs, which remain straight, experience greater intensities of stress than the buckled flanges and webs which take up comparatively smaller stresses. The above study of flexural strains serves as a measure of buckling in the web and flange plate elements in various sections. Experimental values of flexural strains for such thin walled sections stiffened with bulbs, have not been presented earlier elsewhere. Larger number of tests may reveal a consistent pattern of behaviour in these sections, conclusively. The present tests do not reveal any consistent trends that could be generalised.

3.8 Table 3.3 gives comparative longitudinal direct strain levels at various flange and web locations, taking strain at the web or flange bulb as the basis of comparison. The following can be observed from the Table 3.3. In the following, strain at F1 is referred to as  $\epsilon_{F1}$ , and at B1 as  $\epsilon_{B1}$  and so on.

- i) As nominal stress increases the ratios  $\frac{\epsilon_{F1}}{\epsilon_{B1}}$ ,  $\frac{\epsilon_{F2}}{\epsilon_{B4}}$ , etc. decrease.

Hence at higher stress levels the bulbs bear a much higher proportion of the axial strains. Since the order of strains measured is well within the elastic range, virtually in all cases we can conclude that stress levels at bulbs increase more rapidly than at other locations. This means a proportionately larger part of the load is borne by the bulbs at higher levels of loading.

- ii) At the stress level, 10,000 and 12,000 psi the ratios are mostly

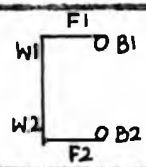
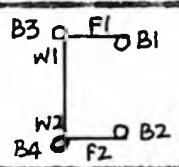
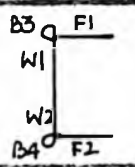
Strain ratios									
	5000 psi	10,000 psi	12,000 psi	5000 psi	10,000 psi	12,000 psi	5000 psi	10,000 psi	12,000 psi
$\frac{\epsilon_{F1}}{\epsilon_{B1}}$	1.46	0.784	0.633	0.80 0.692	0.67 0.7775	0.556 0.755	-	-	-
$\frac{\epsilon_{F2}}{\epsilon_{B2}}$	1.54	0.915	0.62	0.94 0.78	0.552 0.609	0.473 0.5425	-	-	-
$\frac{\epsilon_{F1}}{\epsilon_{B3}}$	-	-	-	0.686 1.50	0.413 1.125	0.33 1.088	0.90	0.679	0.5925
$\frac{\epsilon_{W1}}{\epsilon_{B3}}$	-	-	-	0.94 1.16	0.8375 0.786	0.733 0.81	0.95	0.774	0.6420
$\frac{\epsilon_{F2}}{\epsilon_{B4}}$	-	-	-	0.89 0.603	0.632 0.50	0.54 0.445	0.839	0.6975	0.6375
$\frac{\epsilon_{W2}}{\epsilon_{B4}}$	-	-	-	0.764 0.6475	0.624 0.3682	0.60 0.349	0.806	0.6575	0.575

Table 3.3

less than unity showing that the largest stress intensities occur at the bulbs. However, at a lower nominal stress level, 5,000 psi, bulbs have smaller stress levels in the channel with flange bulbs only. In the channel with 4 bulbs also one flange and one web location show higher stress levels than the bulb. Since these points are not consistent with the general trend it could be that they are affected by residual stresses. Hence the distribution of residual stresses across the cross section may have to be studied in detail by employing slicing techniques. Yielding due to combined direct and flexural stress always occurred at points other than the bulbs, and caused failure of the whole section. This demonstrates the effectiveness of the bulbs.

In most of the test specimens with bulbs it was observed that the strains measured in the bulbs were consistently larger than those in the web and flange plates. However, the flange shown was recorded as being higher than bulb strain in one of the channels with 4 bulbs. This may be due to the distortion undergone by the flange bulb. The bulb strain could be measured with only one strain gauge on the outer surface of the bulb, and the readings could have been vitiated by even the slightest bending of the bulb. A single strain gauge can give longitudinal strain, only if it is mounted along the neutral surface of the bulb section. The strain gauges were mounted on the bulb at a point farthest from the web, i.e. the outer terminal of the diameter of the bulb parallel to the XX axis. This was considered adequate as lateral buckling was anticipated across the XX axis, and the gauge would then be at the neutral surface. But the curves relating bulb strain to the nominal compression in the section are not straight as they would have been if the gauges were exactly at the neutral

surface of the bulbs or lips.

3.9 To determine the Young's Modulus of the material of the channel sections, three coupon tests were conducted which yielded an average value of  $28 \times 10^6$  psi for E and a static tensile yield stress of 40,450 psi. Fig. 3.7 shows the Tangent modulus corresponding to various stress intensities in the transitional range between the limit of proportionality and the static yield. As can be seen on the figure, these are also based on the static values of the stresses at a given strain.

3.10 In analysing stiffened plates, in a semi-empirical manner, a part of the plating adjoining the stiffeners has been assumed to act with the stiffener in resisting axial loading. Codes of practice in Britain, U. S. A. and elsewhere have laid down rules for computing effective widths of plating adjacent to stiffeners. The ratio of effective width to the total width of plating in the cross section has been related to the non-dimensional factor " $\frac{t}{b} \sqrt{\frac{E}{\sigma}}$ ", or " $\frac{b}{t} \sqrt{\frac{\sigma}{E}}$ ". In the present case, at every nominal stress level, the effective width of flange and web plates was computed as that needed to sustain the axial load at a stress equal to the average stress in the bulbs or lips. It should be borne in mind that these bulbs and lips experience the largest stresses. These values of effective width can be compared to the winter curve<sup>15</sup> at present adopted by the American Institute of Steel Construction. The curve is based on the formula:

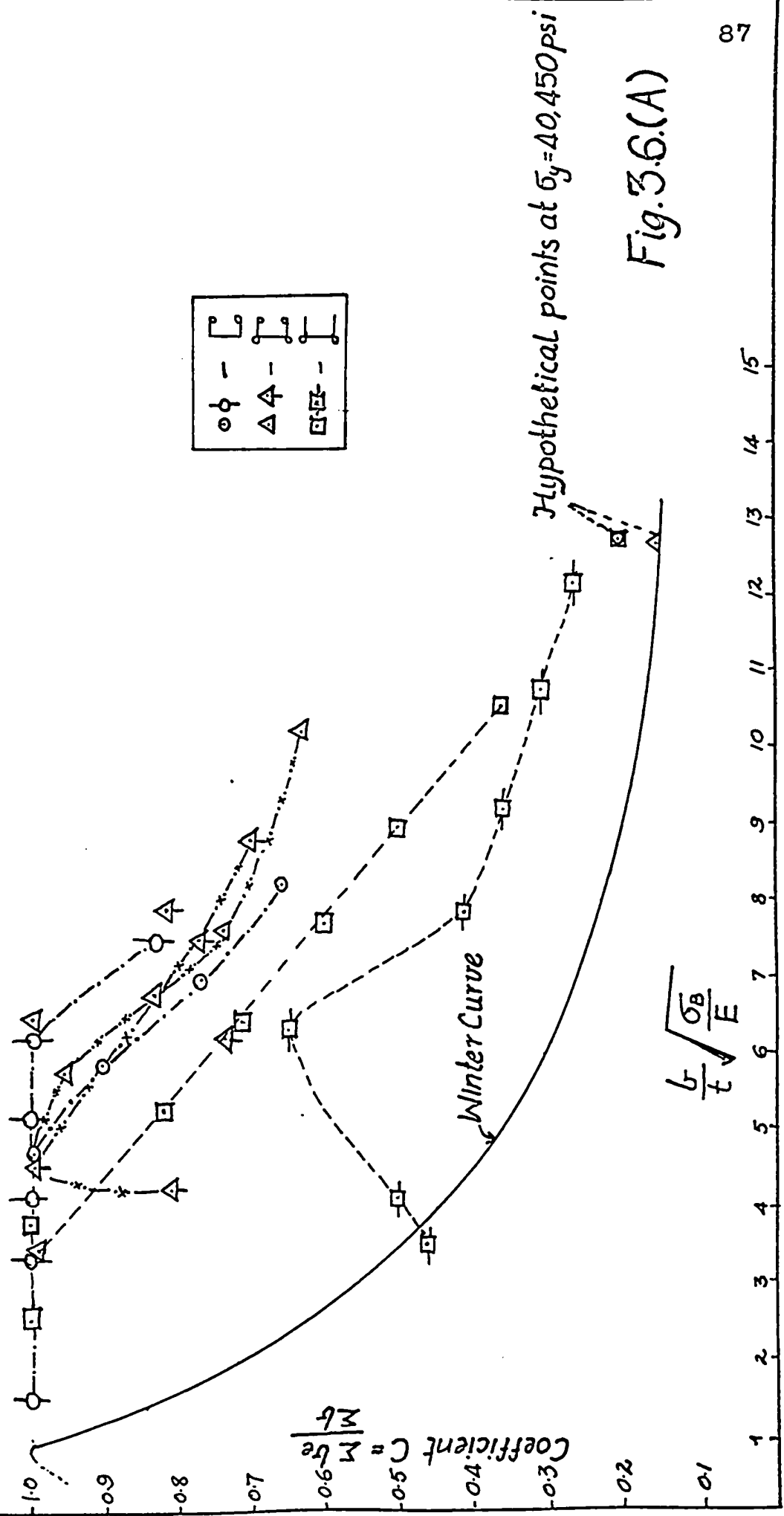


Fig. 3.6.(A)



$$\frac{b_e}{b} = 1.9 \frac{t}{b} \sqrt{\frac{E}{\sigma}} \left( 1 - 0.475 \frac{t}{b} \sqrt{\frac{E}{\sigma}} \right) \quad (3.1)$$

where  $b_e$  = effective width of flange and web plates

$b$  = total widths of flange and web plates

$E$  = Young's Modulus

$\sigma$  = maximum stress in section

$t$  = thickness of plate

applicable within limits of " $\frac{t}{b} \sqrt{\frac{E}{\sigma}}$ " between 0.2 and 0.6. The original formula proposed by Winter was of the form below; yielding lower effective widths than formula 3.1.

$$\frac{b_e}{b} = 1.9 \frac{t}{b} \sqrt{\frac{E}{\sigma}} \left( 1 - 0.574 \frac{t}{b} \sqrt{\frac{E}{\sigma}} \right) \quad (3.2)$$

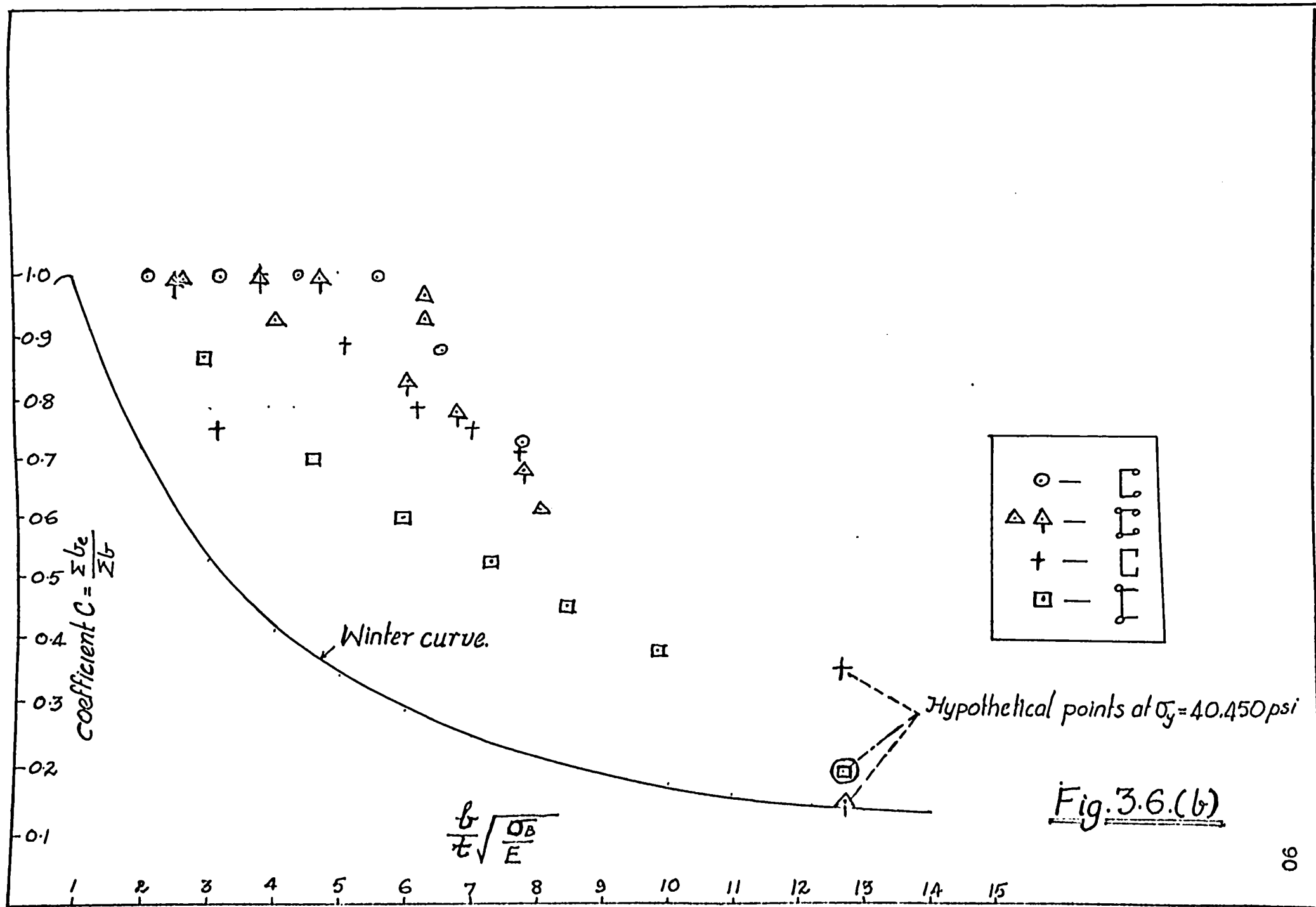
The non-dimensional parameter " $\frac{b}{t} \sqrt{\frac{\sigma}{E}}$ " covers the effect of thickness of the sheeting in relation to width, and also includes the buckling characteristic. That is the reason why investigators into this field have used this parameter as a convenient variable. In the present series of tests the lower limit of the parameter " $\frac{b}{t} \sqrt{\frac{\sigma}{E}}$ " was as low as 0.0835, and as high as 0.668. The Winter curve is recommended for use in the range of " $\frac{t}{b} \sqrt{\frac{E}{\sigma}}$ " 's, 0.2 to 0.6, because, below a ratio of 0.2 the intensity of stress will be very high and the effective widths obtained from the formula may not be realised; also when " $\frac{t}{b} \sqrt{\frac{E}{\sigma}}$ " is 0.6 and

above the stress is so low that the whole section is deemed to be effective.

Figs. 3.6(a) and (b) have been made from the experimental results. Fig. 3.6 (a) gives the points plotted considering the individual bulb or lip separately in the various sections. The values of parameter " $b/t \sqrt{\sigma/E}$ " in Fig. 3.6(a) are plotted for each lip or bulb at various nominal stresses. Fig. 3.6(b) relates to the average values for the lips and bulbs at various nominal stress levels. In both figures the constant "C" which defines the effective width of the section in relation to the total width of plating in web and flanges, has been plotted for varying values of the non-dimensional parameter " $b/t \sqrt{\sigma/E}$ ". The non-dimensional constant "C" is derived from the following relationship:

Effective width of section = Developed width of bulbs + C (Total width of flange and web plate).

In this relationship, the thickness of the sheeting "t" has been eliminated since it is uniform. The effective widths, therefore, are in the same proportion as the effective areas of the section. In Fig. 3.6(a) and (b) the Winter curve is plotted alongside for convenient reference. All the points from the tests lie above the Winter curve showing that Winter's proposals are conservative. Also shown on the same two figures are three points, corresponding to three different sections, plotted to indicate the values when the stress at the bulbs reaches the yield stress for the material, viz. 40,450 psi. These three points are hypothetical since stresses recorded in the bulbs just prior to failure were less than the yield stress, and failure was caused by yield at a section where strain gauges were not provided. The trends observed in these curves are similar



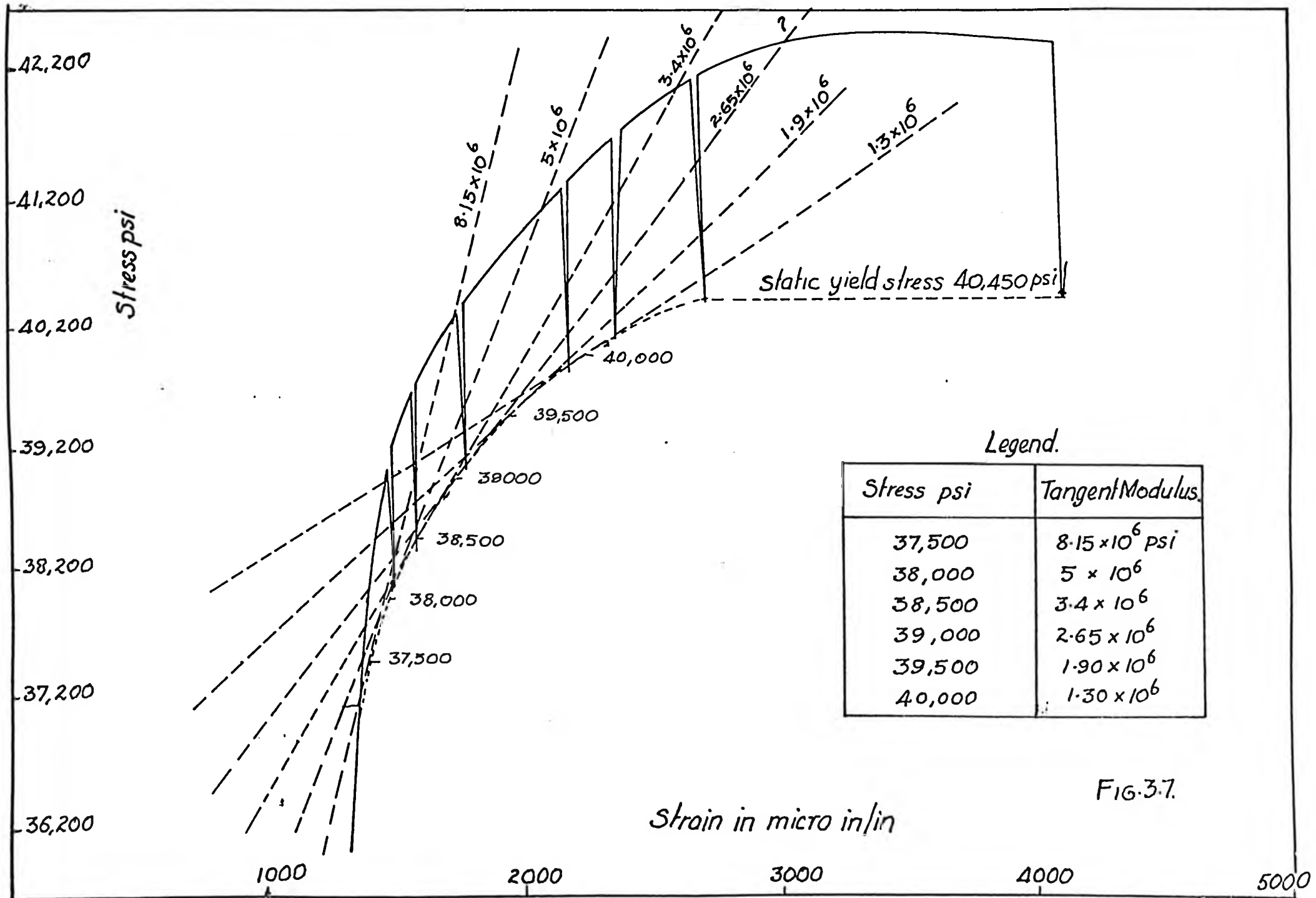


FIG. 3.7.

to those reported by earlier investigators.<sup>16</sup> It is to be noted that the points are generally located higher than the Winter curve, giving a greater effective width than anticipated by Winter. This could be a distinct feature of such thin sheets like the present one (0.0239"), and could be exploited more fully than at present. Lewis<sup>6,7</sup> points out tests carried out on corrugated steel sheet panels yielding test results which are far above the Winter curves. The "b/t" ratio of the section tested by Lewis was 250, compared to 75 which is normally allowed by building codes for load bearing members. At this value of "b/t" (75), the test results would be expected to be closer to the Winter curve. The "b/t" ratio of the sections in the present series of tests is 335, much larger than even the value for the roof cladding referred to.<sup>6,7</sup>

3.11 To determine whether the strain gauge readings on the whole represent the state of overall strain and stress in the section accurately, the following comparison was made. The average strain in the longitudinal direction was taken as the average of all the measured longitudinal strains at a given nominal stress. The stress corresponding to the average strain recorded was then compared to the nominal stress, which is obtained by dividing the load by the cross sectional area of the strut. Table 3.4 contains figures pertaining to two different nominal stress levels.

The section with no flange bulbs, the last one in Table 3.4 indicates that more gauges in the outstanding flanges would be necessary, so that the low strains on these may bring down the average of the strains

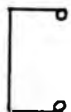
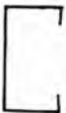


Section	Nominal Stress Level ksi	Stress level as computed from the aver- age of record- ed strains ksi
	10.9 8.72	8.367 6.51
	10.9 8.72	8.17 8.22
	10.9 8.72	9.12 7.71
	10.9 8.72	14.17 12.80

Table 3.4

measured. In the channel with straight lips, the average measured values are smaller than the nominal stress. This would indicate that more gauges should have been located in the vicinity of the corners. In the above tests, gauges were placed 1" from the corners, it being assumed that the influence of edge restraint could be adequately measured at this position, which is only  $1/8$  of the web width away from the corner.

The corners in the sections with no bulbs constitute boundaries between the web and the flange plates, which have different aspect ratios, and go into different modes of buckling as the loading advances. In a strictly physical sense, compatibility demands that the stress at the corner could have only one value, and this could be read by mounting a gauge right at this position. In the sections with corner bulbs, the gauges will have to be always provided as these stiffeners constitute a distinct and separate structural part of the cross section.

3.12 From what has been observed during the tests it would be reasonable to assume that bulbs are fully effective until failure is caused by the yield stress being reached at some point in the cross section; and that parts of the web and the flange plates adjacent to the bulb make a partial contribution to the ultimate strength. It is concluded that many more strain gauges at closer spacing will be required to obtain a better evaluation of variation of stress in the cross section.

Table 3.5 shows the various values of "C" for the different sections taking a yield stress of 40,450 psi as the basis of the calculation. The thickness of the sheeting has been eliminated as before and reference is

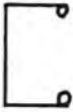
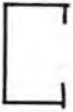
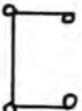

Section	Load lbs.	Total width to sustain load at 40,450 psi	Developed width of bulbs	Total area of plates only	"C"
	6600	6.4"	3.142"	16"	0.203
	5600	5.79"	-	16"	0.362
	8500	8.8"	6.283"	16"	0.157
	6600	6.4"	3.142"	16"	0.203

Table 3.5

(These values of "C" are shown on Fig. 3.6 at " $\frac{b}{t}\sqrt{\frac{\sigma}{E}} = 12.70$ ", and constitute a minimum value for the effective width at the hypothetical maximum load.)



made to widths alone. It should be noted that the coefficient "C" applies only to the effective width of the plates and does not include the developed width of plating in the stiffening elements such as circular or triangular lips. Circular lips on the web or the flange are considered fully effective to the last.

## CHAPTER IV

### COMPARISON OF EXPERIMENTAL RESULTS WITH THEORY

4.1 Theoretical analysis had indicated that the channels considered would fail by overall torsional flexural buckling. All the channels tested failed by local buckling.

4.2 Analytical study placed the sections in the following descending order of strength, the criterion being the value of  $(R_E^2/\Lambda_w)$  in each case:

- i) Channel with 4 bulbs
- ii) Channel with 2 bulbs at the ends of the flanges
- iii) Channel with triangular lips
- iv) Channel with straight lips
- v) Channel with bulbs at the junctions of web and flanges only.

Based on the test results, the following is the descending order of strength of the sections:

- i) Channel with 4 bulbs
- ii) { Channel with 2 bulbs at the ends of the flanges  
Channel with bulbs at the junctions of web and flanges
- iii) Channel with triangular lips
- iv) Channel with straight lips.

It may be seen that the channel with bulbs at the junction of web and flanges is stronger than predicted by theory. One possible explanation may be that due to the heavy flange buckling even at small loads, the web shares most of the load. This was indicated in the tests by larger web strain levels. Winter recommends that the strength of an unstiffened flange should be totally ignored. It may be also that the dimensions 8" x 4" with 1/2" bulbs, results in nearly the same strength for channels with and without flange bulbs. This could be a coincidence. Only tests with channels of different dimensions, and different ratios of web to flange can establish the superiority of the one or the other.

4.3 Table 4.1 shows the comparative theoretical and experimental strengths, the strength of a straight lipped channel being assumed to be unity. The probable causes for the discrepancy between theory and the tests are discussed in the following paragraph.

4.4 All the specimens were tested with their ends flat on the machine platens. In the analysis, the equivalent radius of gyration refers to primary overall buckling. Since this was not the mode of failure actually observed in the tests, the change of mode from primary to local buckling could cause the discrepancy between theory and test results. If sections of larger slenderness ratio than in the present series were tested with their ends pinned or fixed, primary buckling would have ensued, and there would probably be greater agreement between the analytical and experimental strengths.

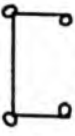
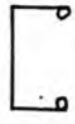
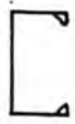
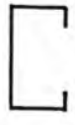
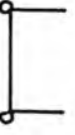
Section	Strength		
	Theoretical based on $R_E^2$ per unit width	Observed in tests	No. of tests
	1.245	1.519	6
	1.185	1.179	5
	1.113	1.16	2
	1.0	1.0	2
	0.9025	1.179	3

Table 4.1

## CHAPTER V

### CONCLUSIONS

5.1 The tests conducted so far have shown that an 8" x 4" channel with 1/2" bulbs at the ends of flanges has greater strength than a similar channel with plain lips, the cross sectional area of both the sections being the same. The bulbed channel has 17.8% greater ultimate strength than the lipped channel. The channel with four bulbs and the lipped channels can be compared by observing the ultimate load borne per unit width of the centre line of the plates in the cross section. This comparison shows the bulbed channel with four bulbs has 30% more ultimate load per unit width of cross section than the channel with straight lips. Channels with web bulbs only also proved to be 17.8% stronger than plain lipped channels. Channels with triangular lips are 16% stronger than plain lipped channels of the same cross sectional area.

5.2 The rotation of the midsection was less than half a degree. The failure was definitely in local buckling. The maximum out-of-plane displacement of web amounted to 4.9 times the plate thickness. Up to 80% of the ultimate load the out-of-plane deformation remained within twice the plate thickness.

5.3 Stiffening elements of triangular or circular shape have been found to be superior to straight lips in enhancing the strength of a channel.

5.4 The values of the coefficient "C" defining the effective width in relation to the parameter " $b/t\sqrt{\sigma/E}$ ", are all above the curve proposed by Winter. The trends in the results show that the effective width concept could be applied to the type of sections under consideration.

5.5 The variation in effective width is dependent on the shape of the stiffening elements.

5.6 Ultimate strength of such sections is a function of the position of the stiffening bulb or lip, and its shape.

## CHAPTER VI

### SUGGESTIONS FOR FURTHER RESEARCH

6.1 From the experience gained from the present investigations the following suggestions for further research are made in order of importance, in the following paragraphs.

6.2 The present series of tests have shown that it will be necessary to test similar sections over greater lengths or sections with smaller cross sectional dimensions over the same length, so that regions of local and overall buckling may be defined by the slenderness ratio, and the thinness ratio " $b/t$ ". The results of these tests could be plotted as functions depending upon the parameter " $L/R_E \times t/b$ ", which could simultaneously take into account both primary and local buckling. These tests should be carried out with the ends of the strut fixed in position and direction. This would enable comparison with the conventional theory based on overall buckling, and would also enable determination of the critical load by the Southwell method. But, where there is local buckling the end conditions are not likely to influence the results significantly. As we cannot determine, at the outset, whether buckling would be primary or local, it would be advisable to presume primary buckling would take place and to make the ends of the struts either fully fixed or pinned.

Should local buckling occur the difference between different end conditions need not be emphasized.

6.3 Since residual stresses are known to precipitate yielding at some points, and generally tend to distort the stress distribution due to superimposed loading, it would be desirable to measure the nature and magnitude of residual stresses by applying slicing techniques.<sup>12</sup> The determination of these residual stresses would give the true stress carried due to loading alone at various points, and could be used for comparison between similar sections, with identical shapes, but with varying metal thicknesses and bulb diameters. Hardening of the material at the corners and bulbs may also influence the stress distribution. Hardening up to 40% over the rest of the section has been reported.<sup>7</sup> Whether this has any direct effect on the test results is a topic for further research. Work hardening in thin sheets is yet to be investigated in detail, and work is progressing at Cornell University, and elsewhere.

6.4 In the present series the sheet used was U.S. gauge 24 of thickness 0.0239". This was chosen as it was readily available and could be formed into the required shapes with a brake press available in the laboratory. Further tests will be more helpful if the sheeting is of any of U.S. gauges 10-14, which is likely to be more acceptable from the point of view of the building codes. Since the flexural rigidity of a plate is directly proportional to the cube of its thickness, thicker sheets



may experience much less out-of-plane deformation than in the present case.

6.5 For the purpose of arriving at some form of design recommendation for such bulbed sections it would be necessary to test sections with the same overall dimensions, but made up of varying sheet thicknesses. This would lead to a more precise determination of the influence of sectional geometry on the crippling strength. For a given thickness of sheeting different overall dimensions may be tried keeping the ratio of web to flange, and the ratio of the radius of bulb to the flange width constant in each case, or in other words, conduct tests on geometrically similar sections. This would pin-point the significance of the thinness ratio " $b/t$ ".

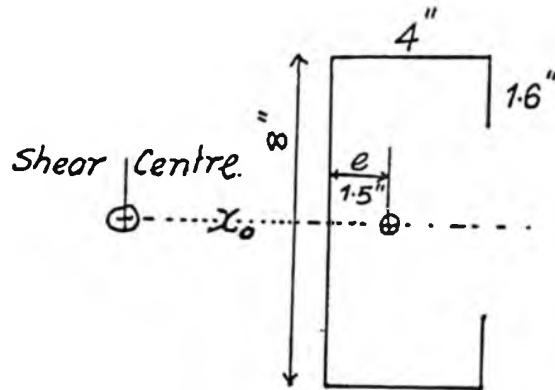
6.6 With regard to instrumentation, in future tests it is recommended that a larger number of strain gauges be used over the cross section in general. In particular, gauges should be closely spaced together in the vicinity of bulbs and lips, and corners. If foil strain gauges of smaller sizes are used, it should be possible to mount gauges as close as  $1/4$ " apart from one another, and at other parts of the cross sections position them at intervals of  $1/2$ ". It is felt this would enable a closer evaluation of the effective widths of the individual flange and web components.

## REFERENCES

1. Wagner, H., Verdrehung und Knickung von offenen Profilen, 25th Anniversary Publication, Technische Hochschule, Danzig, 1904-1929, H.A.C.A. translation Tech. Mem. 807, 1936.
2. Bleich, F., Buckling Strength of Metal Structures, McGraw Hill, 1952.
3. Ostenfeld, A., Politeknisk Laereanstalts Laboratorium for Bygningsstatik, Meddelelse No. 5, Kopenhagen, 1931.
4. Kappus, R., Drillknicken zentrisch gedruckter Stabe mit offenem Profil im elastischen Bereich-Luftfahrt-Forschung, 1939, Translation H.A.C.A. Tech. Mem. 851, 1938.
5. Lundquist, E. E., and C. K. Fligg, A Theory for primary failure of straight centrally loaded columns, H.A.C.A. Tech. Rept. 582, 1937.
6. Chilver, A. H., Structural Problems in the use of cold formed steel sections, Proceedings of the Institution of Civil Engineers, London, October, 1961, Vol. 20, pp. 233-257.
7. See also discussion on above in Proceedings of the Institution of Civil Engineers, London, October, 1962, Vol. 23, pp. 270-297.
8. Kollbrunner, C. F., and Meister, H., Knicken, Biegedrillknicken, Kippen, Springer-Verlag, Berlin, 1961.
9. Winter, G., Chajes, A., Gergely, P., Progress reports on Torsional Flexural Buckling of Thin wall open sections. First report,

- July, 1963, Second report, Nov. 1963, and Third report, Feb. 1964. American Iron and Steel Institute, New York 17.
10. Kollbrunner, C. F., and Meister, H., *Ausbeulern*, Springer Verlag, Berlin, 1958.
  11. Timoshenko, S. P., and Gere, M., *Theory of Elastic Stability*, 2nd Edition, McGraw Hill, 1961, pp. 411-419.
  12. Beedle, Lynn S., and Tall, L., "Basic Column Strength", *Journal of the Structural division of the Proceedings of the American Society of Civil Engineers*, July 1960, pp. 139-173.
  13. Gall, H. W., *Compressive strength of stiffened sheet panels*, 1930, reported by J. S. Newell. *The strength of Aluminium alloy struts*, *Airway Age*, 1930.
  14. Schuman, L., and G. Back, *Strength of rectangular flat plates under edge compression*, N.A.C.A. Tech. Report 356, 1930.
  15. Winter, G., *Performance of thin steel compression flanges*, Prelim. publication 3rd Congress. International Association for Bridge and Structural Engineering, Liege, 1948, p. 137.
  16. Gerard, G., *Introduction to Structural Stability Theory*, McGraw Hill, 1962, p. 76.

## APPENDIX A (SAMPLE CALCULATIONS)



$$\text{Distance of centroid from web} = \frac{2(4 \times 2) + 3.2 \times 4}{19.2} = 1.5''$$

Moment of inertia about xx axis =

$$= \frac{8^3}{12} + 2 \times 4 \times 4^2 + \frac{2}{12} \times 1.6^3 + 2 \times 1.6 \times 3.2^2 = 204.09 \text{ in}^4$$

$x_0$  = Distance between centroid and shear centre

$$= (1.6 \times 2.5 \times 3.2 \times 1.6 \times 2 + 2 \times 128 + \frac{1.5}{3} \times 8^3) / 204.09 = 2.71''$$

$$I_{yy} = \frac{2}{12} \times 4^3 + 8 \times 1.5^2 + 2 \times 1.6 \times 2.5^2 = 48.667 \text{ in}^4$$

Polar moment about shear centre  $I_p$

$$= 204.09 + 48.667 + 19.2 \times x_0^2 = 393.76 \text{ in}^4$$

Polar radius of gyration about shear centre  $R_0$

$$= \sqrt{\frac{393.76}{19.2}} = 4.53''$$

$$R_x = 3.26'' \quad R_y = 1.59''$$

$$\text{Warping constant } \Gamma = \frac{d^2}{4} \left[ I_y + e^2 A \left( 1 - \frac{d^2 A}{4 I_{xx}} \right) \right]$$

$$= 16 \left[ 48.67 + 2.25 \times 19.2 \left( 1 - \frac{16 \times 19.2}{204.09} \right) \right] = 449.12 \text{ in}^6$$

$$L = 36'' \quad t = 0.0239 \quad t^3 = 0.0239^3 \text{ very small}$$

$R_\beta$  = Equivalent radius of gyration for torsion only

$$= \sqrt{\frac{\Gamma}{I_p} + \frac{0.013 t^3 L^2}{I_p}} \quad L = \frac{36}{4} = 9$$

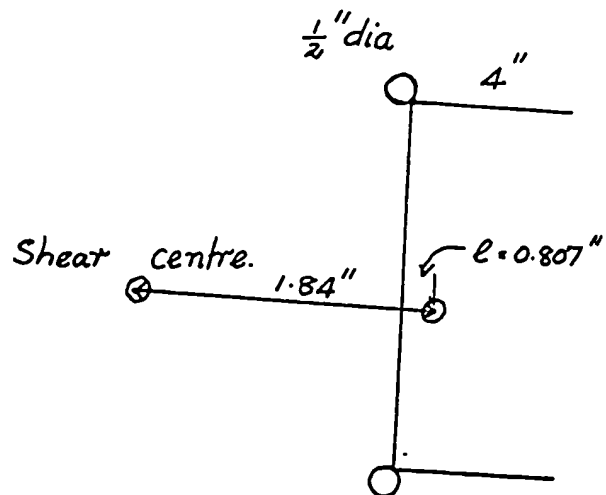
$$= \sqrt{\frac{449.12}{393.76} + \frac{0.0130 \times 0.0239^3 \times 81}{393.76}} = 1.068''$$

$R_E$  = Equivalent radius of gyration for torsion and flexure.

$$= \sqrt{\frac{(\gamma_\beta^2 + \gamma_y^2) - \sqrt{(\gamma_\beta^2 + \gamma_y^2)^2 - 4\gamma_\beta^2 \gamma_y^2 \left(1 - \frac{Ax_o^2}{I_p}\right)}}{2\left(1 - \frac{Ax_o^2}{I_p}\right)}}$$

$$= \sqrt{\frac{3.675 - \sqrt{3.675^2 - 4 \times 2.89 \times 0.642}}{1.284}}$$

$$= \underline{\underline{0.973''}}$$



$$e = 0.807''$$

$$I_{xx} = 225.466 \text{ in}^4$$

$$I_{yy} = 29.338 \text{ in}^4$$

$$R_y = 1.239''$$

$$x_0 = 1.84''$$

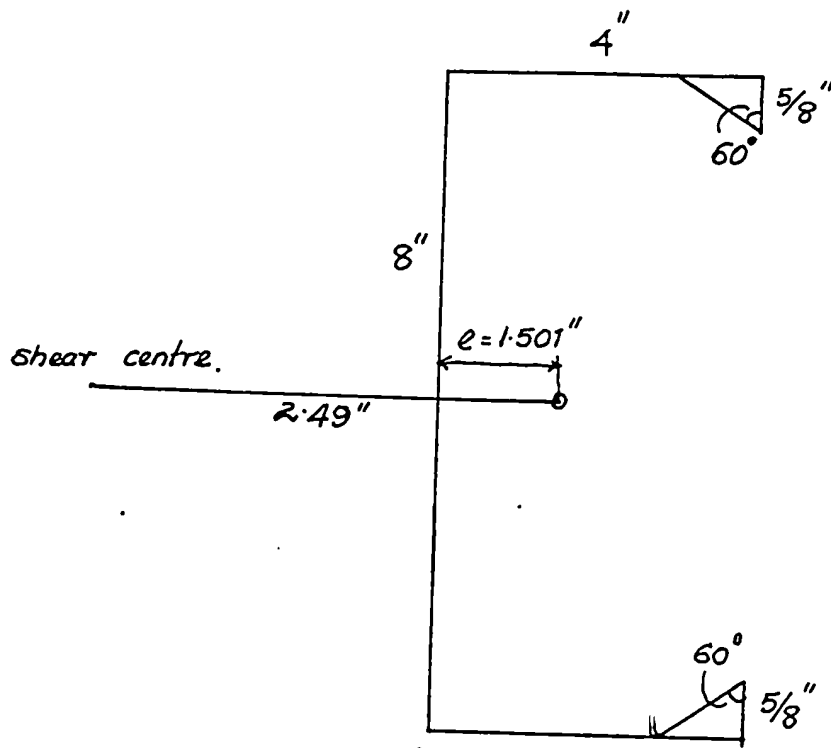
Warping constant  $\Gamma = 398.24 \text{ in}^6$  per unit thickness

$$I_p = 319.534 \text{ in}^4 \quad R_\beta = 1.119''$$

Equivalent radius of gyration  $R_E$

$$= \sqrt{\frac{2.788 - \sqrt{2.788^2 - 4 \times 1.922 \times 0.797}}{1.594}}$$

$$= \underline{\underline{0.914''}}$$



$$e = 1.501"$$

$$I_{xx} = 221.66 \text{ in}^4 \quad I_{yy} = 48.319 \text{ in}^4 \quad I_p = 375.47 \text{ in}^4$$

$$x_o = \left( \frac{5}{8} \times 2.5 \times \frac{5}{8} \times 3.6875 \times 2 + 1.25 \times 5.7 \times 1.25 \times 3.6875 + 2 \times 8 \times 4^2 + 256 \right) / 221.61$$

$$= 2.49"$$

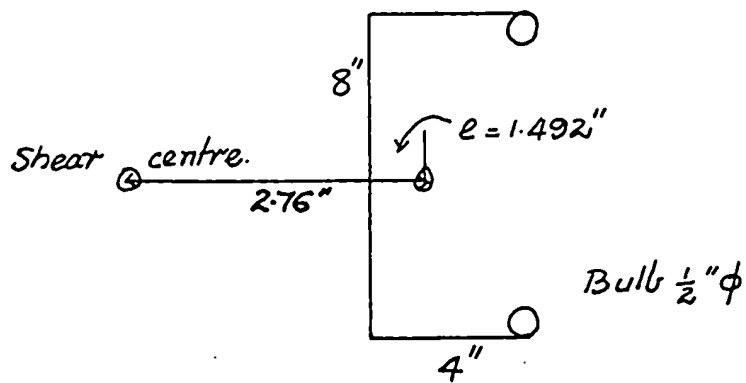
$$R_x = 3.382" \quad R_y = 1.56" \quad R_p = 1.135"$$

Warping constant  $\Gamma = 484.5 \text{ in}^6$  per unit thickness

Equivalent radius of gyration  $R_E$ .

$$= \sqrt{\frac{(R_y^2 + R_p^2) - \sqrt{(R_y^2 + R_p^2)^2 - 4R_y^2 R_p^2 \left(1 - \frac{Ax_o^2}{I_p}\right)}}{2 \left(1 - \frac{Ax_o^2}{I_p}\right)}}$$

$$= \underline{\underline{1.017"}}$$



$$e = 1.492''$$

$$I_{xx} = 214.86 \text{ in}^4$$

$$X_0 = \left( \frac{2^2 \pi^2}{4^2} \sqrt{3.5^2 + 2.508^2} \left( 3.75 \right) + 2 \times 8 \times 4^2 + 1.492 \times \frac{512}{3} \right) / 214.86$$

$$= 2.76''$$

$$I_{yy} = 52.8 \text{ in}^4 \quad I_p = 413.23$$

Warping constant  $\Gamma = 555.2 \text{ in}^6 \text{ per unit thickness}$

$$R_x = 3.448 \quad R_y = 1.664$$

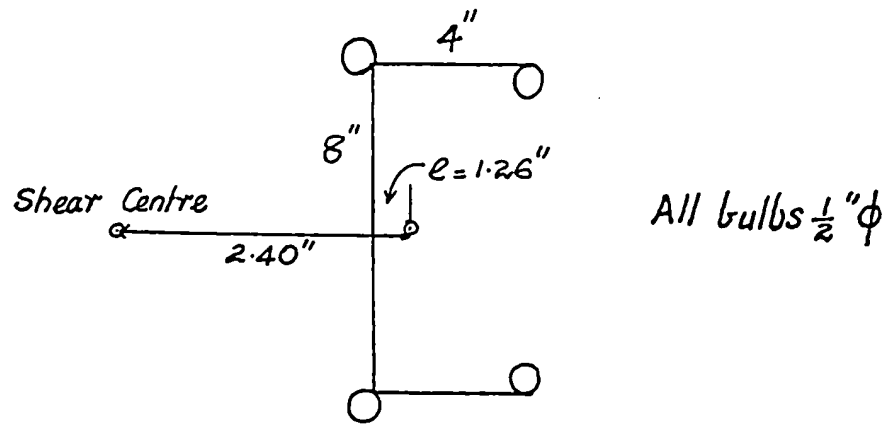
$$R_p = 1.159''$$

Equivalent radius of gyration  $R_E$

$$= \sqrt{\frac{4.112 - \sqrt{4.112^2 - 4 \times 3.719 \times 0.647}}{1.294}}$$

$$= \underline{\underline{1.05''}}$$





$$e = 1.26"$$

$$I_{xx} = 270 \text{ in}^4 \quad I_{yy} = 57.92 \text{ in}^4 \quad I_p = 456 \text{ in}^4$$

$$x_o = 2.40 \text{ in}$$

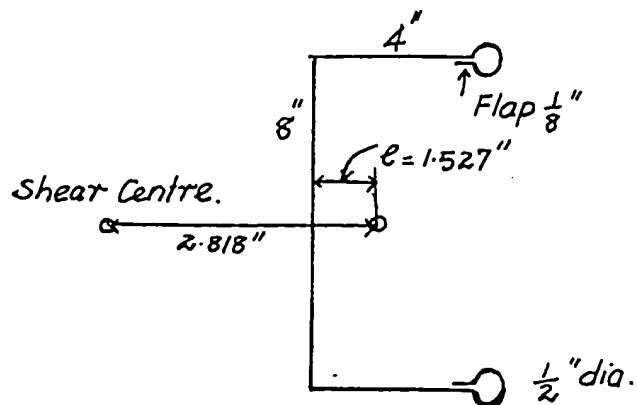
Warping constant  $\Gamma = 782.7 \text{ in}^6 \text{ per unit thickness}$

$$R_\beta = 1.31"$$

Equivalent radius of gyration  $R_E =$

$$= \sqrt{\frac{4.283 - \sqrt{4.283^2 - 4 \times 4.41 \times 0.758}}{1.516}}$$

$$= \underline{\underline{1.16"}}$$



$$e = 1.527"$$

$$I_{xx} = 224.933 \text{ in}^4 \quad I_{yy} = 54.182 \text{ in}^4$$

$$x_0 = 2.818"$$

$$I_p = 433.113 \text{ in}^4$$

Warping constant  $\Gamma = 766 \text{ in}^6$  per unit thickness

Equivalent radius of gyration  $R_E$

$$= \sqrt{\frac{4.562 - \sqrt{4.562^2 - 4 \times 4.94 \times 0.646}}{1.292}}$$

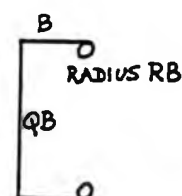
$$= \underline{\underline{1.155''}}$$

## APPENDIX B

TABLE 1

VALUES OF NON-DIMENSIONAL FACTOR GOVERNING  $R_E$ 

R	Q					Remarks
		0.5	1.0	1.5	2.0	
0.01		0.10308	0.16645	0.20657	0.23276	
0.02		0.10414	0.17136	0.21378	0.24162	
0.03		0.10192	0.17310	0.21799	0.24758	
0.04		0.09713	0.17224	0.21972	0.25118	
0.05		0.09021	0.16922	0.21940	0.25280	
0.06		0.08136	0.16438	0.21734	0.25274	
0.07		0.07045	0.15790	0.21378	0.25125	
0.08		0.05679	0.14993	0.20888	0.24850	
0.09		0.03791	0.14049	0.20279	0.24465	
0.10		0.01965	0.12951	0.19558	0.23980	
0.11		0.04689	0.11675	0.18128	0.23404	
0.12		-	0.10172	0.17790	0.22741	
0.13		-	0.08334	0.16737	0.21997	
0.14		-	0.05868	0.15557	0.21171	
0.15		-	-	0.14227	0.20262	
0.16		-	-	0.12709	0.19266	
0.17		-	-	0.10931	0.18176	
0.18		-	-	0.08739	0.16917	
0.19		-	-	0.05676	0.15651	
0.20		-	-	-	0.14166	

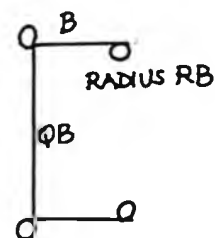


## APPENDIX B

TABLE II

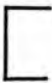
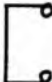
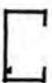

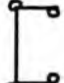

VALUES OF NON-DIMENSIONAL FACTOR GOVERNING  $R_z$ 

$\begin{matrix} Q \\ R \end{matrix}$	0.5	1.0	1.5	2.0	Remarks
0.01	0.10862	0.17210	0.21093	0.23578	
0.02	0.11443	0.18249	0.22265	0.24802	
0.03	0.11622	0.18947	0.23150	0.25772	
0.04	0.11501	0.19364	0.23799	0.26538	
0.05	0.11170	0.19553	0.24254	0.27136	
0.06	0.10706	0.19556	0.24546	0.27595	
0.07	0.10171	0.19410	0.24701	0.27936	
0.08	0.09611	0.19147	0.24743	0.28179	
0.09	0.09058	0.18795	0.24692	0.28340	
0.10	0.08535	0.18380	0.24564	0.28435	
0.11	0.08054	0.17923	0.24377	0.28476	
0.12	0.07621	0.17442	0.24147	0.28478	
0.13	0.07238	0.16954	0.23886	0.28453	
0.14	0.06906	0.16471	0.23603	0.28411	
0.15	0.06621	0.16004	0.23324	0.28364	
0.16	0.06383	0.15563	0.23044	0.28322	
0.17	0.06190	0.15154	0.22777	0.28293	
0.18	0.06039	0.14782	0.22531	0.28281	
0.19	0.05930	0.14452	0.22312	0.28305	
0.20	0.05864	0.14166	0.22125	0.28357	



## APPENDIX C

## PRELIMINARY TESTS

Section 8"x4"	Ultimate load in pounds				
	Test I	Test II	Test III	Test IV	Average
	2,750	2,726	-	-	2,738
	6,560	6,440	6,450	6,550	6,500
	5,450	5,270	-	-	5,360
	6,520	6,440	-	-	6,480
	6,530	6,460	6,500	6,510	6,500
	6,700	6,760	-	-	6,730